

NIST Technical Note XXXX

**Motorcoach Flammability Project
Final Report: Tire Fires - Passenger
Compartment Penetration, Tenability,
Mitigation, and Material Performance**

Erik L. Johnsson
Jiann C. Yang

THIS IS A PREDECISIONAL DRAFT INTERIM REPORT

NIST Technical Note XXXX

Motorcoach Flammability Project Final Report: Tire Fires - Passenger Compartment Penetration, Tenability, Mitigation, and Material Performance

Erik L. Johnsson
Giann C. Yang
*Building and Fire Research Laboratory
National Institute of Standards and Technology*

November 2010



U.S. Department of Commerce
Gary Locke, Secretary

National Institute of Standards and Technology
Patrick D. Gallagher, Director

Certain commercial entities, equipment, or materials may be identified in this document in order to describe an experimental procedure or concept adequately. Such identification is not intended to imply recommendation or endorsement by the National Institute of Standards and Technology, nor is it intended to imply that the entities, materials, or equipment are necessarily the best available for the purpose.

ABSTRACT

Full scale fire experiments were conducted at the National Institute of Standards and Technology (NIST) to investigate tire fire interactions with the passenger compartment of a motorcoach. A burner was designed to imitate the frictional heating of hub and wheel metal caused by failed axle bearings, locked brakes, or dragged blown tires. Two experiments were conducted to determine the mode of penetration of a tire fire into the passenger compartment. For the first experiment, heating to obtain tire ignition was initiated on the exterior of the right side tag axle wheel and for the second, on the exterior of the right side drive axle wheel. Four experiments were conducted to examine fire-hardening of the motorcoach against tire fire penetration. Methods explored were: replacing combustible external components with metal, covering combustible external components with an intumescent coating, and placing a metal fire-deflector shield above the fender. One experiment with a partially furnished interior investigated tire fire growth within the passenger compartment and the onset of untenable conditions. Measurements of interior and exterior temperatures, interior heat flux, heat release rate, and toxic gases were performed. Also, standard and infrared videos and still photographs were recorded.

The experiments showed that the tire fires ignited the plastic fender and glass-reinforced plastic (GRP) exterior side panel (below the windows) upon which the fires spread quickly and penetrated the passenger compartment by breaking the windows. Measurements showed that other potential fire penetration routes (flooring and lavatory) lagged far behind the windows in heating and degradation. Fire-hardening using steel components had the greatest effect, followed by using an intumescent coating. Tenability limits were reached within 11 min after fire penetration throughout the passenger compartment and by 7 min near the fire.

Recommendations are made that address additional testing to improve material flammability performance, motorcoach tire fire hardening options, and tire fire prevention.

KEYWORDS

Motorcoach fire, bus fire, tire fire, vehicle fire, window breakage, fire penetration, fire hardening, compartment tenability, transportation fires

TABLE OF CONTENTS

ABSTRACT..... iii

LIST OF FIGURES vi

LIST OF TABLES..... xiii

LIST OF ABBREVIATIONS..... xiv

INTRODUCTION 1

LITERATURE REVIEW 3

 Previous Studies Related to Bus and Motorcoach Fires 3

 1980s NIST Experiments..... 3

 1990s UK Experiments..... 4

 Experiments in China..... 5

 Experiments at SINTEF (Norway) 6

 Experiments at SP (Sweden)..... 6

 Material Flammability Testing 10

FLAMMABILITY TESTING OF ACTUAL MOTORCOACH MATERIALS..... 13

 Overview..... 13

 Test Results..... 15

EXPERIMENTAL SET-UP 20

 Experimental Preparation..... 20

 Obtaining the Motorcoach 20

 Moving and Securing the Motorcoach..... 20

 Straightening Window Posts..... 21

 Removing Unsafe Materials 25

 Replacement Components 25

 Burner 25

 Modifications for Fire-hardening Experiments 28

 Modifications for the Tenability Experiment 32

 Measurement Instrumentation 36

 Total and Burner Heat Release Rates 37

 Temperature 37

 Heat Flux..... 45

 Gas Volume Fractions..... 49

 Visibility 49

 Image Recording..... 53

 Standard and Infrared Video..... 53

 Still Photography 56

 General Procedures 56

 Extinguishment 57

RESULTS AND DISCUSSION 58

 Penetration Experiments 58

 Event Timing 58

 Photographs..... 60

 Heat Release Rate 74

 Wheel, Tire, and Wheel Well Temperatures 76

 Window and Panel Temperatures 79

Floor, Lavatory, and Central Tunnel Temperatures.....	84
Axle Temperatures.....	88
Heat Fluxes	90
Fire-hardening Experiments.....	92
Event Timing	92
Photographs.....	93
Heat Release Rate	99
ABS Sensor.....	102
Extinguishment	105
Tenability Experiment	105
Event Timing	105
Photographs.....	106
Repeatability	108
Heat Release Rate	109
Interior Gas Temperatures	110
Heat Fluxes	111
Thermal Tenability Analysis.....	112
Other Temperature Measurements.....	115
Gas Volume Fractions.....	116
Toxic Gas Tenability.....	118
Visibility	122
Extinguishment	123
SUMMARY OF FINDINGS AND CONCLUSIONS	124
Material Flammability Testing	124
Penetration Experiments	124
Fire-hardening Experiments.....	125
Tenability Experiment	126
RECOMMENDATIONS	128
ACKNOWLEDGEMENTS	129
REFERENCES	130
APPENDICES	132
Appendix A. Data Channel Description and Hook-up Lists.....	132
Penetration and Fire Hardening Experiments	132
Tenability Experiment	137
Appendix B. Photographs	143
Penetration Experiments	143
Fire-Hardening Experiments.....	155
Tenability Experiment	157

LIST OF FIGURES

Figure 1 A drawing of the motorcoach rear half which was used for tire fire experiments. Dimensions are in meters. Distance measurement uncertainty is $\pm 0.3\%$ 22

Figure 2 A photograph of the cribbing supporting the motorcoach during testing. 23

Figure 3 Window post straightening operation. The top photograph shows the original angle of a bent post. The bottom right photograph shows the notch at the bottom of the post. The bottom left photograph shows the angle bracket with self-tapping screws which reattached the roof to the post..... 24

Figure 4 A schematic of the wheel burner design showing the relative locations of the 10 torch heads and manifold compared to the wheel’s hub, lug nuts, and lug nut covers. The outer circle represents the wheel’s curvature away from the lug nut surface plane..... 26

Figure 5 The burner for heating the wheels. The top photograph shows the whole assembly including the burner ring, wheeled cart, and gas and air valves. The bottom right photograph shows the pre-mixed natural gas and air torches impinging on a tag axle wheel. The bottom left photograph shows the tire shield nested inside a drive axle wheel rim with an insulating cover to minimize convective and radiative heating to the tire from the shield..... 27

Figure 6 A diagram of the right side of the motorcoach for the fire-hardening experiment using stainless steel sheet in place of the fender and exterior side panel. Dimensions are in meters..... 28

Figure 7 A photograph of the fender and exterior side panel replaced with sheet metal. 29

Figure 8 A diagram of the right side of the motorcoach showing the exterior side panel and fender coated with an intumescent coating. Dimensions are in meters..... 30

Figure 9 A photograph of the fender and exterior side panel with an intumescent coating. 30

Figure 10 A diagram of the right side of the motorcoach showing the steel deflector between the fender and exterior side panel. Dimensions are in meters..... 31

Figure 11 Photographs of the deflector installed between the fender and exterior side panel. The left photo shows a view of the side of the motorcoach. The right photo shows an end view from the rear..... 32

Figure 12 Two photographs of the motorcoach front extension construction showing the beginning of the attachment of the galvanized sheet steel to the metal studding on the wooden substructure. 33

Figure 13 Photographs of the motorcoach extension. The top photo shows most of the assembly of the original motorcoach rear half and added front extension. The bottom left photo shows the extension doorway and steps. The bottom right photo shows the front end with the window and visibility camera. 34

Figure 14 A photograph of the seats and parcel rack installed for the tenability experiment. 36

Figure 15 A photograph of the right side wheel well area with the locations of thermocouples shown for the tag axle wheel experiment. The ignited and unignited tires (and their thermocouples) were reversed for the drive axle experiment. Labels (in red) are used in temperature plot legends..... 39

Figure 16 A schematic (top) and photograph (bottom) of the exterior grid of thermocouples on the motorcoach windows. The blue rectangles represent window outlines, red dots represent TCs, green areas represent window frames and post centerlines. Labels pertain to designations in the data file. The pattern of thermocouple labeling is shown in red with O for outside grid, the 1st number for column, and the 2nd number for row. 40

Figure 17 A schematic of the interior grid of thermocouples located near the windows. The blue rectangles represent window outlines, red dots represent TCs, green areas represent window frames and post centerlines. Labels pertain to designations in the data file. The pattern of thermocouple labeling is shown in red with I for inside grid, the 1st number for column, and the 2nd number for row. 41

Figure 18 A diagram of the top view of the motorcoach showing approximate locations of interior floor thermocouples and the locations and directions of heat flux gauges for tenability and hardening tests. 41

Figure 19 Schematic of the whole motorcoach assembly used for the tenability experiment showing locations of the three sampling stations, heat flux gauges, and thermocouples. 43

Figure 20 Two photographs showing the three pairs of seats installed for the tenability experiments. The right photograph shows one of the thermocouples installed on the top of an aisle seat headrest. 44

Figure 21 A photograph showing the right side parcel rack installed for the tenability experiments. Three thermocouples are shown attached about half way up the doors. 44

Figure 22 From the penetration experiments, a photograph of the interior of the motorcoach showing the locations of the heat flux gauges. 47

Figure 23 From the penetration experiments, a photograph of the interior heat flux gauges and their view of the right side windows. 47

Figure 24 From the penetration experiments, a photograph of the interior of the motorcoach showing the proximity to the window of the heat flux gauge at the position of a seat head rest. 48

Figure 25 Schematic of the whole motorcoach assembly used for the tenability experiment showing approximate locations of IR, video, and bullet cameras. 51

Figure 26 A photograph showing the rear gas sampling position, rear visibility sign, rear thermocouple array, and rear heat flux gauge used for the tenability experiment. 52

Figure 27 A photograph of the interior of the motorcoach and front extension looking toward the rear. The lit exit signs were used to determine visibility deterioration during the tenability experiment. 52

Figure 28 A diagram of the video camera layout for the penetration and hardening experiments showing their general locations and the directions they faced. 54

Figure 29 Photograph of the two IR cameras viewing the open end of the motorcoach for penetration and hardening experiments. One camera was set to IR and the other to visual mode for comparison. 55

Figure 30 A photograph of the bullet camera located between the two left (driver’s) side axles. 55

Figure 31 A photograph showing the location of the passenger compartment bullet camera (lower left) and lighting (lower right) to provide better videos and photographs of the interior. 56

Figure 32 Tag axle wheel heating penetration experiment about 1 min after the burner was removed. The fender is already burning and the exterior panel is just igniting..... 61

Figure 33 Tag axle wheel heating penetration experiment about 2 min after the burner was removed. The exterior panel is burning up to the windows. 62

Figure 34 Tag axle wheel heating penetration experiment just under 4 min after the burner was removed. 63

Figure 35 Tag axle wheel heating penetration experiment at fire penetration, about 4 min 40 s after burner removal. 64

Figure 36 Drive axle wheel heating penetration experiment about 1 min before burner was turned off. 65

Figure 37 Drive axle wheel heating penetration experiment just after burner was turned off. 65

Figure 38 Drive axle wheel heating penetration experiment about 30 s after burner was turned off. 66

Figure 39 Drive axle wheel heating penetration experiment showing fire spreading from the drive axle to the tag axle area of the fender..... 67

Figure 40 Drive axle wheel heating penetration experiment about 3 min after the burner was removed showing a view of the fire plume from the interior..... 68

Figure 41 Drive axle wheel heating penetration experiment showing large fire plumes on each tire. 69

Figure 42 Drive axle wheel heating penetration experiment showing the joined fire plumes within 2 min of fire penetration. 70

Figure 43 Drive axle wheel heating penetration experiment just under 5 min after burner removal. 71

Figure 44 Drive axle wheel heating penetration experiment at fire penetration, about 6 min 3 s after burner removal. Window breakage occurred on the more rearward window while the burning tire was fairly centered on post 3 between windows..... 72

Figure 45 Drive axle wheel heating penetration experiment within a few seconds of fire penetration and at the very beginning of extinguishment. 73

Figure 46 Heat release rate plotted versus time for test 1, the heated tag axle wheel passenger compartment penetration experiment. 75

Figure 47 Heat release rate plotted versus time for test 2, the heated drive axle wheel passenger compartment penetration experiment. 75

Figure 48 A plot of test 1 (tag axle) temperatures versus time for the heated wheel (Wh) and tire (Ti). Numbers in the labels represent 12, 3, 6, and 9 o'clock positions (0°, 90°, 180°, and 270° from top). 77

Figure 49 A plot of test 2 (drive axle) temperatures versus time for the heated wheel (Wh) and tire (Ti). Numbers in the labels represent 12, 3, 6, and 9 o'clock positions (0°, 90°, 180°, and 270° from top). 77

Figure 50 A plot of test 1 (tag axle) temperatures versus time for the wheel wells. I and U represent ignited and unignited sides, respectively. 78

Figure 51 A plot of test 2 (drive axle) temperatures versus time for the wheel wells. I and U represent ignited and unignited sides, respectively. 78

Figure 52 A plot of test 1 (tag axle) temperatures versus time for the lowest row of exterior TCs located below the window line 1 cm from the exterior GRP panel. See Figure 16 for labeling system. 80

Figure 53 A plot of test 2 (drive axle) temperatures versus time for the lowest row of exterior TCs located below the window line 1 cm from the exterior GRP panel. See Figure 16 for labeling system. 80

Figure 54 A plot of test 1 (tag axle) temperatures versus time for the highest row of exterior TCs located 1 cm from window surfaces and about 10 cm from the top of the windows. Figure 16 shows labeling. 81

Figure 55 A plot of test 2 (drive axle) temperatures versus time for the highest row of exterior TCs located 1 cm from window surfaces and about 10 cm from the top of the windows. Figure 16 shows labeling. 81

Figure 56 A plot of test 1 (tag axle) temperatures versus time for the lowest row of interior TCs, 1 cm from window surfaces and about 3 cm from the bottom of the windows. Figure 17 shows labeling. 82

Figure 57 A plot of test 2 (drive axle) temperatures versus time for the lowest row of interior TCs, 1 cm from window surfaces and about 3 cm from the bottom of the windows. Figure 17 shows labeling. 82

Figure 58 A plot of test 1 (tag axle) temperatures versus time for the hottest column of interior TCs, array 6, 1 cm from window. T0 was located above the window. See Figure 17 for labeling system. 83

Figure 59 A plot of test 2 (drive axle) temperatures versus time for the hottest column of interior TCs, array 8, 1 cm from window. T0 was located above the window. See Figure 17 for labeling system. 83

Figure 60 A plot of test 1 (tag axle) temperatures versus time for TCs on the interior floor at the bottom of the right side wall. Table 8 and Figure 18 describe thermocouple locations. 85

Figure 61 A plot of test 2 (drive axle) temperatures versus time for TCs on the interior floor at the bottom of the right side wall. Table 8 and Figure 18 describe thermocouple locations. 85

Figure 62 A plot of test 1 (tag axle) temperatures versus time for TCs on the interior floor where the lavatory walls join the exterior wall and floor in the middle of the coach. See Table 8 and Figure 18. 86

Figure 63 A plot of test 2 (drive axle) temperatures versus time for TCs on the interior floor where the lavatory walls join the exterior wall and floor in the middle of the coach. See Table 8 and Figure 18. 86

Figure 64 A plot of test 1 (tag axle) temperatures versus time for TCs inside the central tunnel for wires under the interior floor along the centerline of the coach. R, C, and F represent rear, center, and front, respectively, of the test section. Table 8 and Figure 18 describe thermocouple locations. 87

Figure 65 A plot of test 2 (drive axle) temperatures versus time for TCs inside the central tunnel for wires under the interior floor along the centerline of the coach. R, C, and F represent rear, center, and front, respectively, of the test section. Table 8 and Figure 18 describe thermocouple locations. 87

Figure 66 A plot of test 1 (tag axle) temperatures versus time for TCs above the two axles. P, C, and D represent passenger (right) side, center, and driver (left) side, respectively. 89

Figure 67 A plot of test 2 (drive axle) temperatures versus time for TCs above the two axles. P, C, and D represent passenger (right) side, center, and driver (left) side, respectively. 89

Figure 68 A plot of test 1 (tag axle) total heat flux versus time for the 5 heat flux gauges in the passenger compartment. Table 9 provides additional descriptions of the locations..... 91

Figure 69 A plot of test 2 (drive axle) total heat flux versus time for the 5 heat flux gauges in the passenger compartment. Table 9 provides additional descriptions of the locations. 91

Figure 70 Steel exterior panel fire-hardening experiment about 8 min after burner removal. 94

Figure 71 Steel exterior panel fire-hardening experiment about 39 min after burner removal. 94

Figure 72 Intumescent coating fire-hardening experiment about 4 min after burner removal. 95

Figure 73 Intumescent coating fire-hardening experiment about 6 min after burner removal. 95

Figure 74 Intumescent coating fire-hardening experiment about 19 min after burner removal. 96

Figure 75 Intumescent coating fire-hardening experiment about 28 min after burner removal. 97

Figure 76 Steel deflector fire-hardening experiment about 1 min after burner removal. 98

Figure 77 Steel deflector fire-hardening experiment about 2 min after burner removal. 98

Figure 78 Steel deflector fire-hardening experiment about 8 min after burner removal. 99

Figure 79 Heat release rate plotted versus time for test 3, the metal panel/fender experiment. 100

Figure 80 Heat release rate plotted versus time for test 4, the coated panel/fender experiment. 101

Figure 81 Heat release rate plotted versus time for test 5, the steel deflector experiment. 101

Figure 82 ABS sensor voltage (left axis) and ABS temperature (right axis) plotted versus time for test 3, the steel panel test. 103

Figure 83 ABS sensor voltage (left axis) and ABS temperature (right axis) plotted versus time for test 4, the intumescent coating test. 103

Figure 84 ABS sensor voltage (left axis) and ABS temperature (right axis) plotted versus time for test 5, the steel deflector test..... 104

Figure 85 ABS sensor voltage (left axis) and ABS temperature (right axis) plotted versus time for test 6, the tenability test. 104

Figure 86 Tenability experiment about 12 min after burner removal..... 106

Figure 87 Tenability experiment passenger compartment about 15 min after burner removal. 107

Figure 88 Tenability experiment almost 20 min after burner removal. 107

Figure 89 Comparison of average tag axle wheel temperatures plotted versus time for the experiments initiated on the tag axle wheel..... 109

Figure 90 Heat release rate plotted versus time for test 6, the tenability experiment. 110

Figure 91 A plot of test 6 (tenability) interior rear, middle, and front gas temperatures versus time. Numbers 30 through 180 represent distance from the floor in centimeters. 111

Figure 92 A plot of test 6 (tenability) total heat flux versus time for the 5 heat flux gauges in the passenger compartment. Table 10 provides additional descriptions of the locations. 112

Figure 93 Fractional effective doses from thermal radiation plotted versus time for the six heat flux gauges located 1m, 2 m, 3 m, 4 m, and 6 m from the rear (lavatory door) of the motorcoach. 113

Figure 94 Fractional effective doses from thermal convection plotted versus time for the thermocouples 1.5 m from the floor at the rear (R), middle (M), and front (F) thermocouple arrays. The type 1 analysis treats occupants as fully clothed while type 2 is for more lightly clothed occupants with more skin exposure. 114

Figure 95 Fractional effective doses from radiation and convection plotted versus time for the rear (1 m) and middle (6 m) heat flux gauges and thermocouples 1.5 m above the floor. The type 1 analysis treats occupants as fully clothed while type 2 is for more lightly clothed occupants with more skin exposure. 115

Figure 96 Seat headrest and parcel rack door temperatures plotted versus time for the tenability experiment. Locations were on or over the rear (R), middle (M), and front (F) seats. 116

Figure 97 O₂, CO₂, and CO volume fractions measured at the rear (R), middle (M), and front (F) sampling locations plotted versus time for the tenability experiment. 117

Figure 98 CO, HCN, and HCl volume fractions measured with FTIR at the rear sampling location plotted versus time for the tenability experiment. 118

Figure 99 Fractional effective doses for HCN and CO measured at the rear (R), middle (M), and front (F) sampling locations plotted versus time for the tenability experiment. 120

Figure 100 Total (both CO and HCN) fractional effective doses for the rear (R), middle (M), and front (F) sampling locations plotted versus time for the tenability experiment. 120

Figure 101 Fractional effective concentration for HCl measured with FTIR at the rear sampling location plotted versus time. 121

Figure 102 Visibility distance plotted versus the time from burner removal for the exit signs during the tenability experiment. 123

Figure 103 Tag axle wheel heating penetration experiment showing burner, shield, melted hub, and early thermal damage to tire. 143

Figure 104 Tag axle wheel heating penetration experiment about 2.5 minutes after the burner was removed showing the large quantity of black smoke on the far (driver's) side of the motorcoach. 144

Figure 105 Exterior fire damage due to tag axle wheel heating penetration experiment 145

Figure 106 Exterior view of window damage after tag axle wheel heating penetration experiment. 146

Figure 107 Interior view of window damage after tag axle wheel heating penetration experiment. 146

Figure 108 Damage to wall behind exterior panel after tag axle wheel heating penetration experiment.	147
Figure 109 Damage to back side of exterior panel showing little penetration of fire through the GRP.	147
Figure 110 Motorcoach ready for start of drive axle wheel heating penetration experiment.	148
Figure 111 Positioning of burner for drive axle wheel heating penetration experiment.	148
Figure 112 Close up view of burner near beginning of drive axle wheel heating penetration experiment.	149
Figure 113 Drive axle wheel heating penetration experiment showing smoke coming from the external air vents.	150
Figure 114 Drive axle wheel heating penetration experiment just over 1 min after burner was removed.	151
Figure 115 Drive axle wheel heating penetration experiment showing large fire plumes on each tire.	152
Figure 116 Drive axle wheel heating penetration experiment showing smoke on driver's side 4 min after burner removed.	153
Figure 117 Interior view of damage to the window over the tag axle after the drive axle wheel heating penetration experiment fire.	154
Figure 118 Interior view of damage to the window over the drive axle after the drive axle wheel heating penetration experiment fire.	154
Figure 119 Steel exterior panel fire-hardening experiment at the beginning of suppression.	155
Figure 120 Steel exterior panel fire-hardening experiment paper-covered wall foam damage from fire.	156
Figure 121 Intumescent coating fire-hardening experiment close-up of coated fender.	156
Figure 122 Intumescent coating fire-hardening experiment damage to coated fender and exterior panel.	157
Figure 123 Tenability experiment at the beginning of suppression.	157
Figure 124 Tenability experiment seat damage from fire.	158
Figure 125 Tenability experiment seat and parcel rack damage from fire.	158
Figure 126 Tenability experiment seat damage from fire.	159

LIST OF TABLES

Table 1 Material selection and appropriate flammability tests 13

Table 2 Flammability test descriptions 14

Table 3 Parcel rack door flammability test results..... 15

Table 4 Seat cushion flammability test results 16

Table 5 Interior wall panel flammability test results 17

Table 6 Seat back rear flammability test results 19

Table 7 Test matrix 20

Table 8 Numbers of thermocouples and location descriptions common to all
experiments..... 38

Table 9 Heat flux gauge locations for the penetration and fire-hardening experiments..... 45

Table 10 Heat flux gauge locations for the tenability experiment..... 46

Table 11 Timing of events and observations during the penetration experiments.
(uncertainty = ± 3 s) 58

Table 12 Duration of periods of heating and between heating and window penetration. 59

Table 13 Timing of events and observations during the fire-hardening experiments.
(uncertainty = ± 3 s) 92

Table 14 Duration of periods of heating and between heating and penetration for the tag
axle experiments with and without fire-hardening 93

Table 15 Timing of events and observations during the tenability experiment.
(uncertainty = ± 3 s) 105

Table 16 Comparison of times from fire penetration to untenable conditions 122

Table 17 List of distances and time visibility ended for the tenability experiment exit
signs..... 122

LIST OF ABBREVIATIONS

ABS	Anti-lock braking system	L	Length
ASTM	American Society of Testing and Materials	LFL	Large Fire Laboratory (NIST)
CBUF	Combustion behaviour of upholstered furniture programme	LIFT	Lateral ignition and flame spread test apparatus
CFD	Computational fluid dynamics	M	Middle position
CFR	Code of Federal Regulations	MCI	Motor Coach International
CO	Carbon monoxide	NDIR	Non-dispersive infrared
CO ₂	Carbon dioxide	NHTSA	National Highway Traffic Safety Administration
DAQ	Data acquisition system	NIST	National Institute of Standards and Technology
DOT	Department of Transportation	NO	Nitric oxide
D _s	Specific optical density (optical density measured over unit path length in a unit volume from a unit surface area specimen irradiated by a heat flux of 2.5 W/cm ²)	NO ₂	Nitrogen dioxide
ECE	Economic Commission for Europe	NTSB	National Transportation Safety Board
F	Front position	O ₂	Oxygen
FAA	Federal Aviation Administration	OD	Outside diameter
FAR	Federal Aviation Regulations (Title 14 of CFR)	OEM	Original equipment manufacturer
FDS	Fire Dynamics Simulator	R	Rear position
FEC	Fractional effective concentration	SCBA	Self-contained breathing apparatus
FED	Fractional effective dose	SINTEF	Norwegian Fire Research Laboratory
FID	Flame ionization detector	SO ₂	Sulfur dioxide
FMVSS	Federal Motor Vehicle Safety Standard	SP	Technical Research Institute of Sweden
FRA	Federal Railroad Administration	TC	Thermocouple
FTIR	Fourier transform infrared	TX	Texas
FTA	Federal Transit Administration	UK	United Kingdom
GRP	Glass reinforced plastic	W	Width
H	Height		
H ₂ O	Water		
HBr	Hydrogen bromide		
HCl	Hydrogen chloride		
HCN	Hydrogen cyanide		
HRR	Heat release rate		
ID	Inside diameter		
IR	Infrared		
I _s	Flame spread index (product of flame front progress rate and heat release rate)		
ISO	International Standards Organization		

INTRODUCTION

Research concerning vehicle fires is important for the prevention of life and property losses. While death by fire in a burning vehicle is a tragedy, fires in vehicles such as motorcoaches which carry as many as 56 passengers are especially tragic as they impact whole communities, regions, or even nations. One such fire occurred during the evacuation of Gulf Coast residents during Hurricane Rita in 2005. On September 23, 2005, near Wilmer, TX, a motorcoach carrying nursing home residents experienced a failed right bearing on the tag axle resulting in a tire fire which spread to consume the motorcoach. Twenty-three occupants died because many were not mobile and could not escape the motorcoach before being overcome by smoke and flames. [1] Even when there are no fatalities in motorcoach or bus fires, complete loss of the coach and passenger property is typical. [2]

The National Highway Traffic Safety Administration (NHTSA) has sponsored the National Institute of Standards and Technology (NIST) to conduct research to support NHTSA's current effort on improving motorcoach fire safety based on recent National Transportation Safety Board (NTSB) recommendations [1]. The recommendations were:

H-07-04: Develop a Federal Motor Vehicle Safety Standard to provide enhanced fire protection of the fuel system in areas of motorcoaches and buses where the system may be exposed to the effects of a fire.

H-07-05: Develop a Federal Motor Vehicle Safety Standard to provide fire-hardening of exterior fire-prone materials, such as those in areas around wheel-wells, to limit the potential for flame spread into a motorcoach or bus passenger compartment.

H-07-06: Develop detection systems to monitor the temperature of wheel-well compartments in motorcoaches and buses to provide early warning of malfunctions that could lead to fires.

H-07-07: Evaluate the need for a Federal Motor Vehicle Safety Standard that would require installation of fire detection and suppression systems on motorcoaches.

The pertinent recommendations for NIST's experimental research were H-07-05 and H-07-06. The research conducted by NIST was intended to accomplish the following tasks:

- Establish an understanding of the development of a motorcoach fire and its subsequent spread into the passenger compartment.
- Evaluate and identify bench-scale material flammability test methods that are most likely to give a meaningful measure of the resistance of interior materials of a motorcoach to a typical wheel-well fire.
- Determine the feasibility of establishing requirements for fire-hardening or fire resistance of motorcoach exterior components, including fuel system components.
- Assess tenability within the passenger compartment in the event of a wheel-well fire and identify potential mitigation strategies.

Whereas motorcoach fires may result from electrical system malfunctions, engine compartment leaks, component overheating, or tire fires, this research was focused on the penetration of motorcoach *tire fires* into the passenger compartment, methods of fire-hardening of the motorcoach passenger compartment against tire fires, and untenable conditions and available time to escape for motorcoach tire fires. The causes of tire fires (failed axle bearings, locked brakes, or dragged blown tires) are common to all makes and models of motorcoaches. [2]

For the NIST research project, only the rear half of a motorcoach was used. Six full scale fire experiments were performed: two passenger compartment penetration experiments, three fire-hardening experiments, and one tenability experiment. In order to imitate the frictional heating of hub and wheel metal caused by failed axle bearings, locked brakes, or dragged blown tires, a unique burner was designed to only heat the metal of the wheel without preheating the tire rubber.

For the two penetration experiments, each experiment was ignited by heating a different wheel. The heated wheels for all of the experiments were on the right side (when facing forward) of the motorcoach which was also the passenger entry door side and opposite the driver's side. The first tire fire was started on the tag (rearmost, also called dead or lazy) axle, which only had one wheel and tire per side. This experiment most closely emulated the Hurricane Rita evacuation motorcoach tire fire. The second experiment started on the drive axle (in front of the tag axle), which had two wheels and tires per side. For the fire-hardening experiments, the tag axle wheel was heated. The penetration experiments are described in a previous interim report. [3]

Three methods of fire-hardening the motorcoach passenger compartment against tire fires were explored: replacing combustible external components with metal, covering combustible external components with an intumescent coating, and placing a metal fire-deflector shield above the fender.

A final experiment was conducted to investigate tire fire growth within the passenger compartment after penetration and to determine the onset of untenable conditions due to thermal effects and toxic gases. For this experiment, the original rear of the motorcoach was complemented by a constructed front to recreate a realistic passenger compartment volume, and the interior was partially furnished to provide fuel for fire spread.

For each tire fire experiment, temperature measurements were made and recorded in the interior near the windows and on the floor, on the exterior near the windows and body panels, on the wheels and tires, and in the wheel well and axle regions. Interior heat fluxes were measured in several locations, and the total heat release rate of the fire was calculated from the hood exhaust using oxygen depletion calorimetry. For the tenability experiment, toxic gases were measured, and visibility was analyzed. Standard and infrared videos and still photographs were recorded.

LITERATURE REVIEW

The review consists of two parts. The first part discusses material flammability test methods related to materials used in the transportation sector. The second part reviews previous studies related to bus and motorcoach fires.

Previous Studies Related to Bus and Motorcoach Fires

Although our study focuses on wheel-well fires, the literature review provided here also covers other aspects related to bus and motorcoach fires because proper assessment of how a fire spreads from a wheel-well into the passenger compartment cannot be systematically performed until we know more about wheel-well fires and what affects the rate of fire development on the tires, on the components near the wheel-well, and on the interior materials.

1980s NIST Experiments

In May of 1988, a fiery collision between a pickup truck traveling the wrong way on an interstate highway in Kentucky and a former school bus (1977 model) returning from a church youth excursion resulted in twenty-seven fatalities on the bus. This occurred even though the bus seat assemblies were presumably compliant with fire performance requirements stipulated by the Federal Motor Vehicle Safety Standards (FMVSS) 302. This tragedy prompted NHTSA to task the National Institute of Standards and Technology (NIST) to assess the fire performance of school bus seat assemblies and to develop a test protocol to evaluate the fire performance of materials used in school bus seats. [4]

In the NIST study, laboratory-scale cone calorimeter and lateral ignition and flame spread test (LIFT) apparatus were used to assess ignitability, flame spread, heat release rates (HRRs), and specific gaseous products (CO, CO₂, HCN, HCl) and smoke yields of representative bus seating materials. To evaluate the fire performance of fully assembled seats, a large-scale furniture calorimeter was used to determine the HRRs, mass loss rates, and yields of specific gaseous products (CO, CO₂, HCN, HCl) of the seats exposed for 200 s to a 50 kW or 100 kW heat source. The heat source was either a line natural-gas burner placed in the cushion back crevice to simulate a fire on the seat or a box natural-gas burner with a surface area of 0.05 m² placed adjacent to the side edge of the seat to simulate a fire under the seat.

Full-scale fire tests were conducted in an enclosure with dimensions of 8.23 m (L) × 2.44 m (W) × 2.13 m (H) to simulate a school bus. Ventilation for the enclosure was provided by a doorway with dimensions of 1.83 m (H) × 1.02 m (W). Three seat assemblies placed on a load cell and with seating arrangement similar to a real school bus were placed in the rear corner of the enclosure. The box burner placed adjacent to the aisle edge of the rearmost seat assembly was used to ignite the seat. In the test series, gas temperatures in the upper and lower layers, gas (CO₂, O₂, CO) volume fractions in the upper layer, and mass loss rates of the burning seat assemblies were measured to determine the HRRs and to assess tenability inside the simulated bus.

The NIST study concluded that the fire performance of a material depended not only on the ignition propensity of the material but also on other parameters such as flame spread, HRR, toxicity of the combustion products generated, and smoke development, and could not be uniquely determined by any one simple small-scale test. Based on the full-scale test results, a full-scale test protocol was proposed as a basis for compliance testing of seat assemblies for use in school buses. The procedure required the determination of the tenability conditions in the compartment and comparison of results to tenability limits.

1990s UK Experiments

A study of life threat in bus fires was conducted in the United Kingdom (UK) by Fardell et al. [5] using a combination of material flammability testing, fire tests of mock-up and full-scale single deck and double deck buses, computer field modeling, and tenability assessment based on mass loss fractional effective dose models. [6] The focus of the study was on vandalism, intentionally set fires, and engine fires.

For the material flammability testing, normal and vandalized (simulated by ripped fabric, exposing polyurethane foam underneath) seating materials were used and subjected to various ignition sources likely to be used in intentionally set fires, which included a match, a glowing cigarette, a butane cigarette lighter, methylated spirits spread on a seat or on a rag, pieces of torn bus ticket, a sheet of newspaper, and lighter fuel. The normal un-vandalized materials were found to perform better. However, the flammability test protocol and the performance metrics were not described, and it was unclear if the materials contained flame retardants.

A full-sized mock-up of a single-deck or double-deck bus interior with authentic materials and seating arrangement was used in the fire tests. The intent of using the mock-ups was largely for the identification and selection of test conditions for the subsequent full-scale bus fire experiments. A vandalized seat with exposed upholstery foam soaked with lighter fuel was ignited. HRRs, volume fractions of carbon dioxide, carbon monoxide, and oxygen, mass losses, and smoke densities were measured. With several seats (number and configuration unspecified in the paper) used in the fire tests, flashover occurred in 16 min in the single-deck mock-up and 37 min for the double-deck mock-up. Based on the mass loss model, the approximate times to incapacitation and death were 6 min and 8 min respectively for double-deck mock-up and 8 min and 10 min for the single-deck mock-up. It was argued, together with other unpublished studies, that this represented sufficient time for escape.

A fire on the lower deck in a seat close to the foot of the central staircase, which was considered to be a worst case scenario, was chosen for the full-scale double-deck bus fire test because the location of the fire could potentially block the main exit door situated on the lower deck of the bus and facilitate smoke transport up the staircase, thus making it increasingly difficult for the upper deck passengers to escape. For the full-scale single-deck bus fire test, a tray of burning fuel (type not given) placed under the engine which was running at the beginning of the test was used to simulate a fire originating from the engine compartment with potential for spread into the passenger compartment. Both buses were instrumented to measure volume fractions of carbon monoxide, carbon dioxide, and oxygen, temperatures, heat fluxes, and smoke optical densities at various locations on both decks of the double deck bus and near the front and rear exits on the

single deck bus; however, the exact sampling positions were not given in the paper except all sampling points were 1.5 m above the floor (standing “nose height”). In addition, detailed experimental set-up and conditions for both buses were not provided.

The full-scale double-deck bus test results showed that conditions on both decks remained tenable 40 min into the test. For reasons unknown, the fire was confined to the original burning seat without spreading to adjacent seats. For the single-deck bus, the test results indicated incapacitation would have occurred after 8 min at the rear door but was never reached at the front door throughout the test; however, the test duration was not given in the paper.

In addition to fire tests, computational field modeling was employed to study the smoke transport and fire dynamics on the single and double deck buses. The field model used was JASMINE. [7] The full-scale fire test results were used to fine-tune the model and validate the predictions.

Experiments in China

A series of studies on bus fires was initiated by Chow and co-workers as the result of several fires on double-deck buses in Hong Kong in 1999 and 2002. [8, 9, 10, 11] They raised and discussed various key bus fire safety issues, which included material fire safety, fire scenarios, HRRs, potential fire protection strategies, flashover, and smoke spread and control. The approach involved the uses of material flammability test data from literature, empirical equations, a two-layer zone model, and scale-model experiments.

Chow et al. suggested the use of the cone calorimeter to study sandwich panels used on buses in order to understand how these materials behaved in a bus fire. They pointed out that ASTM E162 (flame spread), ASTM D3675 (flame spread), ASTM E662 (smoke density chamber), ASTM E648 [12] (floor covering), ASTM E119 (fire endurance), and FAR-25.853 were potential test methods that could be used to assess material flammability.

They applied the CFAST zone model to study the smoke filling process for a typical double-deck bus with a simulated seating fire. [13] A 1/10-scale empty (without seats) double-deck bus model was fabricated to study the effect of fire origin on smoke spreading and control. The material used to construct the model bus was not specified in the study. The fire was a gasoline pool fire with various pool diameters placed at different locations close to the front exit on the lower deck of the scale model bus. Two natural vents, one at the upper deck ceiling and one in the rear of the upper deck, were used for smoke control. Temperatures inside the model bus were monitored using three vertical thermocouple arrays placed at the front, in the middle, and in the rear of the bus on both decks. The observations revealed smoke spread from the lower deck (fire origin) to the upper deck, and smoke could be removed and its temperature reduced by opening the ceiling vent or rear vent on the upper deck. Their studies resulted in confirmation that fire testing of a full-scale bus was needed to understand the actual fire behavior including the structural integrity of the bus.

Experiments at SINTEF (Norway)

Several full-scale mock-up tire fire experiments have been conducted by the Norwegian Fire Research Laboratory (SINTEF). [14, 15, 16] A set of two tires with wheels was mounted on a steel pipe (a simulated axle) through which the hot combustion gas from a 700 kW propane burner was fed. The wheels, which were in direct contact with the steel pipe, were preheated and subsequently the tires were ignited by a small gas burner. The study involved the measurements of HRRs of burning tires, the structural response of the vehicle to the tire fires, and the penetration of tire fires in a simulated wheel well into the interior compartment. The experiments used a mock-up box truck made of aluminum with or without floor lining (plywood or aluminum punched hole plank) and a simulated cargo (two wooden pallets with concrete blocks) placed on the floor inside the truck and directly above the wheel well.

After preheating for about 30 min, the two tires were ignited, and the peak HRR was about 900 kW. Peak temperature measured in the tires just before pilot ignition was approaching 350 °C. Depending on the test configuration, various extents of damage to the floor and wall of the mock-up was observed, including burn-through and melting of the aluminum skin.

Extinguishment of tire fires was also investigated using the same mock-up and various types of portable fire extinguishers containing dry powder, foam, water, and wet chemicals. No single fire extinguishing agent was identified that exhibited all of the desired attributes for putting out tire fires. Based on the 22 tire fire trials, dry powder and water mist with anti-freeze additives appeared to be the most promising.

These studies do not indicate what real situation conditions were being mimicked or what vehicle types the mock-ups were designed to evaluate. However, these tests do provide lessons learned and some valuable information as to the heat release and propagation rates of tire fires.

Experiments at SP (Sweden)

A comprehensive study on bus fire safety was recently completed by the SP Technical Research Institute of Sweden. [17] The study included:

- a statistical survey of bus fires in Norway and Sweden
- flammability testing of interior materials
- identification of fire risks from design, construction, maintenance, and cost perspectives
- prevention and mitigation strategies
- CFD simulations of fire development and spread, and
- full-scale fire tests.

Flammability testing of bus interior materials from seats, walls, ceilings, and floors using FMVSS 302/ISO 3795 was conducted. [18] Standard fire test methods developed for the maritime and rail transportation and building sectors were also applied to assess the fire performance of these materials. The test methods examined included ISO 5660-1 [19] (cone calorimeter), ISO 5659-2 (smoke box), ISO 5658-2 (flame spread), ISO 9239-1 (radiant panel), ISO 11925-2 [20] (small flame), CBUF [21] (full-scale seat), and ISO 6941 [22] (curtain flame spread). Based on this battery of standard fire tests, it was concluded that FMVSS 302/ISO 3795

alone was inadequate to address material fire performance in an actual bus fire. In addition, the fire resistance performance of partition materials used on buses should also be assessed to enhance fire safety requirements, and other standard test methods should be explored.

Fire risks in association with the electrical system, engine compartment, passenger compartment, and maintenance were assessed; however, it was unclear why wheel-well tire fires were not considered as a risk in the study. The risk factors in the electrical system were aging of cables, mechanical and physical damage to cables, short circuits, arcing, and overloaded or improperly-rated fuses. Exposure of combustible materials (e.g., rubber hoses, fuel and/or hydraulic fluid leaks) to hot surfaces was identified to be the risk factor in an engine compartment. Fire risk in the passenger compartment was attributed to intentionally set fires, electrical fires, fire spread from the engine compartment, and the presence of combustible materials (e.g., seats, flooring). Inadequate maintenance and inspection was also considered as a potential risk factor. Some general mitigation strategies on fire detection and extinguishment of bus fires were qualitatively discussed, and the recommendations drawn from the general discussion were the installation of fire detection and extinguishment systems in the engine compartment, improved electrical systems, better maintenance and inspection crew training, and better fire safety education and fire-fighting training for drivers.

The development of a 1/3-scale city bus rear engine compartment with an engine mock-up to evaluate the performance of water-based fire extinguishing systems in putting out engine fires was included in the SP study. The surface temperature of the mock-up could be controlled using heated water to mimic different engine operating conditions (cruising, idling, and engine-off). This prototype test rig could be used to study the impact on fire extinguishment effectiveness of: fire location, fire type (spray fire, pool fire, smoldering, and glowing), fire size, air temperature and ventilation through the mock engine compartment, and re-ignition.

The SP study also demonstrated the application of computational fluid dynamics (CFD) to understand the development of a bus fire in the passenger compartment. The computer code, Fire Dynamics Simulator [23] (FDS version 4) developed by NIST, was employed in the study. FDS is especially suited to study the transport of hot smoke and product gases from fires. A computational domain analogous to a bus with a typical seating arrangement was constructed and gridded. The modeled bus had one door located at the front and one at the mid section of the bus. The bus also had two hatches, one on the front roof and one on the rear roof. The fire source was a prescribed burning seat in the rear of the bus. Several fire scenarios were examined and compared, which included both roof hatches opened or closed with both doors opened and both doors opened or closed with both roof hatches opened. The simulation results indicated that roof hatches provided an effective way to vent fire smoke, and combustible materials at the ceiling played a major role in fire propagation in a bus.

The culmination of the SP study was the three real-scale fire tests using a 49-passenger motorcoach from Volvo Buses AB (model unspecified, driver side on the right-hand side of the coach, no bathroom onboard). The overall dimensions of the coach were 13 m (L) × 2.6 m (W) × 3.6 m (H). Since the real-scale testing part of the SP study is closely aligned with this NIST study, it will be reviewed in detail. The Volvo test coach, with the interior fully furnished and gear box fitted with a retarder to simulate a loaded engine, had mainly been used for product

development purposes and had never been used to transport the public. From the photograph, the engine compartment seemed to be situated in the mid section on the left side of the coach, and the below-deck baggage compartments were on both sides and in the rear of the coach.

The first full-scale fire test was intended to simulate an engine compartment fire. The fuel used to ignite the fire was a mixture of diesel, engine oil, hydraulic fluid, and sawdust and was applied on the top of the engine block. The engine was running for at least 10 min before ignition. Upon ignition, the engine was put in a no-load running condition for 6 min. Then, the engine was stopped. Temperatures were monitored using thermocouples at several locations in the engine compartment. Two aspirated detectors were also placed in the compartment for fire detection. Each of the four below-deck baggage compartments was equipped with a smoke detector. Observations made were: (1) the two aspirated detectors in the engine compartment were falsely activated 2 min 15 s before ignition due to the presence of nuisance fuel vapor, (2) the four smoke detectors in the baggage compartments were alarmed less than 20 s after ignition, (3) the fire was out in less than 1.5 min after the engine was stopped due to the lack of oxygen supply in the closed engine compartment, and (4) the plywood hatch over the engine compartment was slightly damaged by the fire. Based on the observations, it was suggested that given the closed environment of an engine compartment, an engine fire was unlikely to spread if the engine was stopped upon detection of the fire by a rapid, reliable fire detection system.

The second full-scale test involved the use of a rear wheel well of the motorcoach to study an in-situ tire fire. A small pan of kerosene-diesel mixture placed under the wheel was used to ignite the tire, which was also wrapped with cotton fabric soaked with a kerosene-diesel mixture to facilitate the ignition process. In order to preserve the motorcoach for the final full-scale test and prevent damage to the floor and the side panels, the wheel well, part of the fender, and part of the exterior side panel directly above the wheel well were protected from the tire fire by being covered with mineral wool. The following sequence of events was observed. At 1 min after ignition, the fire had reached the lower edge of the window directly above the wheel well. At 2 min, the tire was engulfed by fire. At 5 min, smoke appeared in the passenger compartment. At 12 min, poor visibility was noted inside the motorcoach. At 14 min, smoldering was observed; however, the report did not describe which part of the interior was smoldering. The window remained intact with flame covering a small part of it at 15 min after ignition. At that time, the decision was made to extinguish the fire with water to prevent further damage to the coach because a small fire was growing inside the coach. The outer pane of the window was eventually cracked by sudden water cooling as the fire was being extinguished. The maximum temperatures measured by the two thermocouples mounted on the lower part of the outer pane of the window were about 300 °C. In this particular test, smoke and hot gases were transported into the passenger compartment from the wheel well through the floor and the side panels. However, given the experimental arrangement (a thermally protected wheel well, fender, and side panel), it was unclear if the test conditions could truly reflect a real-life wheel well fire. It was noted in the report that since wheel well fires were normally caused by frictional heating due to malfunctioning brakes or wheel bearings, a temperature sensor installed in the wheel bearings could potentially prevent many wheel well fires.

The last of the SP full-scale test series examined the development of a simulated rear engine compartment fire from ignition, burn-through, to flash-over inside the coach. The objectives of

the test were to investigate the following: how rear engine compartment fires penetrate into the passenger compartment, smoke transport, smoke obscuration, and toxic gas volume fractions inside the passenger compartment, and HRR from a developed motorcoach fire.

The rear baggage compartment of the coach was used to simulate a *rear* engine compartment. Holes were drilled on the floor of the baggage compartment to simulate ventilation in an engine compartment. A 100 kW propane burner was used as the fire source. The burner was enclosed between two mineral wool side walls in order to compartmentalize the fire to a specific location beneath the passenger compartment. At the location directly above the burner, five thermocouples were placed on the floor and two 20 cm above the floor inside the passenger compartment to assess fire endurance of the floor. The distance from the burner to the underside floor of the passenger compartment was about 60 cm. Inside the passenger compartment, two vertical thermocouple arrays, one in the front of the compartment and one in the rear, were placed on the centerline of the compartment and used to measure the gas temperatures. In addition, thermocouples were mounted on several specified seat headrests on both sides of the aisle.

Visibility inside the passenger compartment was assessed during smoke spread using four video cameras to monitor the visibility of the seven targets placed on the sides of the seven specified seat headrests (six next to the aisle and one in the back row) at eye level at standard seat positions and locations at the thermocouples on the two thermocouple arrays. From the photographs in the report, the targets appeared to be white index cards with a number (from 1 to 7) printed on each card. The four cameras were all pointed towards the back of the motorcoach. One camera was mounted outside of the coach in the middle of the windshield and was tilted downward at eye level. One was located horizontally off of the aisle center by the front door at eye level at a seat position. One was positioned horizontally near the floor in the middle of the coach near the center of the aisle. One was placed near the window on the driver side in the middle of the coach at eye level in a standing position and was pointed downwards.

Toxic gases (CO, CO₂, HCl, HCN, HF, HBr, SO₂, NO, NO₂) in the passenger compartment were measured using an FTIR (Fourier transform infrared spectrometer) by extracting the gas using a sampling probe mounted at the ceiling directly above the location of the rear right side wheel well. To prevent hot gases and smoke from escaping readily through the front door, the upper part of the door was covered with a plywood soffit to reduce the door opening. The fire test was conducted with the door opened and the soffit in place. Although no explanation was given in the report, the use of a soffit to reduce the door opening area was probably meant to artificially create a worse-case scenario to assess tenability.

Since SP's industrial-scale calorimeter was not large enough to accommodate the full length of the motorcoach and the fire was initiated at the rear simulated engine compartment, only two-thirds of the rear part of the coach was placed under the calorimeter hood for HRR measurements during the fire test.

Although the precise times for smoke and fire penetration into the passenger compartment were not noted, smoke was observed in the passenger compartment from the photograph taken at 3 min after ignition. At about 13 min, the exterior of the rear of the coach was seen from the

photograph to be fully engulfed with fire. At about 17 min after ignition, the rear side windows on the left hand side of the coach broke and the interior materials in the passenger compartment started to burn intensely. At about 19 min, the fire was so intense that the hood was overrun, and the fire test had to be terminated for safety reasons using manned fire hoses. The HRR just before the termination of the fire test was estimated to be about 15 MW.

Viewed from the camera mounted outside the windshield, the target at the ceiling lamp location inside the motorcoach 12 m from the camera was visible at 180 s after ignition. The visibility decreased to 6 m at 360 s. Eventually, it reduced to 2 m at 510 s. For targets at eye level, the visibility decreased from about 13 m at 120 s to about 3.7 m at 330 s. At headrest level, the visibility decreased from about 13 m at 120 s to 4 m at 390 s. From the photograph, it appeared that all of the interior lights were turned on during the fire test.

Toxic gas measurements were reported during the first 8 min after ignition. The maximum volume fractions of CO, CO₂, HCl, HCN, HF, HBr, SO₂, NO, and NO₂ were 3030 µL/L, 1.71 %, 51 µL/L, 65 µL/L, < 5 µL/L, < 10 µL/L, < 10 µL/L, < 15 µL/L, and < 5 µL/L, respectively. Tenability criteria were not assessed using the fractional effective dose (FED) approach in the study; however, based on visibility, toxic gas measurements, and HRRs, it was concluded that at most 5 min was available to safely egress the test motorcoach, had there been a fire in the simulated rear engine compartment.

Material Flammability Testing

The intent of this review is to delineate the differences between the various material fire safety test standards. This review focuses on the following test standards: FMVSS 302 [24], Economic Commission for Europe (ECE) Regulation No. 118 [25], Federal Railroad Administration (FRA) 49 CFR Part 238.103 [26], and Federal Aviation Administration (FAA) 14 CFR Part 25.853 [27], also referred to as FAR Part 25.853. The FRA and FAA test standards are included because they evaluate, in addition to flame spread, ignition propensity or resistance, smoke and toxic gas generation, and HRR.

FMVSS 302, as described in 49 CFR Part 571.302, specifies burn resistance requirements for materials used in the occupant compartments of motor vehicles (passenger cars, multipurpose passenger vehicles, trucks, and buses). The materials are seat cushions, seat backs, seat belts, headlining, convertible tops, arm rests, all trim panels, compartment shelves, head restraints, floor coverings, sun visors, curtains, shades, wheel housing covers, engine compartment covers, mattress covers, and any other interior materials including padding and crash-deployed elements (e.g., air bag materials).

FMVSS 302 is a horizontal flame spread test using a Bunsen burner placed underneath the open end of a pre-conditioned test material which is supported by a U-shaped sample holder or frame in a fully-ventilated enclosure with an observation window. As stated, the standard is intended to reduce the deaths and injuries to motor vehicle occupants caused by vehicle fires, originating in the interior of the vehicle from small ignition sources such as matches or cigarettes. The pass/fail test criterion is based on the observed burn rate of the material. A material is considered in compliance if it does not burn, has an observed burn rate of less than 102 mm/min,

or stops burning before 60 s and has not burned more than 51 mm from the start. Several recent studies have suggested that FMVSS 302 is inadequate to accurately assess material fire safety characteristics associated with the interior content of a vehicle. [28, 29, 30]

ECE Regulation No. 118 consists of three tests, a horizontal flame spread test, a material melting behavior test, and a vertical flame spread test. This regulation applies to the burning behavior of interior materials used in vehicles carrying more than 22 passengers, not designed for standing passengers and urban use (e.g., city buses).

The horizontal flame spread test is the European equivalent of FMVSS 302. This test applies to materials used for seat upholstery and accessories, interior roof lining, floor, luggage racks, heating and ventilation pipes, side and rear walls (including separation walls), thermal and/or acoustic functions, and light fittings.

The test apparatus used to determine the melting behavior of materials consists of a stand which anchors a metallic ring on which a grill is placed to support a sample in a horizontal position. An electric radiator with an applied heat flux of 30 kW/m^2 to the exposed sample surface is located 30 mm above the sample. A drip pan filled with cotton wool is placed underneath the sample support to collect melt drip and verify any flaming drop. This test applies to materials used for the interior roof lining, luggage racks, heating and ventilation pipes in the roof, and for lights located in luggage racks and/or the roof. Materials, after being exposed to the prescribed thermal radiation for a pre-determined period, are said to be in compliance if no melt drip is formed which ignites the cotton wool.

The vertical flame spread test only applies to curtains and blinds (and/or other hanging materials). The test involves exposing a pre-conditioned vertical sample to a small gas burner flame and determining the flame spread rate over the test material. The test apparatus consists of a sample holder, a template, a gas burner, an exhaust system to vent combustion products, and cotton threads placed horizontally in front of the test sample at three specified locations as markers to facilitate burn rate measurements. A material is considered to be in compliance if the vertical burn rate is less than 100 mm/min.

Recently, a draft proposal to amend ECE 118 was submitted by the Norwegian and Swedish authorities to improve fire safety in buses. [31] The proposed draft calls for the inclusion of three additional ISO test standards and one European standard: ISO 5658-2 [32] to evaluate lateral flame spread of materials in vertical configurations exposed to thermal radiation, ISO 5659-2 [33] to determine smoke generation and toxicity of smoke gases from a burning material, ISO 9239-1 [34] to assess lateral flame spread of flooring materials in horizontal configurations exposed to thermal radiation, and prCEN/TS 45545-2 [35] to determine burning behavior of seats by measuring their HRRs when exposed to flaming ignition. The draft proposal argues that the most rational way to improve fire safety in buses is to take advantage of the experience from other public transport, like passenger trains and ships which have far more stringent fire safety requirements. The adaptation of existing standards with known satisfactory levels of fire safety to amend ECE 118 will minimize the amount of research needed.

The Federal Railroad Administration (FRA) 49 CFR Part 238.103 describes the test performance criteria for flammability and smoke characteristics of materials used in constructing a passenger car or a cab of a locomotive. The test methods are based on a collection of American Society for Testing and Materials (ASTM International) standards, ASTM C1166 [36], ASTM D3675 [37], ASTM E119 [38], ASTM E162 [40], and ASTM E662 [41], and the vertical test in FAA 14 CFR Part 25.853. Materials, which are tested according to their types and functions using the corresponding test methods, are considered to be in compliance if they meet the performance criteria set forth in the table in Appendix B to Part 238 of the CFR.

The Federal Transit Administration (FTA) and its predecessor, the Urban Mass Transportation Administration, published the recommended fire safety practices for transit bus and van materials in the 1993 Federal Register (vol. 58, No. 201, pp. 54250-54254) and the recommended fire safety practices for rail transit materials in the 1984 Federal Register (vol. 49, No. 158, pp. 32482-32486), respectively. The test procedures listed in the two publications are largely adopted from ASTM standards and are very similar to those described in Appendix B to Part 238 of CFR 49 (FRA).

The Federal Aviation Administration (FAA) 14 CFR Part 25.853 describes test procedures and performance criteria for materials used in the interior compartments of passenger airplanes. Depending on the type and function of a material, the regulation requires a variety of fire tests to be performed which may include vertical burn test, horizontal burn test, HRR measurement, smoke emission test, and/or seat cushion burn test. Detailed descriptions of the test apparatus and procedures can be found in FAA Aircraft Materials Fire Test Handbook. [41] It appears that the recent proposed amendment to ECE 118, as discussed above, closely follows the fire safety practices for materials used in airplane interior compartments.

FLAMMABILITY TESTING OF ACTUAL MOTORCOACH MATERIALS

Overview

In order to evaluate how typical motorcoach interior materials contribute to a passenger compartment fire, flammability testing was applied to a set of materials taken from used motorcoaches. Since the list of materials used in the passenger compartment of a motorcoach is extensive, the selection of materials for testing was carefully made and prioritized based on the estimated fire load a particular material might contribute due to its mass and location.

Representative interior materials were selected from seat, wall, and ceiling constructions for fire tests since these materials constitute the bulk of the contents in the interior compartment. The materials were obtained from two Motor Coach Industries (MCI) E-series motorcoaches (2000 model year) except for the parcel rack doors which were from 2003 to 2009 J-series models. Since a very limited sample of motorcoach models was surveyed, the flammability test results only provide a small sampling of how some typical motorcoach components perform. While the results cannot be assumed to reflect how similar components on all other motorcoach models would perform, the components tested are representative of those used by other manufacturers so the results are expected to be typical as well.

Table 1 lists the materials that were tested with appropriate fire tests chosen from these regulations: FMVSS 302, ECE 118, FRA 49 CFR Part 238.103, and FAA 14 CFR Part 25.853. New vehicles manufactured since 1972 already have to meet the FMVSS 302 standard, but the selected materials were subjected to that test to verify compliance. From the other standards, a test procedure was considered appropriate for a motorcoach material when the corresponding material for the same function (e.g. seat), but different application (i.e. train or airplane versus bus) would be subject to that test under the regulations for trains or airplanes. Table 2 provides more detailed descriptions of the standard tests including the titles, regulation sources, and failure or acceptance criteria.

Table 1 Material selection and appropriate flammability tests.

Material	Regulations and Relevant Tests			
	FMVSS 302	ECE 118	FAA 14 CFR Part 25.853 (also called FAR Part 25.853)	FRA 49 CFR Part 238.103
Seat bottom and back cushion	Horizontal spread	Horizontal spread; drip test	Horizontal and vertical burn tests; heat release rate; smoke tests; seat cushion test	ASTM D3675; ASTM E662
Wall trim panel	Horizontal spread	Horizontal spread; drip test	Horizontal and vertical burn tests; heat release rate; smoke tests	ASTM E162; ASTM E662
Parcel rack door (MCI J-series coach)	Horizontal spread	Horizontal spread; drip test	Horizontal and vertical burn tests; heat release rate; smoke tests	ASTM E162; ASTM E662
Back of seat back	Horizontal spread	Horizontal spread; drip test	Horizontal and vertical burn tests; heat release rate; smoke tests	ASTM E648; ASTM E662

Table 2 Flammability test descriptions.

Short Title	Official Title, Source	Failure or Acceptance Criteria
FMVSS302	Flammability of Materials Used in the Interior of Motor Vehicle Occupant Compartments, 49 CFR Part 571.302	burn rate > 102 mm/min for any specimen
ECE/324 No. 118	Uniform technical prescriptions concerning the burning behaviour of materials used in the interior construction of certain categories of motor vehicle, E/ECE/324 and E/ECE/TRANS 505 Addendum 117: Regulation No. 118	falling drips observed (whether flaming or not), and cotton wool beneath specimen ignites
FAA Heat Release	Test Method to Determine the Heat Release Rate from Cabin Materials Exposed to Radiant heat, FAR Part 25, Appendix F, Part IV, FAR 25.853(d)	2 min: 65 kW/m ² pk, 65 kW min/m ² avg.
ASTM E662 Smoke Density	Standard Test Method for Specific Optical Density of Smoke Generated by Solid Materials (NFPA Designation No. 258), FRA/FTA 49 CFR Part 238.103 Appendix B	¹ D _s (1.5)<100, D _s (4)<200, no flaming or running
ASTM E162 Radiant Panel	Standard Test Method for Surface Flammability of Materials Using a Radiant Heat Energy Source, FRA/FTA 49 CFR Part 238.103 Appendix B	² I _s <35, no flaming or running
FAA Vertical Test (12 s)	FAA Vertical Test (12 s flame application), FAR Part 25, Appendix F, Part I(b) (4)	15 s max avg. afterflame, 5 s max avg. drip burn, 20 cm (8") max avg. burn length
FAA Vertical Test (60 s)	FAA Vertical Test (60 s flame application), FAR Part 25, Appendix F, Part I(b) (4)	15 s max avg. afterflame, 3 s max avg. drip burn, 15 cm (6") max avg. burn length
ASTM D3675 Radiant Panel for Cellular Materials	Standard Test Method for Surface Flammability of Flexible Cellular Materials Using a Radiant Heat Energy Source, FRA/FTA 49 CFR Part 238.103 Appendix B	I _s <25, no flaming or running (test may not apply to surface fabric)
ASTM D3675 Radiant Panel for Cellular Materials	Standard Test Method for Surface Flammability of Flexible Cellular Materials Using a Radiant Heat Energy Source, FRA/FTA 49 CFR Part 238.103 Appendix B	I _s <25, no flaming or running
FAA Heat Release	Test Method to Determine the Heat Release Rate from Cabin Materials Exposed to Radiant heat, FAR Part 25, Appendix F, Part IV, FAR 25.853(d)	max avg. peak HRR 65 kW/m ² , max avg. total HRR 65 kW min/m ²
FAA Seat Cushion Flammability	FAA Flammability of Seat Cushions, FAR Part 25, Appendix F, Part II	10 % max avg. weight loss, max 1 specimen which may exceed 10 %, max 1 specimens that may exceed 43 cm (17") surface char length

¹ In the testing tables, D_s is the specific optical density. See the LIST OF ABBREVIATIONS for a full definition.

² In the testing tables, I_s is the flame spread index. See the LIST OF ABBREVIATIONS for a full definition.

Short Title	Official Title, Source	Failure or Acceptance Criteria
FAA Seat Cushion Flammability	FAA Flammability of Seat Cushions, FAR Part 25, Appendix F, Part II	10 % max avg. weight loss, max 1 specimen which may exceed 10 %, max 1 specimens that may exceed 43 cm (17") surface char length

Test Results

This section provides tables for each motorcoach interior component tested. The tables include the flammability test title, failure or acceptance criteria, and the performance of the component for each test. In reviewing the results, consider that current federal regulations only require compliance of these motorcoach interior materials with FMVSS 302 and that they were not designed for compliance with the additional tests. In the tables, green shaded sections indicate compliance while red shaded sections and red performance values indicate non-compliance.

Table 3 shows the results for the parcel rack door testing. The door passed the FMVSS 302 horizontal burning test and the European equivalent. The door failed the FAA heat release test, ASTM E662 smoke density test, and ASTM E162 radiant panel test. Based on these results, the parcel rack door would not pass FRA or FAA flammability requirements.

Table 3 Parcel rack door flammability test results

Short Title	Failure or Acceptance Criteria	Parcel Rack Doors (J-series) Performance
FMVSS302	burn rate > 102 mm/min for any specimen	<u>Pass</u> , max burn rate 23 mm/min
ECE/324 No. 118	falling drips observed (whether flaming or not), and cotton wool beneath specimen ignites	No, No (<u>complies</u>)
FAA Heat Release	2 min: 65 kW/m ² pk, 65 kW min/m ² avg.	<u>Does not comply</u> : 20 s, 352 kW/m ² avg. pk (<u>fail</u>), 342 kW min/m ² avg. (<u>fail</u>)
ASTM E662 Smoke Density	D _s (1.5)<100, D _s (4)<200, no flaming or running	<u>Fail</u> : 90 s D _s avg. 286 (flaming mode) avg. 5 (non flaming mode) <u>Fail</u> : 4 min D _s avg. 871 (flam), avg. 117 (non flam) w/in 20 min D _s avg. 871 (flam), avg. 428 (non flam) <u>Pass</u> : No flaming, dripping, or flaming running
ASTM E162 Radiant Panel	I _s <35, no flaming or running	<u>Fail</u> : I _s avg. 450.5 , no flaming, dripping, flaming running, 38 cm (15") flame front length (max avail), sustained flame front ignition at 10 s, still burning at end of test 38 cm (15") (4:41-5:15)

Table 4 shows the results for the seat bottom and backrest (front) testing. These parts of the seats passed the FMVSS 302 horizontal burning test and the European equivalent. The seat

failed every other test performed and failed most of them significantly. Based on these results, these seat components would not pass FRA or FAA flammability requirements.

Table 4 Seat cushion flammability test results

Short Title	Failure or Acceptance Criteria	Seat Bottom & Backrest Performance
FMVSS302	burn rate > 102 mm/min for any specimen	Pass, max burn rate 25 mm/min
ECE/324 No. 118	falling drips observed (whether flaming or not), and cotton wool beneath specimen ignites	No, No (complies)
ASTM E662 Smoke Density	D _s (1.5)<100, D _s (4)<200, no flaming or running	Fail: 90 s D _s avg. 110 (flaming mode), avg. 82 (non flaming mode) Fail: 4 min D _s avg. 138 (flam) avg. 334 (non flam) w/in 20 min D _s max avg. 132 (flam), avg. 316 (non flam) Pass: No flaming, dripping, or flaming running
FAA Vertical Test (12 s)	15 s max avg. afterflame, 5 s max avg. drip burn, 20 cm (8") max avg. burn length	Does not comply: 30+ s (fail), 0 s (pass), 30 cm (12") (fail)
FAA Vertical Test (60 s)	15 s max avg. afterflame, 3 s max avg. drip burn, 15 cm (6") max avg. burn length	Does not comply: 30+ s (fail), 0 s (pass), 30 cm (12") (fail)
ASTM D3675 Radiant Panel for Cellular Materials	I _s <25, no flaming or running (cover fabric tested, test may not apply)	Fail: avg. I _s 136.1 Pass: no flaming dripping or flaming running, no non-sustained flame front off gas ignition, sustained flame front ignition at 8 s avg., all flaming out range 4:55 (still burning but ran out of material) to 6:10, test end 4:55 to 7:49, no drip flame on test floor
ASTM D3675 Radiant Panel for Cellular Materials	I _s <25, no flaming or running	Fail: avg. I _s 1177.4 Fail: yes flaming dripping or flaming running, yes non-sustained flame front off gas ignition, sustained flame front ignition at 1 s avg., all still burning at test end, test end 0:35 to 0:44, yes drip flame on test floor
FAA Heat Release	max avg. peak HRR 65 kW/m ² , max avg. total HRR 65 kW min/m ²	Does not comply: 182 kW/m ² (fail), 120 kW min/m ² (fail)
FAA Seat Cushion Flammability	10 % max avg. weight loss, max 1 specimen which may exceed 10 %, max 1 specimens that may exceed 43 cm (17") surface char length	Does not comply: 15.4 % avg. weight loss for 3 specimens (20.1 lb frame weight included in starting weight of 26.3 lbs). 46 cm (18") char length (flame consumed material).

Short Title	Failure or Acceptance Criteria	Seat Bottom & Backrest Performance
FAA Seat Cushion Flammability	10 % max avg. weight loss, max 1 specimen which may exceed 10 %, max 1 specimens that may exceed 43 cm (17") surface char length	Does not comply: 66.1 % avg. weight loss for 3 specimens (frame weight not included, starting weight 6.2 lbs). 46 cm (18") char length (flame consumed material).

Table 5 shows the results for the interior wall panel testing. The panel passed the FMVSS 302 horizontal burning test and the European equivalent. The panel also passed the ASTM E662 smoke density test and two FAA vertical tests. The panel failed the ASTM E162 radiant panel test. Based on these results, the interior wall panel would pass the FAA flammability requirements, but would fail those for the FRA.

Table 5 Interior wall panel flammability test results

Short Title	Failure or Acceptance Criteria	Interior Wall Panel Performance
FMVSS302	burn rate > 102 mm/min for any specimen	Pass, max burn rate 0 mm/min, self-extinguishing
ECE/324 No. 118	falling drips observed (whether flaming or not), and cotton wool beneath specimen ignites	No, No (complies)
ASTM E662 Smoke Density	D _s (1.5)<100, D _s (4)<200, no flaming or running	Pass: 90 s D _s avg. 1 (flaming mode) avg. 1 (non flaming mode) Pass: 4 min D _s avg. 36 (flam) avg. 6 (non flam) w/in 20 min D _s max avg. 164 (flam) avg. 165 (non flam) Pass: No flaming, dripping, or flaming running
ASTM E162 Radiant Panel	I _s <35, no flaming or running	Fail: I _s avg. 81.8 Fail: yes flaming, dripping, flaming running, 38 cm (15") flame front length (max avail), sustained flame front ignition at 2.5 s, still burning at end of test 38 cm (15") (2:20-4:21), yes drips flame on test floor
FAA Vertical Test (12 s)	15 s max avg. afterflame, 5 s max avg. drip burn, 20 cm (8") max avg. burn length	Complies: 0 s (pass), 0 s (pass), 5.3 cm (2.1") (pass)
FAA Vertical Test (60 s)	15 s max avg. afterflame, 3 s max avg. drip burn, 15 cm (6") max avg. burn length	Complies: 0 s (pass), 0 s (pass), 7.4 cm (2.9") (pass)

Table 6 shows the results for the rear side of the seat back. The seat back rear failed the FMVSS 302 horizontal burning test by having a burning rate which was about 25 % higher than allowed. The seat back rear passed the ASTM E662 smoke density test and passed the FAA heat release test by staying about 20 % below the failure criteria. The seat back rear failed the FAA vertical tests and ASTM D3675 radiant panel test for foam. Based on these results, the seat back rear would fail current flammability requirements for motorcoaches and would also fail the FRA and FAA flammability requirements.

Four motorcoach interior materials (interior wall panels, parcel rack doors, seat fronts, and seat backs) were tested using FMVSS 302, FAA, and FRA flammability tests. Of the four materials tested using FMVSS 302, the currently required flammability test, only the back of the seat backrest failed by exceeding the horizontal burn rate criteria by 25 %. The fact that this was a ten year old, used seat could have had some impact on its performance. Of the four components tested under the FAA flammability requirements (standards not required for motorcoach materials), only the interior wall panel passed. All four components failed the FRA flammability requirements (also not required for motorcoach materials). The degree to which the failure criteria were exceeded in the tests failed by the seat components and the parcel rack door indicate that these motorcoach interior materials burn significantly more easily than comparable components approved for use in aircraft and railcars.

Table 6 Seat back rear flammability test results

Short Title	Failure or Acceptance Criteria	Seat Back Rear Performance
FMVSS302	burn rate > 102 mm/min for any specimen	<u>Fail</u> : max burn rate 127 mm/min
ECE/324 No. 118	falling drips observed (whether flaming or not), and cotton wool beneath specimen ignites	Yes/No (<u>complies</u>)
ASTM E662 Smoke Density	D _s (1.5)<100, D _s (4)<200, no flaming or running	<u>Pass</u> : 90 s D _s avg. 24 (flaming mode) avg. 1 (non flaming mode) <u>Pass</u> : 4 min D _s avg. 30 (flam) avg. 3 (non flam) w/in 20 min D _s max avg. 50 (flam) avg. 46 (non flam) <u>Pass</u> : No flaming, dripping, or flaming running
FAA Vertical Test (12 s)	15 s max avg. afterflame, 5 s max avg. drip burn, 20 cm (8") max avg. burn length	<u>Does not comply</u> : 30+ s (fail), 6.2 s (fail, other dir 3.6 s), 29 cm (11.6") (fail)
FAA Vertical Test (60 s)	15 s max avg. afterflame, 3 s max avg. drip burn, 15 cm (6") max avg. burn length	<u>Does not comply</u> : 26.6 s (fail), 2.4 s (pass), 29 cm (11.4") (fail)
ASTM D3675 Radiant Panel for Cellular Materials	I _s <25, no flaming or running (test may not apply to surface fabric)	<u>Fail</u> : avg. I _s 43.2 <u>Fail</u> : yes flaming dripping or flaming running, no non-sustained flame front off gas ignition, sustained flame front ignition at 2 s avg., all flaming out range 01:00 to SB (still burning but ran out material), test end 1:55 to 3:22, yes drip flame on test floor
ASTM D3675 Radiant Panel for Cellular Materials	I _s <25, no flaming or running	<u>Fail</u> : avg. flame spread index 2855 <u>Fail</u> : yes flaming dripping or flaming running, 2 yes/2 no non-sustained flame front off gas ignition, sustained flame front ignition at 1 s avg., all still burning at test end, test end 0:30 to 0:36, yes drip flame on test floor
FAA Heat Release	max avg. peak HRR 65 kW/m ² , max avg. total HRR 65 kW min/m ²	<u>Complies</u> : 52.57 kW/m ² (<u>pass</u>), 49.6 kW min/m ² (<u>pass</u>)

EXPERIMENTAL SET-UP

Experimental Preparation

This section describes the preparation and modifications to the motorcoach required for the test series. The test matrix is listed in Table 7.

Table 7 Test matrix

Test No.	Date	Experimental Focus	Axle of Heated Wheel
1	3/25/09	Passenger compartment penetration	Tag
2	3/27/09	Passenger compartment penetration	Drive
3	11/2/09	Fire-hardening, metal exterior	Tag
4	11/5/09	Fire-hardening, intumescent coating	Tag
5	11/10/09	Fire-hardening, flame deflector	Tag
6	11/19/09	Passenger compartment tenability	Tag

Obtaining the Motorcoach

The motorcoach used for these experiments was a 2000 Motorcoach Industries model 102EL3 which is the same model as the one which burned near Wilmer, TX, during the Hurricane Rita evacuation. [1] This model has a capacity of 55 passengers, includes a lavatory, has a mass of approximately 17 000 kg (38 000 lb) empty, and has a length of 13.92 m (45.7 ft), width of 2.59 m (8.5 ft), and height of 3.59 m (11.77 ft). Prior to these experiments, the motorcoach had been used in a front-end crash test in Ohio. Damage to the rear half of the motorcoach was minor and expected to have negligible effect on the tire fire experiments. A specialist at cutting motorcoaches cut the motorcoach approximately in half using multiple types of saws. Undamaged or intact components from the crashed front of the motorcoach, such as exterior glass reinforced plastic (GRP) panels, windows, seats, luggage racks, and trim panels, were salvaged and secured in the rear of the bus. The bus was transported to the Large Fire Laboratory (LFL) at the NIST campus in Maryland, where a large fork lift was used to unload and park the motorcoach. Figure 1 is a drawing which shows the rear half of the motorcoach with labels and dimensions of the most important components. Expanded uncertainties on the measured dimensions are estimated to be $\pm 0.3\%$. The width of the interior floor (not shown) was 2.44 m.

Moving and Securing the Motorcoach

A large forklift was used to transfer the motorcoach to the high-bay experimental area in the LFL with the steering assistance of another forklift. The larger forklift generally pushed the motorcoach from the rear to prevent it from dragging on the ground. The motorcoach was able to roll on its own six tires. Once the test section was safely transported to the designated anchoring area underneath the hood, it was secured with the undercarriage approximately 30 cm above the floor (above protective gypsum panels) on wooden cribbing [multiple 15 cm (6 in) by 15 cm (6 in) timber beams and smaller pieces of wood]. Figure 2 is a photograph of some of the cribbing used to support the motorcoach during testing. The lifting and securing was accomplished with jacks and jack stands.

Straightening Window Posts

During the crash test, the roof was pushed backward between 7 cm and 10 cm. The window posts were angled back with the tops behind the bottoms which created non-rectangular window openings preventing window closure. To straighten the posts and maintain the latching mechanisms in the centers of the window openings, the tops of the posts were cut completely and the bottoms were notched on 3 sides to enable the top to be bent towards the front. In the new vertical positions, the posts were reattached to the roof with self tapping screws. Figure 3 shows photographs of the cutting operation, notched post, and reattachment.

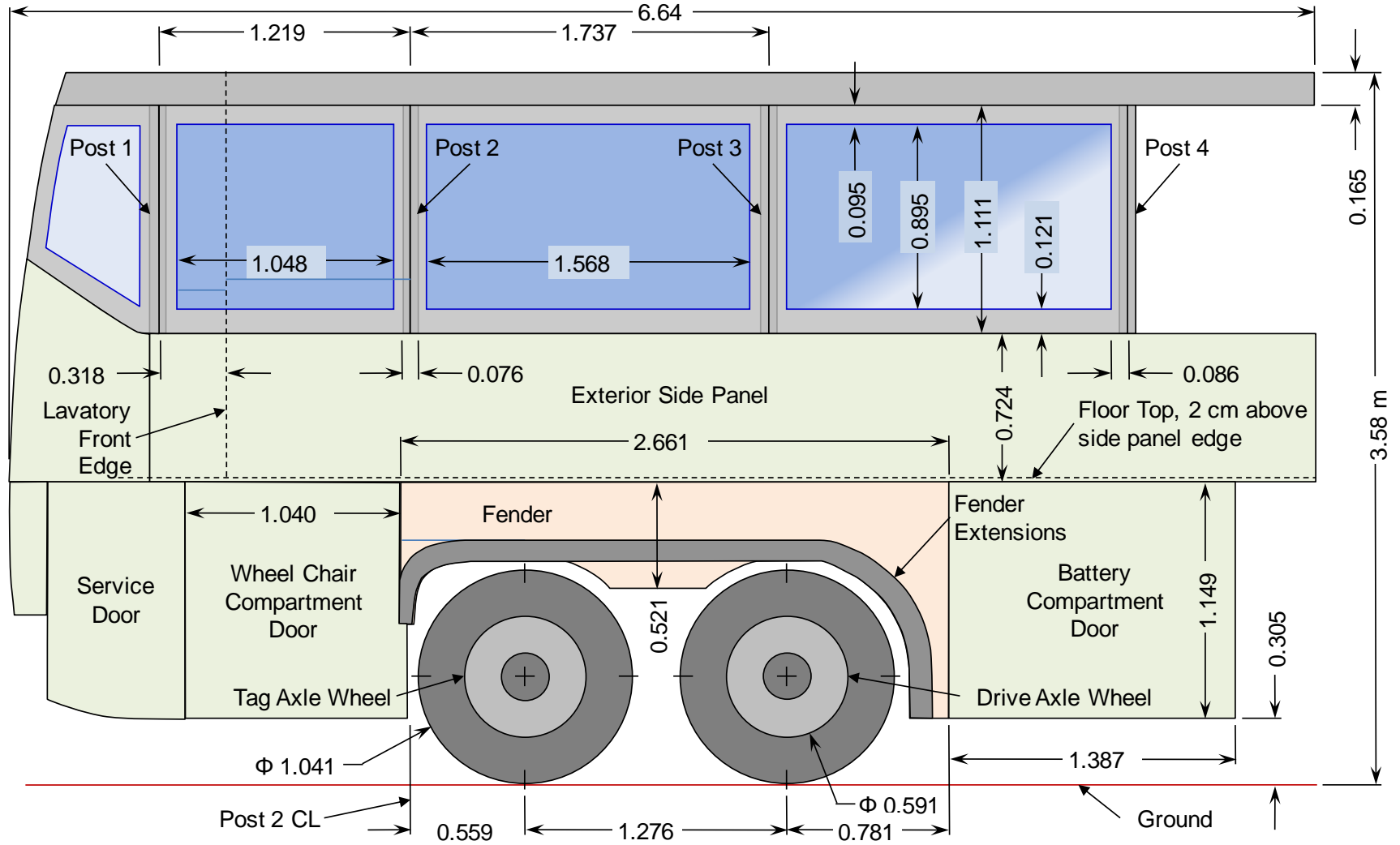


Figure 1 A drawing of the motorcoach rear half which was used for tire fire experiments. Dimensions are in meters. Distance measurement uncertainty is $\pm 0.3\%$.



Figure 2 A photograph of the cribbing supporting the motorcoach during testing.



Figure 3 Window post straightening operation. The top photograph shows the original angle of a bent post. The bottom right photograph shows the notch at the bottom of the post. The bottom left photograph shows the angle bracket with self-tapping screws which reattached the roof to the post.

Removing Unsafe Materials

For safety reasons, motorcoach components that might prove dangerous during the fire experiments were removed or made safe. The tires were deflated, and then 1.3 cm (0.5 in) holes were drilled in their sidewalls so they could not burst under pressure. The coach was supported by the cribbing under the frame and axles and not by the tires during testing. The batteries and the fuel tank were removed. Pressurized air and nitrogen tanks for the pneumatic and other systems were removed or punctured. Coolant, transmission, hydraulic, and brake fluids were drained from their systems.

Replacement Components

For the second and subsequent experiments, fire damaged parts of the motorcoach were replaced. Wheels [aluminum, 57 cm (22.5 in) diameter by 23 cm (9.00 in) wide], tires (315/80R22.5), and long side windows were replaced with non-fire-exposed components. For the second experiment, the exterior side panel was replaced with the front right portion salvaged from the front of the motorcoach. For later experiments, panel sections were salvaged from another motorcoach used in a roll over crash test. As needed, replacement windows and new fender and fender trim were purchased from the manufacturer. Installation of the fender and exterior panel generally followed the maintenance manual for the motorcoach and used comparable off-the-shelf sealants and fasteners.

Tires from different manufacturers were assumed to have similar burning characteristics, and differences between them were not a focus of this study. The tire brands and models used in these experiments were: Goodyear G409 MBA, Michelin XZA2 Energy, Hercules S-203, and Firestone FS400. All of the tires weighed (unmounted, new) within 0.4 kg of 66.3 kg. Their official dimension variations were also narrow: 107.4 cm \pm 1.4 cm (42.3 in \pm 0.6 in) inflated OD and 31.5 cm \pm 0.7 cm (12.4 in \pm 0.3 in) for the inflated width. All of the tires were used and had unknown age and mileage.

Burner

A special burner was designed and built that would focus substantial heat, (up to 100 kW) on the metal of a motorcoach wheel without the flames or exhaust gases impinging on the rubber. The purpose of this design was to cause the rubber to ignite just from heat conduction with hot metal, which qualitatively simulates the frictional heat generated from failed axle bearings, locked brakes, or dragged blown tires.

The design of the burner was a 25 mm OD stainless steel (type 304) tube bent into a 30.5 cm circle with ten high output heating torch nozzles attached perpendicular to the plane of the circle. Figure 4 shows a schematic of this design. The torch tips were brass National Torch model N-6 which has a 3.49 cm (1 3/8 in) OD and 0.99 mm (0.39 in) diameter center hole. A Belchfire Corporation model 4F assembly of valves and a mixing chamber for the natural gas and high-pressure air was attached to the circular tube. The flames were meant to be pre-mixed so nearly all of the heat was efficiently generated at the flames. Flame arresting torch tips were used. The

burner was designed with the requirement of a heat output between 50 kW and 100 kW based on a calculation using an estimate of the total mass of the wheel and associated metal and a target heating duration between 30 min and 1 h.

The burner was mounted on a long, wheeled cart to enable positioning of the flame tips and fast removal of the burner after tire ignition. A tire shield was fabricated and placed between the wheel and tire to prevent direct heating of the tire by burner flames and gases. For the second test, a calcium silicate blanket was placed on top of the shield for additional insulation to minimize radiation and convection from the shield to the tire. Figure 5 shows photographs of the burner and shield.

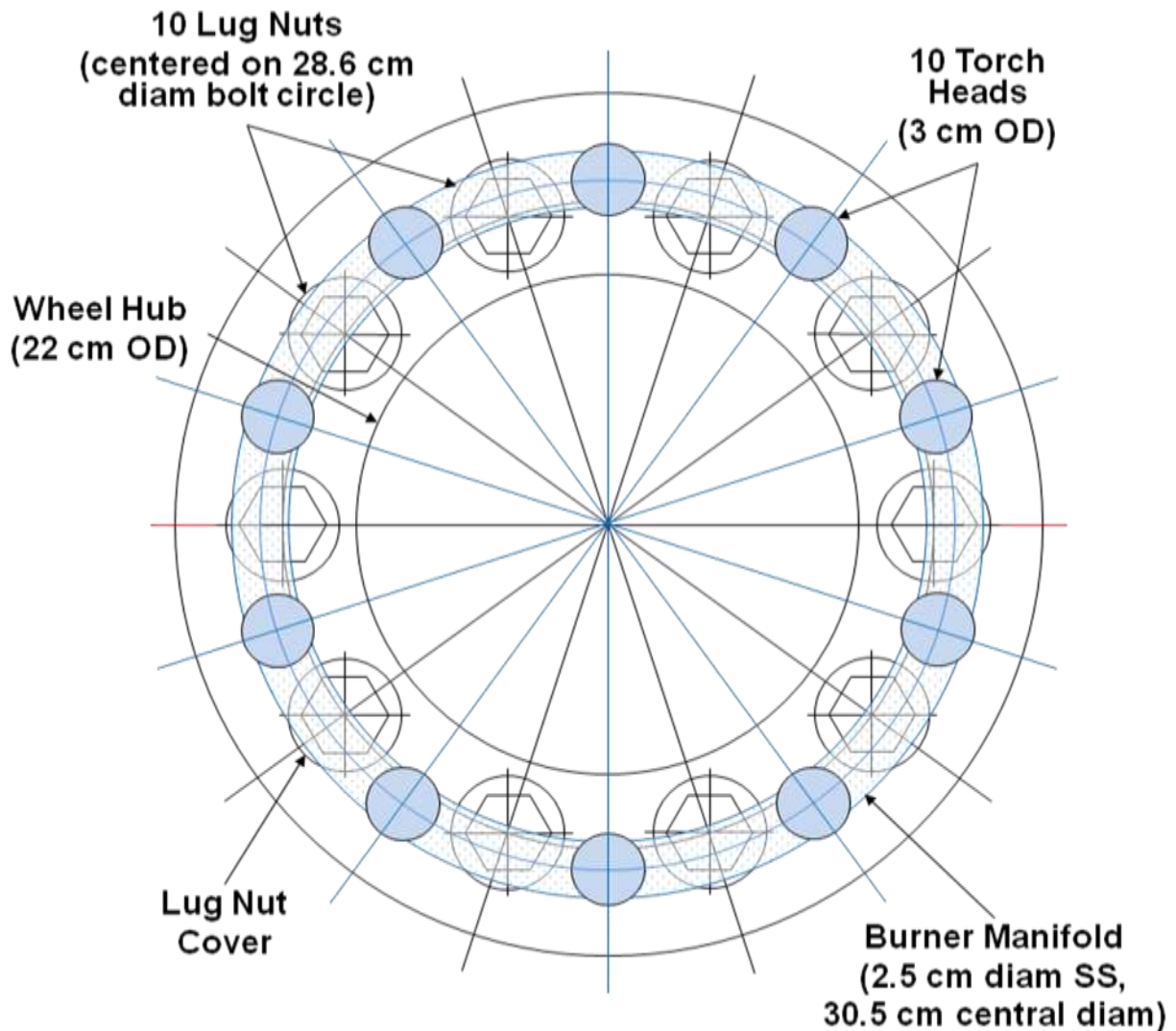


Figure 4 A schematic of the wheel burner design showing the relative locations of the 10 torch heads and manifold compared to the wheel's hub, lug nuts, and lug nut covers. The outer circle represents the wheel's curvature away from the lug nut surface plane.



Figure 5 The burner for heating the wheels. The top photograph shows the whole assembly including the burner ring, wheeled cart, and gas and air valves. The bottom right photograph shows the pre-mixed natural gas and air torches impinging on a tag axle wheel. The bottom left photograph shows the tire shield nested inside a drive axle wheel rim with an insulating cover to minimize convective and radiative heating to the tire from the shield.

Modifications for Fire-hardening Experiments

Three methods of fire-hardening, to limit penetration of the passenger compartment by tire fires, were explored: replacing combustible exterior with steel, covering combustible exterior with intumescent coating, and adding a flame deflector. The first method involved removing material which acts as fuel during a tire fire by replacing the external GRP exterior side panel below the windows and the fender with sheet metal. The type of sheet metal used for the side panel and fender was 22 gauge (0.79 mm or 1/32 in thick) type 304 stainless steel. Three sections of 0.724 m wide stainless steel sheet were required for the panel. The sections of steel had varied lengths and overlapped by about 5 cm for a total combined length of about 5.8 m (19 ft). The fender was made from two pieces of steel and was cut to match the outline of an OEM fender. A diagram and a photograph of the motorcoach with both the stainless steel panel and fender are shown in Figure 6 and Figure 7, respectively.

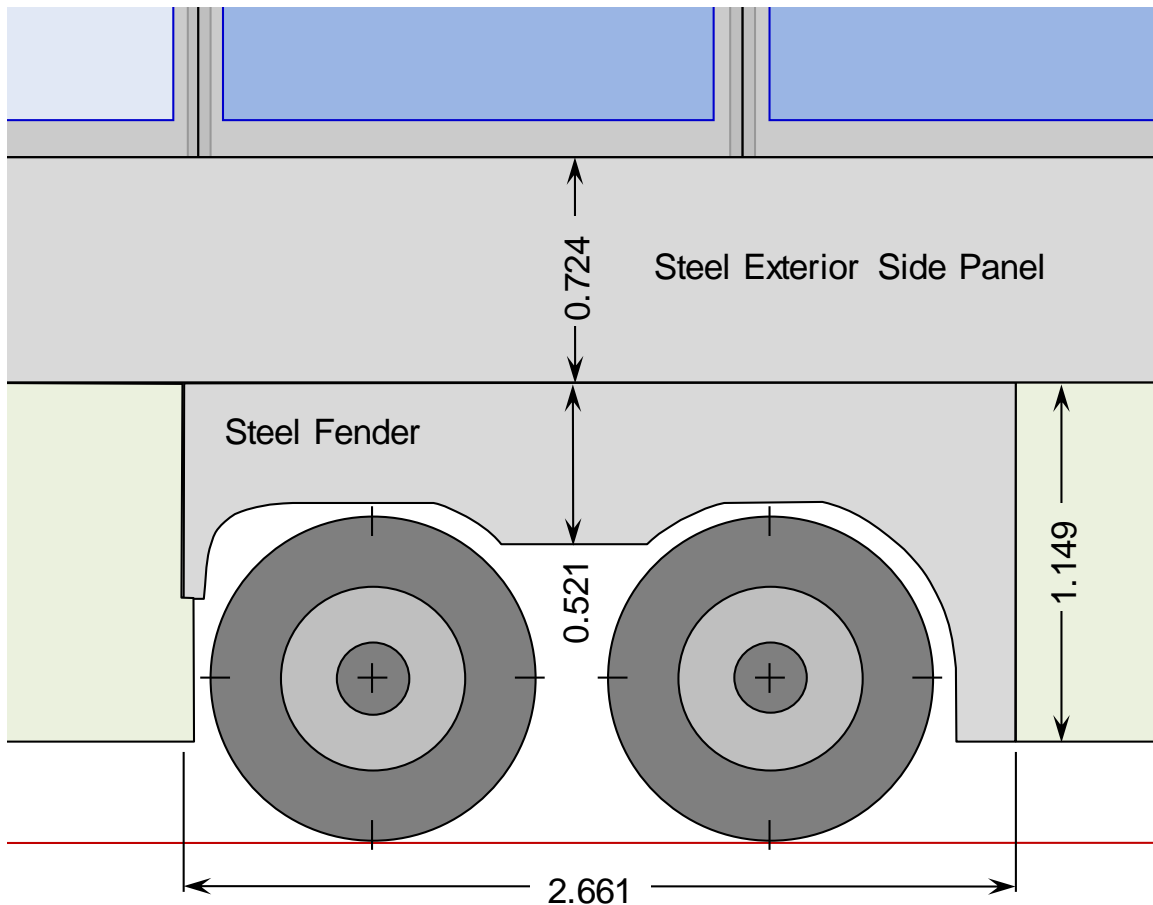


Figure 6 A diagram of the right side of the motorcoach for the fire-hardening experiment using stainless steel sheet in place of the fender and exterior side panel. Dimensions are in meters.



Figure 7 A photograph of the fender and exterior side panel replaced with sheet metal.

The second fire-hardening method was to cover the motorcoach exterior above the tires with an intumescent coating which put a physical barrier between the combustible materials and the tire fire plume. An intumescent coating is a polymer that swells and creates a char barrier to heat and mass transfer when heated by flame. An effective char barrier can limit pyrolysis of the combustible material underneath and prevent fuel vapors that are generated from escaping and burning. A used exterior GRP panel and used fender were shipped to PPG Industries Protective & Marine Coatings for application of the coating. The particular coating, PITT-CHAR XP[®], is designed for marine applications. The manufacturer describes the coating as an epoxy which is weather and abrasion resistant. A diagram of the motorcoach with the coated panel and fender is shown in Figure 8 and a photograph is shown in Figure 9.

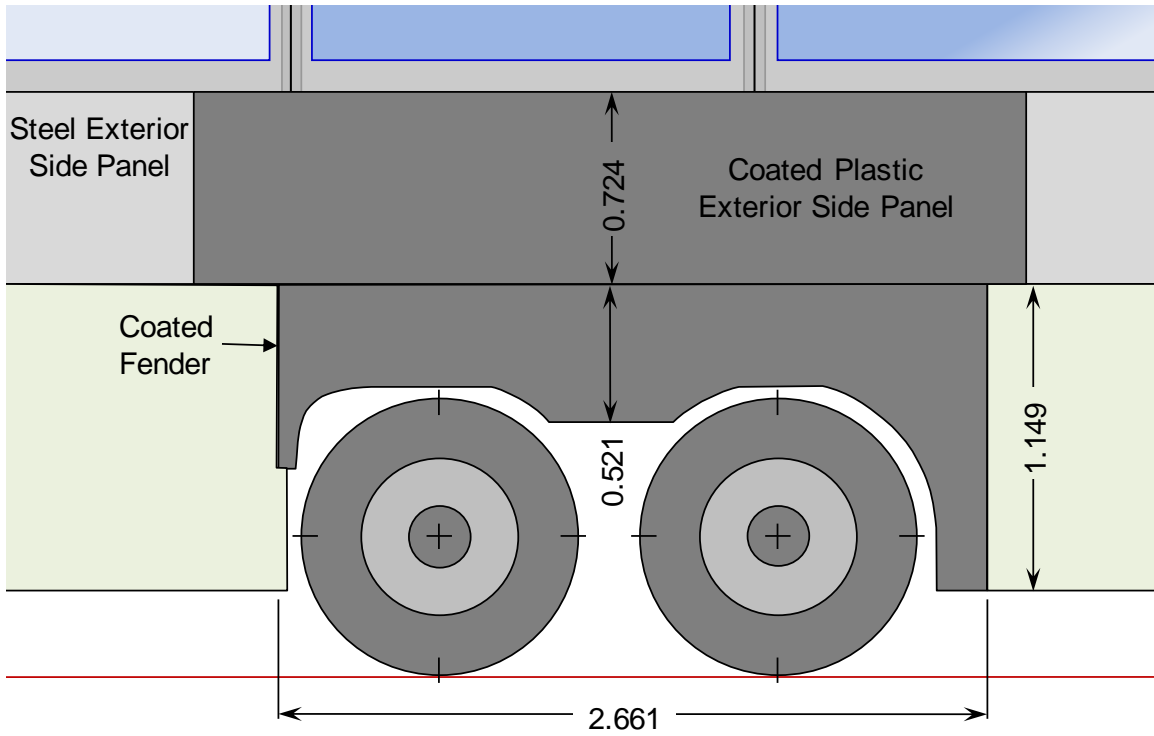


Figure 8 A diagram of the right side of the motorcoach showing the exterior side panel and fender coated with an intumescent coating. Dimensions are in meters.



Figure 9 A photograph of the fender and exterior side panel with an intumescent coating.

The third fire-hardening method consisted of a deflector shield located above the fender and below the exterior side panel. The deflector was designed to deflect the fire plume away from side of the motorcoach sufficiently to impede flame spread to the exterior side panel and thus delay or prevent window breakage. The shield was 22 gauge (0.79 mm or 1/32 in thick) type 304 stainless steel. The deflector protruded from the side of the motorcoach at a 45° angle above horizontal. The deflector was 15 cm wide with an additional 2 cm inserted in the channel that holds the exterior side panel. The deflector was about 3.5 m (11.5 ft) long and extended about 17 cm (6.5 in) in front of the fender and 68 cm (27 in) behind the fender. A diagram of the motorcoach with the deflector between the panel and fender is shown in Figure 10 and the corresponding photograph is shown in Figure 11. Application of the Fire Dynamics Simulator (FDS) [23] software was used to estimate the effect of such a shield on the tire fire plume. While wider designs had slightly larger effects on the average plume temperatures near the windows, we chose the 15 cm width due to the combination of its plume temperature impact and less protruding profile.

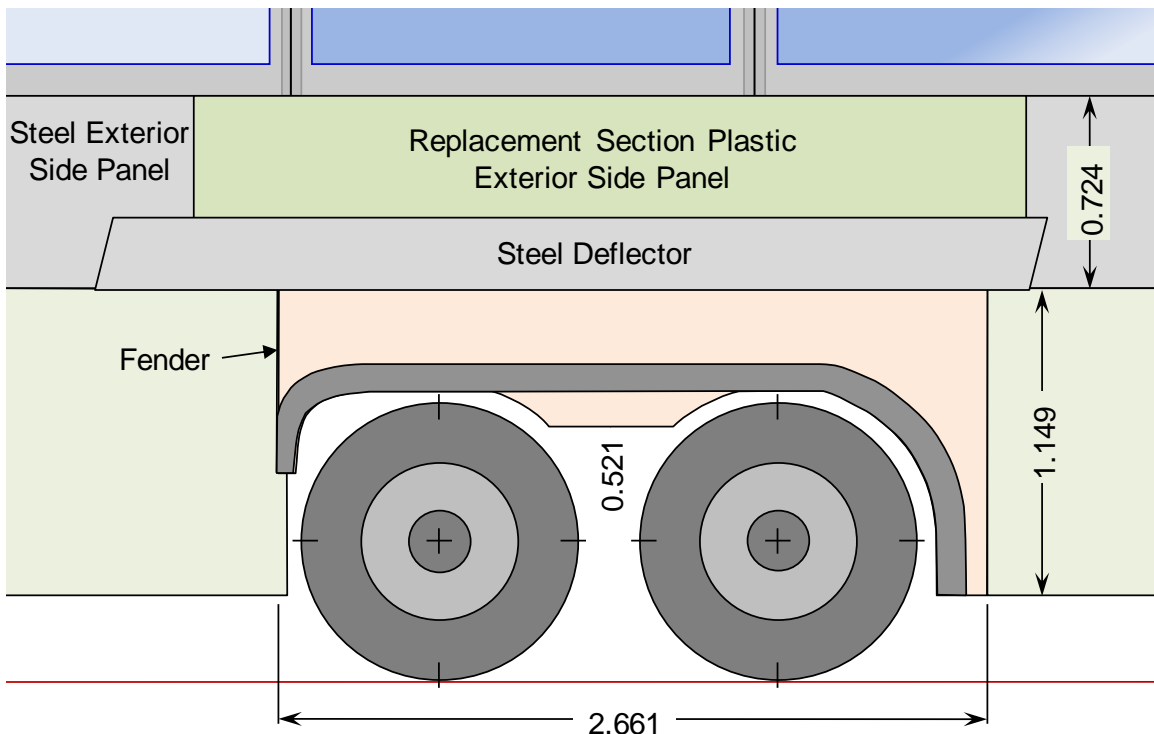


Figure 10 A diagram of the right side of the motorcoach showing the steel deflector between the fender and exterior side panel. Dimensions are in meters.



Figure 11 Photographs of the deflector installed between the fender and exterior side panel. The left photo shows a view of the side of the motorcoach. The right photo shows an end view from the rear.

Modifications for the Tenability Experiment

For the tenability experiment, a complete interior motorcoach volume was necessary in order to provide realistic results for temperatures, heat fluxes, toxic gas volume fractions, and the time for the passenger compartment to reach dangerous thresholds for each of these hazards. A motorcoach front half was constructed to complement the original rear and make a whole interior volume with similar dimensions to an E-series model coach.

The constructed front of the motorcoach consisted of a wood frame structure supporting a plywood deck upon which a steel stud frame was built and to which a galvanized steel interior skin was attached. A photograph taken part way through the construction process is shown in Figure 12. The wood used for the support framing was 38 mm × 89 mm (nominal 2 in × 4 in) boards. The boards were nailed with 8.3 cm (3 ¼ in) long, 3.3 mm (0.131 in) diameter, 30° smooth shank Paslode framing nails. The wood framing used 41 cm (16 in) centers spacing. The plywood was 16 mm (5/8 in) thick tongue and groove subflooring. The metal framing studs were made of galvanized steel. The interior steel skin for the sides, roof, and front cap was 26 gauge (0.55 mm or 0.022 in thick) galvanized sheet steel. The steel components were all attached using 11 mm (7/16 in) long, semi-flat head, self tapping screws. Photographs of the added front with part of the rear, the front end, and the doorway area are shown in Figure 13. The front end cap had access holes cut into it for a glass observation window and visibility camera access. The right side wall of the extension was constructed with a 5° slant in at the top to match the slant of the rear of the original motorcoach which was caused by the front end crash test. The slant was such that the interior width across the extension was about 8.6 cm (3.4 in) less at the top than at the extension floor.



Figure 12 Two photographs of the motorcoach front extension construction showing the beginning of the attachment of the galvanized sheet steel to the metal studding on the wooden substructure.



Figure 13 Photographs of the motorcoach extension. The top photo shows most of the assembly of the original motorcoach rear half and added front extension. The bottom left photo shows the extension doorway and steps. The bottom right photo shows the front end with the window and visibility camera.

The doorway was sized to approximately match that of an MCI E-series coach. Its dimensions were 2.27 m (89.5 in) high by 0.81 m (32 in) wide. The doorway and stairs were located 31.8 cm (12.5 in) from the inside front wall of the constructed end of the motorcoach. Stairs were built to allow easy access for instrumenting the interior and also to approximate the footprint of the original stairwell, but not the spiral design used in a real E-series motorcoach.

Treads were constructed with 38 mm × 140 mm (nominal 2 in × 6 in) boards. The lowest step was about 35 cm (14 in) above the test bay floor with 56 % of its horizontal depth within the walls of the motorcoach. The five steps had average vertical rises of 22.1 cm (8.7 in) and horizontal runs of 24.3 cm (9.6 in) and extended into the interior floor by 1.21 m (4 ft). The sides of the steps were enclosed with plywood since they were within the plane of the side of the motorcoach. Railings were added for safety.

For the tenability experiment, it was necessary to provide a representative and realistic fuel load that would ignite and become a substantial fire within the motorcoach after penetration of the tire fire through the windows. Some of the actual interior furnishings were reinstalled on the motorcoach since most had been removed for the penetration and fire-hardening experiments to prevent flame spread into the interior. The reinstalled furnishings included: three pairs of seats positioned on the right side over the rear axles, a parcel rack with doors along the right side of the entire original rear half, the interior wall trim (extending from the floor duct to the bottom of the windows) on both sides, the foam rubber window post covers, and the right side window curtain rods and screens (rolled up). The seats were installed with the original 86.4 cm (34 in) spacing in positions corresponding to the second to last row and the next two rows in front of it. This centered the three pairs of seats in the anticipated fire breakthrough area. The parcel rack was installed approximately 12 cm (4 ³/₄ in) forward of its original position. Figure 14 shows a view of the seats and parcel rack installed in the motorcoach.



Figure 14 A photograph of the seats and parcel rack installed for the tenability experiment.

Measurement Instrumentation

Measurements of heat release rate, heat fluxes, and interior and exterior temperatures were recorded for each experiment. The details of the types of measurements and locations are described below. A data acquisition system (DAQ), described in Bryant et al. [42], was used to record 151 channels of sensor output voltages every second. Each voltage was the average of 200 readings scanned each second. This DAQ was separate from that used for the calorimetry system described below.

Total and Burner Heat Release Rates

The total HRR was measured using oxygen depletion calorimetry. Details of the constituent measurements and calculations can be found in Bryant et al. [42]. The experiments were performed under the NIST Large Fire Laboratory (LFL) 9 m by 12 m hood which utilizes up to two fan trains, each of which can be set to a maximum flow of about 21 m³/s (45 000 ft³/min). The LFL exhaust hood is capable of capturing the smoke from a steady 10 MW fire and transients up to 30 MW over periods less than 15 s. Calibrations of the hood up to 8 MW are performed with metered natural gas fires. The calorimeter combined expanded uncertainty for natural gas was about $\pm 7.6\%$ based on a natural gas calibration burner test performed two weeks before the motorcoach penetration experiments. That uncertainty was calculated over the whole range of the calorimeter's operation. For the fire-hardening experiments, the uncertainty was slightly less at $\pm 6.3\%$, and for the tenability experiment which used two hoods, it was $\pm 7.3\%$. Uncertainties in a narrow range, for example around 1 MW as for these fires, can be much lower. Since the motorcoach experiments involved an unknown mixture of fuels, the expanded uncertainty increased by 5% (in quadrature) to $\pm 9.1\%$, $\pm 8.1\%$, and $\pm 8.9\%$ for the penetration, fire-hardening, and tenability experiments, respectively. The increased uncertainty is from an empirical constant for heat released per mole of oxygen consumed for a range of hydrocarbon fuels. [43]

The flow of natural gas to the burner was measured with the DAQ of the calorimeter for an accurate and independent calculation of ideal (assumed 100% efficient) HRR solely related to the burner. The expanded uncertainty of the burner HRR was calculated to be $\pm 2.5\%$ for the 60 kW level at which it operated for these experiments.

Temperature

Temperatures were measured on and around the wheels and tires, along the exterior panel and windows, and inside the motorcoach along the windows and on the floor. K-type thermocouples (TCs) were used throughout. For locations where flames were expected, such as near the heated wheels and over the exterior panel and windows, TC wires with special Nextel (ceramic fiber) insulation were used while the rest of the thermocouple wires had a fiberglass braid. The Nextel insulated thermocouples used 20 or 24 gauge wire, and the fiberglass insulated thermocouples used 30 gauge wire. The numbers and locations of temperature measurements which were in common for all six experiments are listed in Table 8. Extra thermocouples used for the tenability experiment are described later. Additional descriptions of the TC locations are in the channel description and instrument hook-up list which is provided in Appendix A. The DAQ channel descriptions also provide a key to measurement label names used in the plots. Thermocouples were attached to the floor with staples, and the beads were bent to touch the surface. Wheel TCs were secured with screws and washers and tire TCs were held in place with screws. Figure 15 shows the locations of the tire and wheel TCs. The locations are labeled with the same scheme used in the channel list (Appendix A) and temperature plots.

The uncertainties associated with the gas and surface temperature measurements away from the fire were approximately $\pm 2\text{ }^{\circ}\text{C}$. [42] For thermocouples impinged by fire, the gas temperatures recorded may be as much as 90 $^{\circ}\text{C}$ low for a 600 $^{\circ}\text{C}$ reading and 220 $^{\circ}\text{C}$ low for a 850 $^{\circ}\text{C}$

reading. [44] These offsets are due to radiative heat losses from the thermocouple beads to the relatively cool surroundings. Uncertainties of surface temperatures for thermocouples exposed to fire were estimated to be approximately ± 10 °C. The main purposes of the temperature measurements were to monitor progress of the tires toward ignition and identify relatively hotter locations generated by the tire fire in and around the motorcoach. The uncertainties in the temperature measurements were not detrimental to either of these purposes. Expanded uncertainty on thermocouple locations is about ± 1 cm.

Table 8 Numbers of thermocouples and location descriptions common to all experiments.

General Location	Specific Location	Number of TCs
Wheels	Heated wheel on back side in a plus pattern, 0°, 90°, 180°, and 270° from top	4
Tires	Heated tire on front side between wheel rim and tire in plus pattern, 0°, 90°, 180°, and 270° from top	4
Wheel well	Rearmost corner of wheel well, over center of rear (tag axle) wheel, above center between wheels, over center of front (drive axle) wheel, and at front most corner of wheel well	5
Above axles	Left, center, and right above each axle	6
Outside windows and exterior panel	In a grid with 38 cm spacing consisting of 12 columns and 4 rows; bottom row over exterior panel, other rows over windows	48
Inside windows and in space above	In a grid with (generally) 38 cm spacing consisting of 12 columns and 4 rows; bottom 3 rows over windows, top row in space above window 17 cm above top window row	48
Interior floor	Along fire-side wall aligned with wheel well TCs with extra 46 cm behind rearmost and 46 cm in front of front most	7
	Along outside and inside of lavatory wall joint with floor	3
	In central cable tunnel under center of floor aligned with the rear most, center, and front most interior TCs at the side wall	3

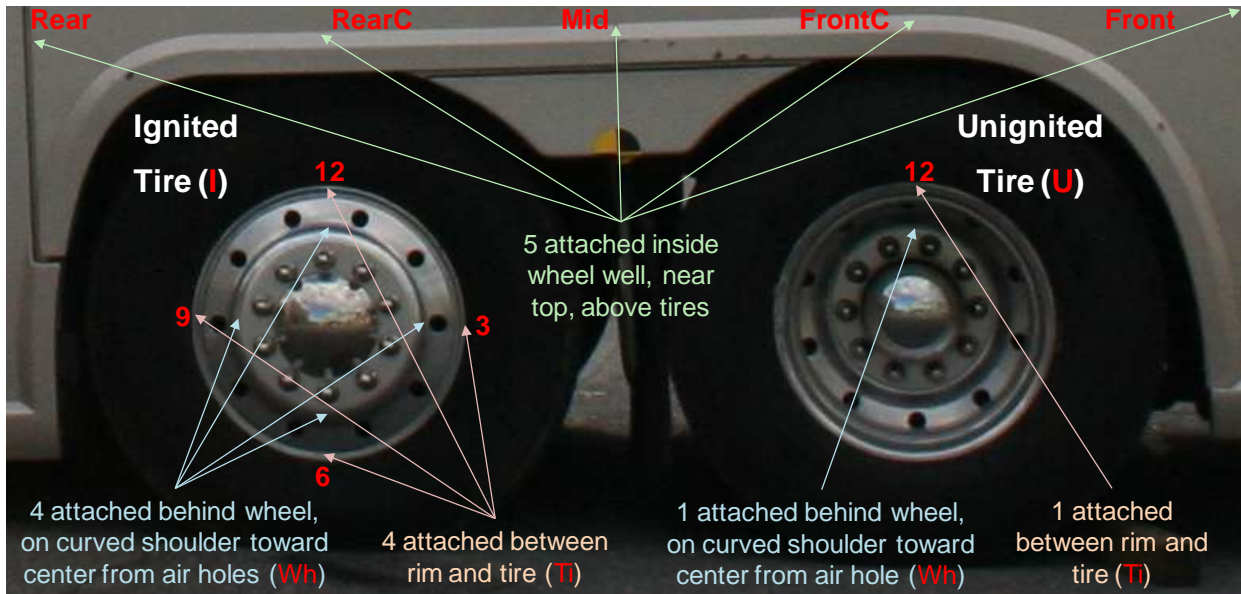


Figure 15 A photograph of the right side wheel well area with the locations of thermocouples shown for the tag axle wheel experiment. The ignited and unignited tires (and their thermocouples) were reversed for the drive axle experiment. Labels (in red) are used in temperature plot legends.

The exterior window and panel thermocouples were spaced 38 cm apart (vertically and horizontally) in 12 columns of 4 rows each for a total of 48 measurements. Three of the rows were over the window glass, whereas the bottom row was over the exterior panel.

Thermocouples were placed about 1 cm from the window surface. Figure 16 (top) shows a diagram with the spacing of the thermocouples and locations relative to the windows and posts. The diagram shows that the gap between columns of thermocouples and adjacent window posts was about 2.4 cm, and the gap between the bottom window row and the bottom of the window was about 3 cm. Figure 16 (bottom) is a photograph of the grid of exterior thermocouples as installed.

For the interior thermocouples near the windows, the spacing was generally the same as the exterior, and over the window area, both interior and exterior thermocouples were aligned on the same grid. The interior grid of thermocouples was shifted upward by one row so that the bottom row was over the window glass, and the top row was above the window in the space below the parcel rack. That top interior row was spaced only 17 cm above the top window row as the only exception to the 38 cm spacing. Figure 17 shows a diagram of the interior grid spacing. As on the exterior, the distance of the thermocouples from the glass was about 1 cm.

The approximate locations of interior floor thermocouples are depicted in Figure 18. The diagram differentiates those near the wall under the windows, those along the lavatory wall and door, and those under the floor in the central tunnel. The locations are further described in Table 8.

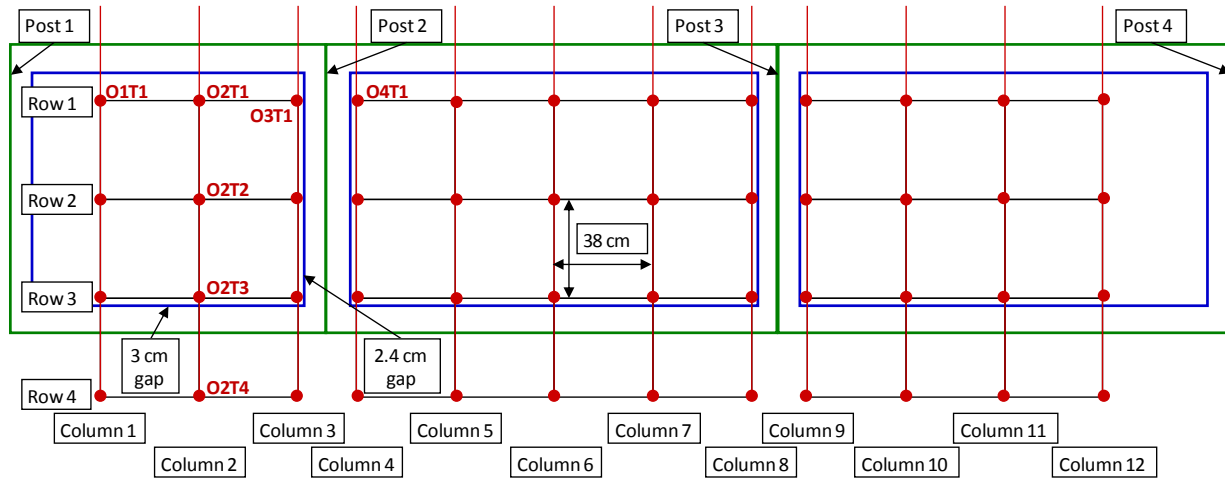


Figure 16 A schematic (top) and photograph (bottom) of the exterior grid of thermocouples on the motorcoach windows. The blue rectangles represent window outlines, red dots represent TCs, green areas represent window frames and post centerlines. Labels pertain to designations in the data file. The pattern of thermocouple labeling is shown in red with O for outside grid, the 1st number for column, and the 2nd number for row.

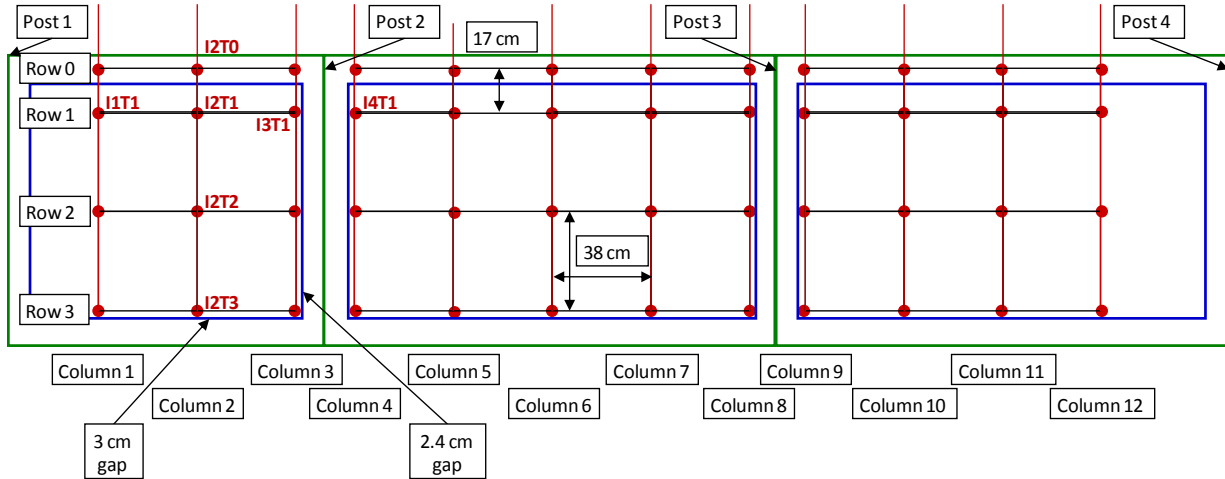
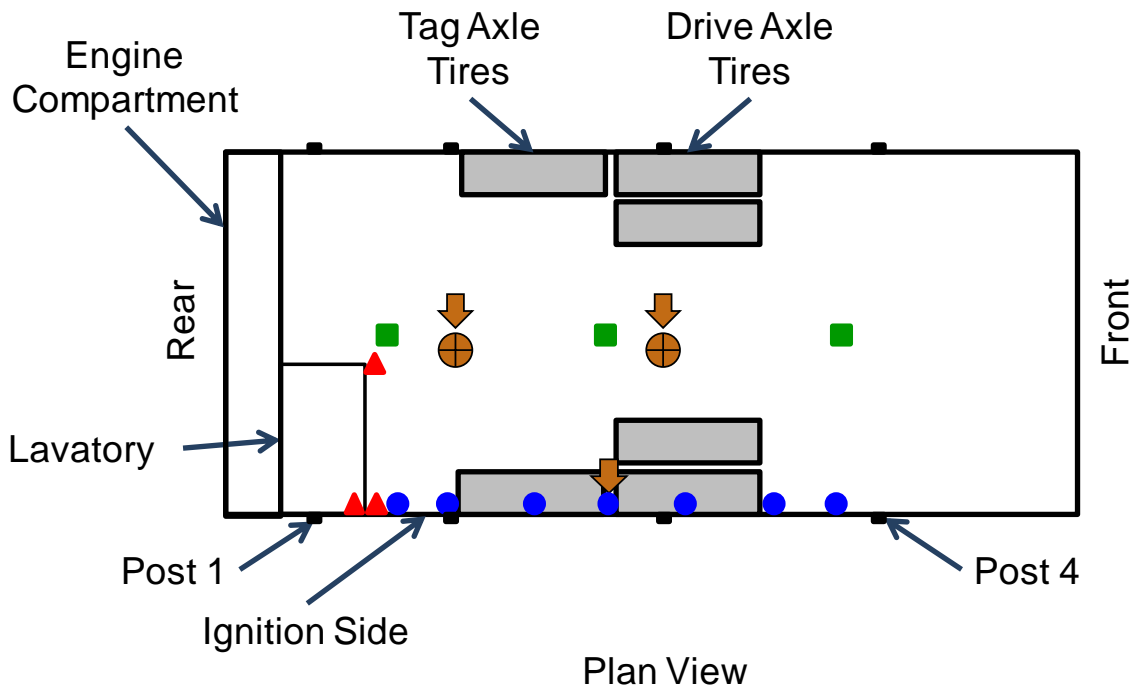


Figure 17 A schematic of the interior grid of thermocouples located near the windows. The blue rectangles represent window outlines, red dots represent TCs, green areas represent window frames and post centerlines. Labels pertain to designations in the data file. The pattern of thermocouple labeling is shown in red with I for inside grid, the 1st number for column, and the 2nd number for row.



- Heat Flux Gauges (5)
- Wall/Floor Thermocouples (7)
- Lavatory/Floor Thermocouples (3)
- Central Tunnel/Floor Thermocouples (3)

Figure 18 A diagram of the top view of the motorcoach showing approximate locations of interior floor thermocouples and the locations and directions of heat flux gauges for tenability and hardening tests.

For the fire-hardening and tenability experiments, additional thermocouples were positioned inside and around the motorcoach. Four thermocouples were located behind and half way up the width of the exterior side panel at positions behind the tag axle, above the tag axle, centered between the two axles, and above the drive axle. These were used to ascertain the thermal penetration through the exterior panel and to help determine if the foam material behind the panel was at risk for burning.

For the fire-hardening and tenability experiments, an OEM anti-lock braking system (ABS) sensor from Meritor and an accompanying thermocouple were installed (and replaced for each experiment) on the tag axle near the normal installation location for the ABS sensor. These were to discover if there was any kind of response by the ABS sensor to increasing temperature and whether it correlated with the thermocouple temperature. An ABS sensor typically provides a signal based on cyclical contact with metal which is rotating. In this case, there was no rotating metal to provide a stimulus to the sensor so instead, a 9 V battery was connected to the sensor, and its voltage was monitored. The sensor's behavior under heating was observed to determine if its output had any value as a heat indicator while in a passive mode.

For the tenability experiment, vertical thermocouple arrays of five thermocouples each were installed at rear, middle, and front locations. A thermocouple array consisted of a main wire (stringer) attached between the ceiling and floor to which thermocouples wires were attached, and the beads extended out from the stringer approximately 2 cm. Figure 19 shows the locations of these arrays inside the motorcoach. The heights where temperature was measured on each array were: 180 cm, 150 cm, 120 cm, 60 cm, and 30 cm above the floor. While 150 cm is the typical target for assessing tenability conditions because it is the average location for a person's nose and mouth, the other locations were of interest for observing maximum temperatures (usually near the ceiling) as well as what conditions were like near the floor where the air would remain cool the longest during a fire.

Also for the tenability experiment, thermocouples were attached to the top center positions of the headrests of each of the three aisle seats. The centers of the headrests were about 82.3 cm (32.4 in) from the right side windows and 113.7 cm (44 ¾ in) above the floor. Fiberglass tape was used about 1 cm from the bead to hold each thermocouple on the headrest material. Photographs of the seats and an example of the thermocouple installation are shown in Figure 20.

Thermocouples were attached (with tape) to the parcel rack doors above each of these headrest thermocouple positions. The thermocouples were placed about half way up the doors which was 1.78 m (70.2 in) from the floor. The rearmost thermocouple was located at the same height as the others but in the air since the parcel rack didn't extend far enough back. A photograph of the parcel rack and the thermocouples is shown in Figure 21.

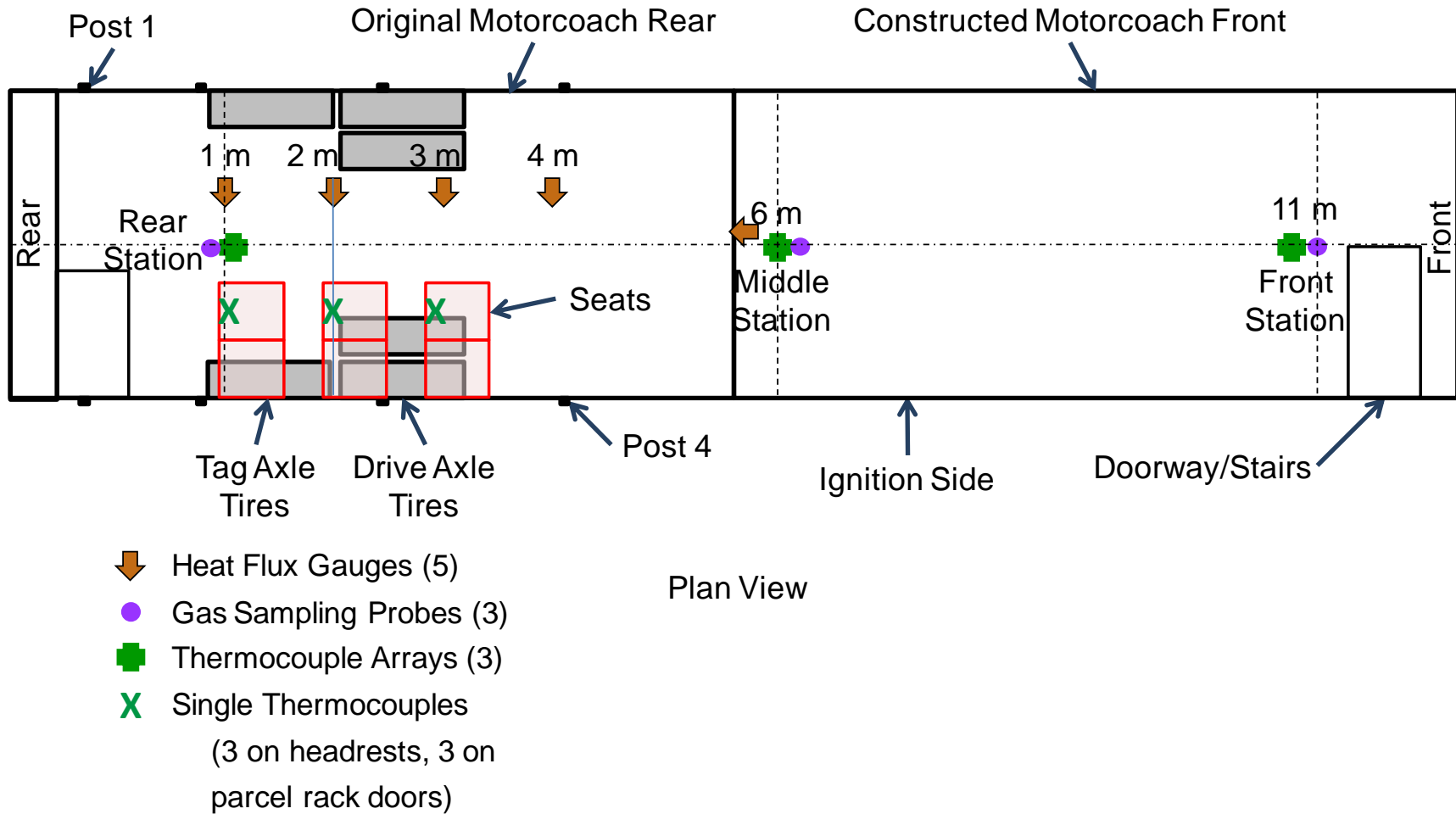


Figure 19 Schematic of the whole motorcoach assembly used for the tenability experiment showing locations of the three sampling stations, heat flux gauges, and thermocouples.



Figure 20 Two photographs showing the three pairs of seats installed for the tenability experiments. The right photograph shows one of the thermocouples installed on the top of an aisle seat headrest.

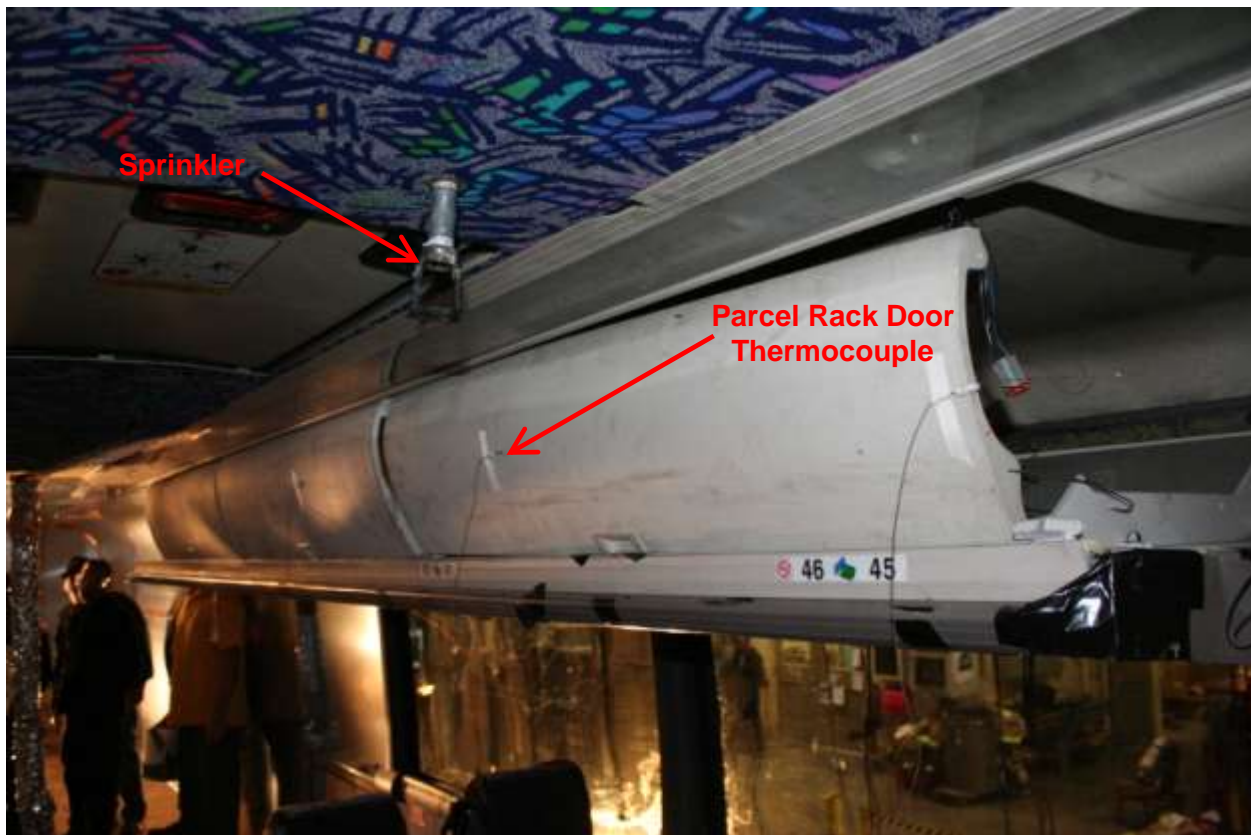


Figure 21 A photograph showing the right side parcel rack installed for the tenability experiments. Three thermocouples are shown attached about half way up the doors.

Heat Flux

For the penetration and fire-hardening experiments, heat flux was measured in five locations to help indicate the transfer of heat from the fire through the windows or floor. These measurements also provided insight as to when interior heat fluxes threatened to ignite combustible materials, if they had been present. Table 9 lists the locations and directions of the gauges, and Figure 18 is a diagram depicting the top view of the motorcoach and the approximate locations and directions of the gauges. Expanded uncertainties for the heat flux location measurements are estimated to be ± 3 mm. Figure 22 and Figure 23 are photographs of the installation of the gauges, and Figure 24 is a photograph of the gauge at the seat headrest location showing its proximity to the window. The heat flux gauges were water-cooled (using unheated tap water), Schmidt-Boelter type, which measured total heat flux, including both radiation and convection. The uncertainties (combined, expanded, relative) associated with the heat flux measurements were approximately ± 3 % based on the assumption that the measurement conditions were not significantly different from the gauge calibration conditions. [45]

Table 9 Heat flux gauge locations for the penetration and fire-hardening experiments.

Gauge Label	Location Description	Location Details
HFRS	Rear position, facing horizontally toward windows	127.8 cm from floor, centerline of bus, centered over rear tire (tag axle)
HFFS	Front position, facing horizontally toward windows	130.9 cm from floor, centerline of bus, centered over front tire
HFRD	Rear position, facing down toward floor	132.8 cm from floor, centerline of bus, centered over rear tire (tag axle)
HFFD	Front position, facing down toward floor	133.8 cm from floor, centerline of bus, centered over front tire
HFS _{Seat}	At seat headrest position, facing horizontally toward windows	111.2 cm from floor, 14.9 cm from window, centered between tires which is 51.8 cm rearward of rear facing side of window post 3 above front (drive axle) tire

For the tenability experiment, the five heat flux gauges were rearranged to monitor wider areas of the passenger compartment. Four gauges were located in the original rear of the motorcoach at 1 m, 2 m, 3 m, and 4 m from the rear of the interior as defined by the lavatory door. Their height was 1.5 m, and each faced the right side windows. The lateral location was 69 cm toward the driver's side from the centerline of the motorcoach. The fifth heat flux gauge was at the same height, but near the middle gas sampling and thermocouple array location, and it faced rearward. Its location was 8 cm from the centerline and 5.66 m from the rear of the motorcoach. The Figure 19 diagram shows the locations of the heat flux gauges relative to other features of the motorcoach.

Table 10 Heat flux gauge locations for the tenability experiment.

Gauge Label	Location Description
HF1m	1 m forward of lavatory door, 1.5 m high, facing horizontally toward windows, 69 cm toward driver's side from motorcoach centerline
HF2m	2 m forward of lavatory door, 1.5 m high, facing horizontally toward windows, 69 cm toward driver's side from motorcoach centerline
HF3m	3 m forward of lavatory door, 1.5 m high, facing horizontally toward windows, 69 cm toward driver's side from motorcoach centerline
HF4m	4 m forward of lavatory door, 1.5 m high, facing horizontally toward windows, 69 cm toward driver's side from motorcoach centerline
HF6m	5.66 m forward of lavatory door, 1.47 m high, facing rearward, 8 cm toward driver's side from motorcoach centerline



Figure 22 From the penetration experiments, a photograph of the interior of the motorcoach showing the locations of the heat flux gauges.

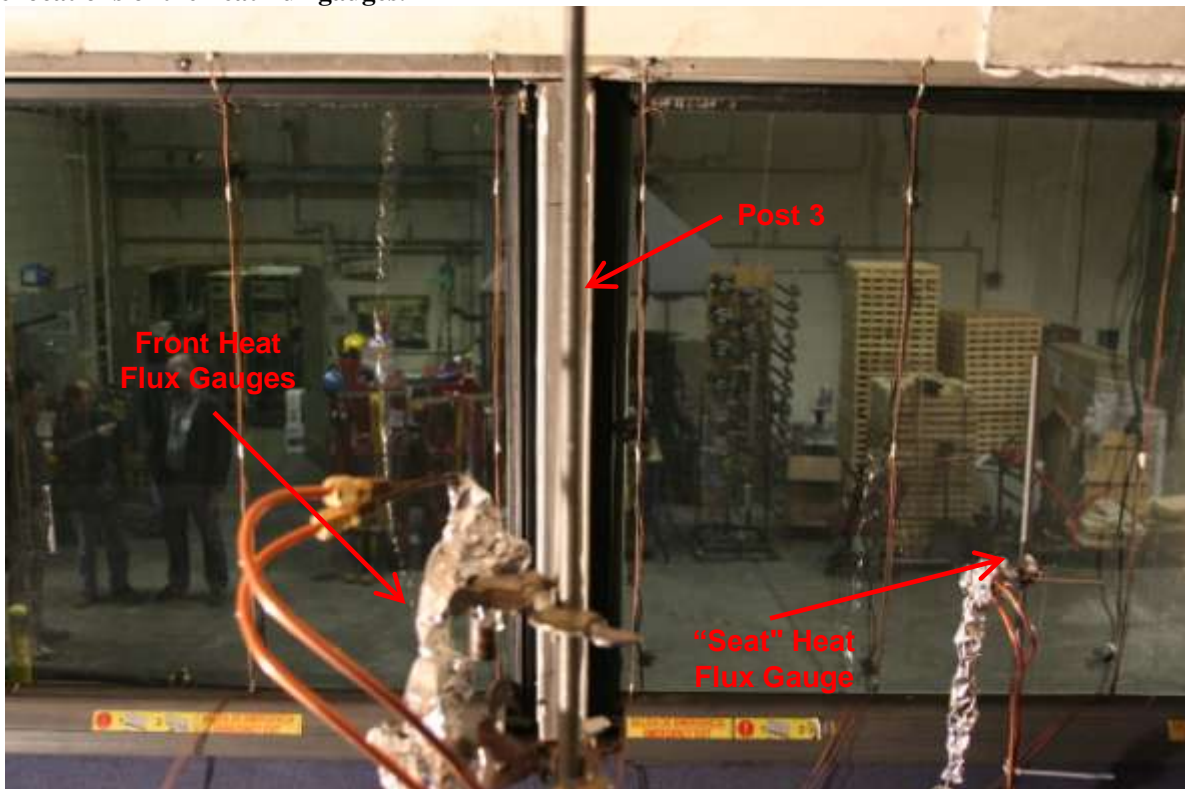


Figure 23 From the penetration experiments, a photograph of the interior heat flux gauges and their view of the right side windows.

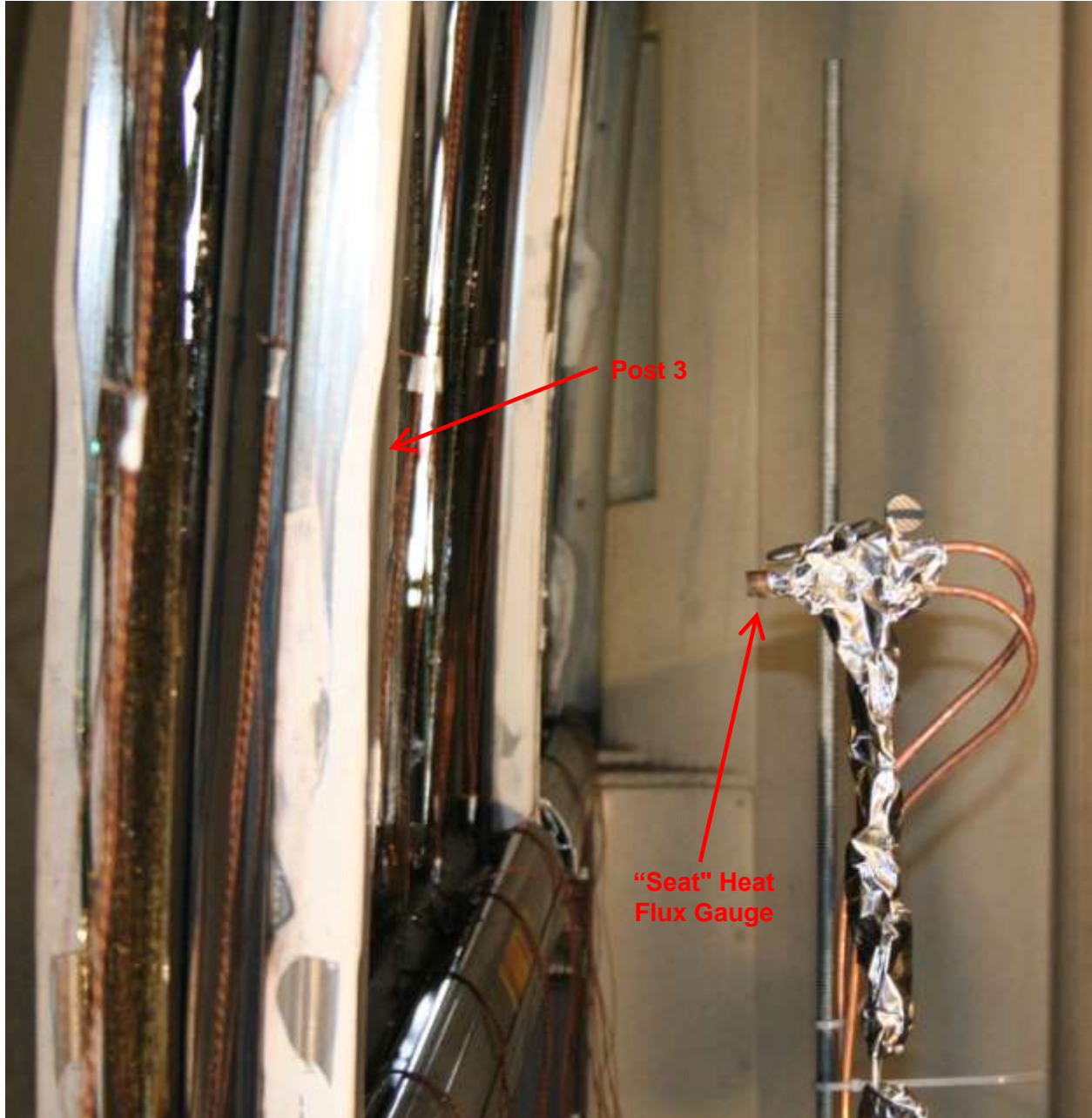


Figure 24 From the penetration experiments, a photograph of the interior of the motorcoach showing the proximity to the window of the heat flux gauge at the position of a seat head rest.

Gas Volume Fractions

Gas volume fractions in the interior of the motorcoach were measured only during the tenability experiment. Three 9.5 mm (3/8 in) OD stainless steel probes were installed at rear, middle, and front positions. The three probe locations are shown in the Figure 19 schematic. The rigid straight probes protruded out through the floor or ceiling at which point they were attached to more flexible copper tubing which was routed to the analyzer racks. Each probe was associated with a rack of gas analyzers with its own sample pump and conditioning unit. The analyzers were non-dispersive infrared (NDIR) Siemens Ultramat 6 for carbon monoxide (CO) and carbon dioxide (CO₂), paramagnetic Servomex 4100 or 540 for oxygen (O₂), and flame ionization detector (FID) Baseline-Mocon 8100H for total unburned hydrocarbons. The conditioning units filtered soot and trapped water vapor from the gas sample. The sample analysis delay relative to the time of extraction from the motorcoach was between 26 s and 34 s for the CO, CO₂, and O₂ analyzers. The NDIR, paramagnetic, and FID type analyzers had measurement uncertainties of around ± 1 % of their reported values. These inherent analyzer uncertainties along with uncertainties in the calibration gases used with the analyzers (1 % to 2 %) and uncertainties imposed by the mixing and spreading of gas samples in the sampling system (estimated at 2 %) combine for overall combined expanded uncertainties in the gas measurements of about ± 3 % of the measured values.

The rear sample probe also provided sample gas to a MIDAC Corporation Fourier transform infrared spectrometer (FTIR) which was used to measure hydrogen cyanide (HCN), hydrogen chloride (HCl), water (H₂O) and other gases with relatively lower volume fractions. The FTIR sample was extracted at a flow of about 10 L/min prior to the main sample reaching the rear rack and its conditioning unit. No soot filters were used to condition the FTIR sample since acid gases would collect on them. A heated sample line was used and maintained at 170 °C to prevent condensation of water and other species so the FTIR was able to accurately measure water vapor. The FTIR open cell path length was about 10 cm and the sample analysis delay relative to the time of extraction from the motorcoach was about 4 s. The FTIR measurements generally had total uncertainties estimated at ± 10 % of the measured values. Larger uncertainties were estimated for measurement ranges far from the gas volume fractions at which the FTIR was calibrated. These instances are discussed in the results section.

Visibility

For the tenability experiment, two methods were used to try to determine when passenger compartment smoke reached sufficient levels to inhibit visibility. One method involved installing a smoke meter across the motorcoach interior near the middle sampling station. The position is shown in Figure 25. The smoke meter consisted of a laser and detector. Decreases in the detector signal indicated smoke attenuation of the laser beam. The laser model was Thorlabs LDM635 Red Laser Diode Module (635 nm wavelength and 4.5 mW power), and the detector model was Thorlabs PDA 100A Silicon Detector. Holes for the laser and detector were made in the sheet metal walls of the front extension of the motorcoach. The laser and detector were mounted on stands that did not touch the walls so as to prevent thermal expansion effects on their mountings which would change the laser beam alignment. The centers of the holes were located

1.5 m from the floor and 6.26 m from the lavatory door or 67 cm forward of the front edge of the original motorcoach rear half.

A second method to determine visibility involved mounting six luminous signs spaced at 2 m intervals from the lavatory door forward 10 m to about 2 m from the front wall. Figure 25 shows their positions in the motorcoach. A video camera, Hitachi KP-D20, was mounted in the front end cap of the motorcoach to record the deterioration of visibility. The luminous signs selected were Lithonia Lighting EXR EL exit signs. The signs were made of white thermoplastic with LED lights and red letters and operated on rechargeable NiCd batteries. The signs were installed with their centers 69 cm (27 in) toward the driver's side from the centerline. Their vertical centers were located 1.5 m from the floor or about 47.5 cm (18.7 in) from the ceiling. The signs were attached to the ceiling with 2.5 cm × 2.9 cm (1 in × 1 1/8 in) steel angle with the 16.5 cm (6 1/2 in) horizontal segment attached to the ceiling and the 54.6 cm (21 1/2 in) vertical segment attached to the sign. Each sign had a different letter left unmasked to enable easier analysis of the video recording. Figure 26 shows the rearmost sign as installed. Figure 27 shows the front most visibility sign and the others toward the rear.

Visibility was determined based on a visual analysis of the video recording. During the course of the experiment, after a sign could no longer be distinguished from its surroundings due to smoke, visibility was considered impossible for that particular sign. The motorcoach interior was not lit during the experiment so it was relatively dark inside except for some low level laboratory light which came in through the windows. Uncertainty in this somewhat subjective measurement was considered to be approximately ± 5 s.

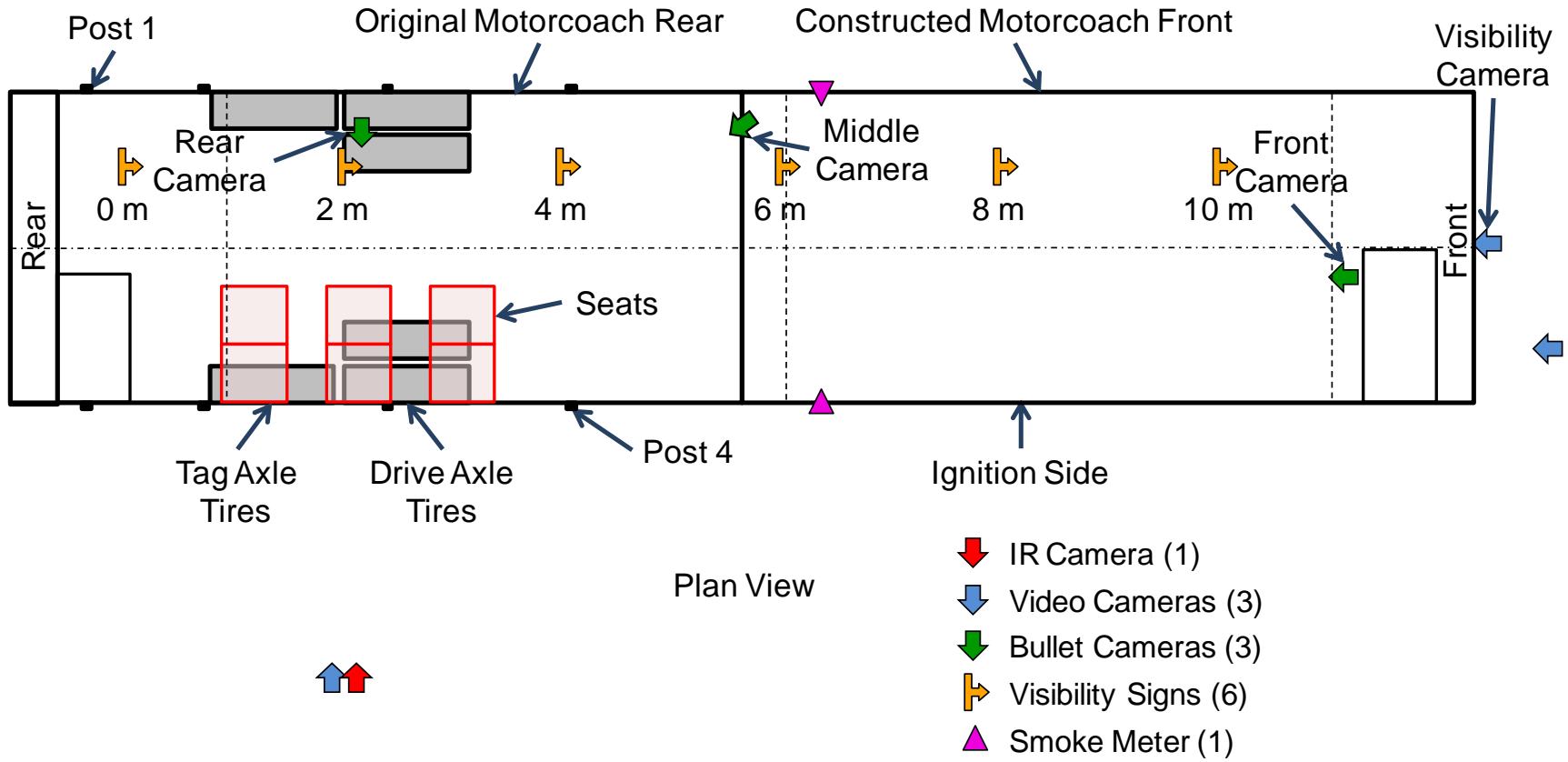


Figure 25 Schematic of the whole motorcoach assembly used for the tenability experiment showing approximate locations of IR, video, and bullet cameras.

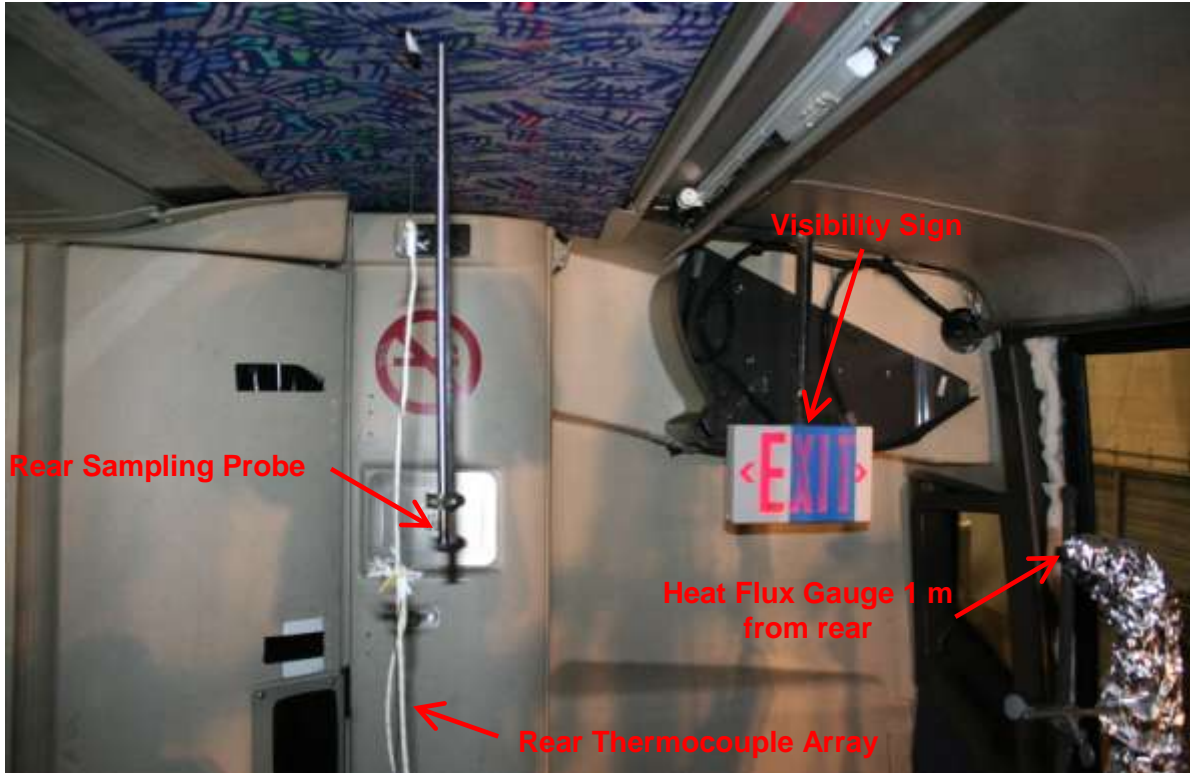


Figure 26 A photograph showing the rear gas sampling position, rear visibility sign, rear thermocouple array, and rear heat flux gauge used for the tenability experiment.

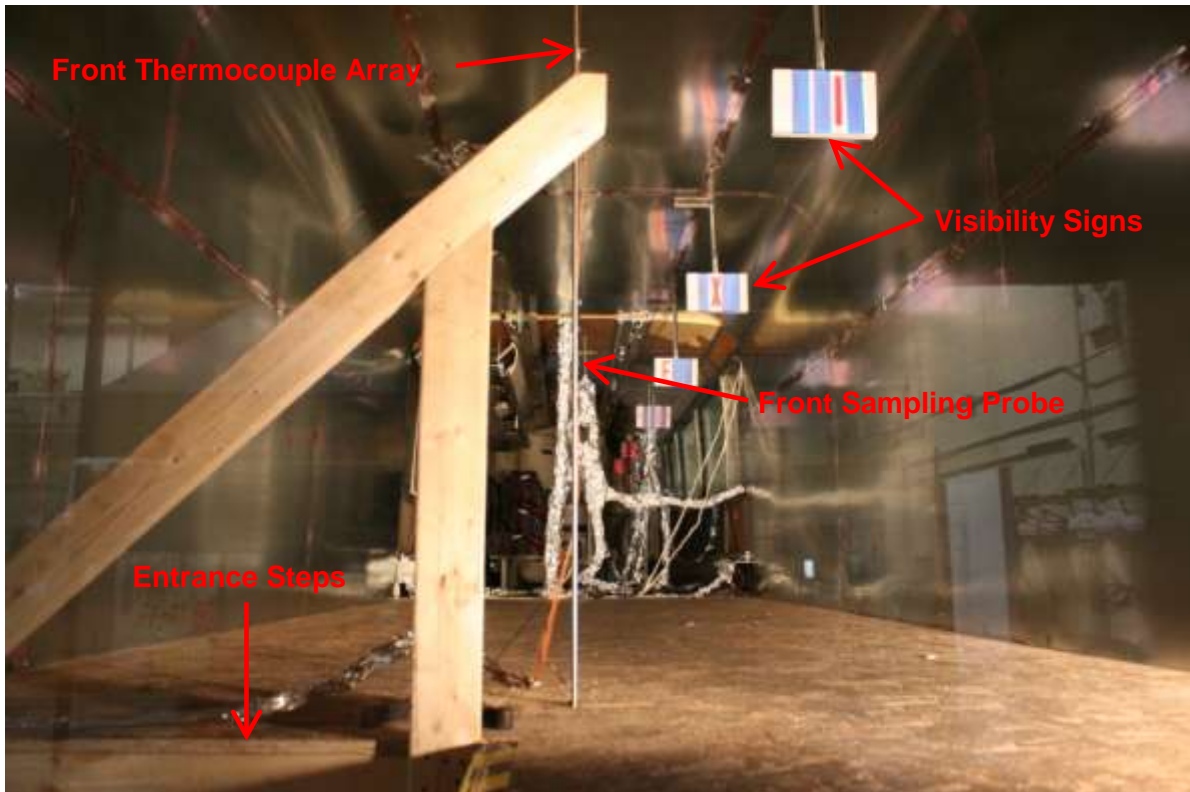


Figure 27 A photograph of the interior of the motorcoach and front extension looking toward the rear. The lit exit signs were used to determine visibility deterioration during the tenability experiment.

Image Recording

Standard and Infrared Video

For the penetration and fire-hardening experiments, seven standard and two infrared (IR) video recordings were made around and inside the motorcoach. The IR cameras were used to determine if fire penetration into the passenger compartment could be better observed using infrared imaging. The approximate positions of all of the cameras are shown in Figure 28. The cameras shown outside the motorcoach were located relatively further away than depicted. Two of the standard video cameras were high resolution versions. One was located at a position facing the tire fire from the side of the motorcoach, and the other was directed at the interior from a position several meters in front of the motorcoach's cut end. The video camera facing the tire fire from the side was paired with an infrared (IR) camera. Two other IR video cameras were mounted together on a ladder at the front end of the motorcoach and trained on the interior, but one of these IR cameras was set to normal mode to provide contrast to the IR images. The two IR cameras on the ladder are shown in Figure 29. The remaining four video cameras were located closer to the motorcoach. These cameras were "bullet" type, low cost cameras which could be damaged from heat during the testing. Figure 30 is a photograph of one of the bullet cameras in position on the far side (driver's side or left side facing forward) of the motorcoach between the axles. Figure 31 is a photograph of the bullet camera inside the passenger compartment opening, viewing the rear of the motorcoach interior. Interior lighting was added to improve image quality.

For the tenability experiment, video recordings were made with one IR camera, three standard cameras, and three standard bullet cameras. Figure 25 is a schematic showing the approximate locations or viewing directions of the various interior and exterior cameras. The cameras shown outside the motorcoach were located relatively further away than depicted.

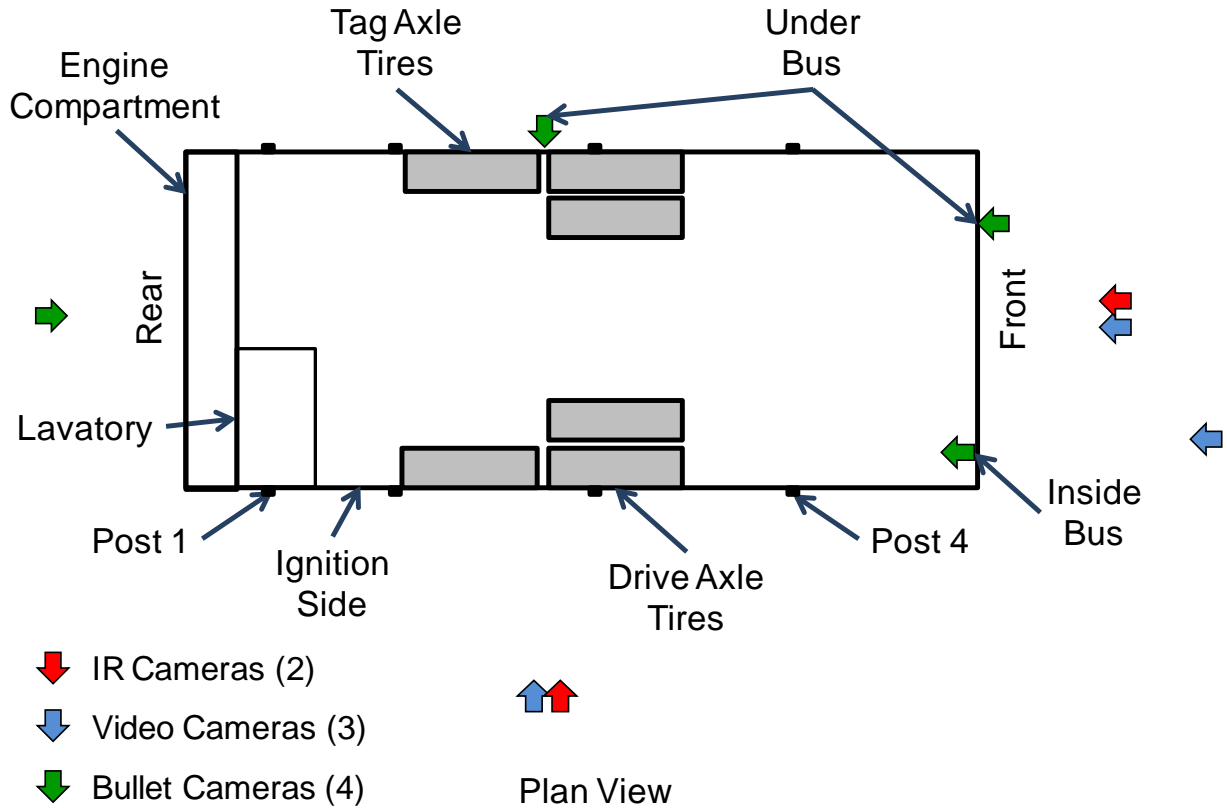


Figure 28 A diagram of the video camera layout for the penetration and hardening experiments showing their general locations and the directions they faced.



Figure 29 Photograph of the two IR cameras viewing the open end of the motorcoach for penetration and hardening experiments. One camera was set to IR and the other to visual mode for comparison.



Figure 30 A photograph of the bullet camera located between the two left (driver's) side axles.



Figure 31 A photograph showing the location of the passenger compartment bullet camera (lower left) and lighting (lower right) to provide better videos and photographs of the interior.

Still Photography

One main camera was used to take still digital photographs before, during, and after each experiment. Since the main camera was located where it could primarily view the passenger compartment from the open end and record fire penetration, it was supplemented during the second experiments with another digital camera, which captured more views of the developing fire involving the tire, wheel well, and exterior panel. For the fire-hardening and tenability experiments, two and sometimes three cameras were used to acquire a sufficient number of images from multiple views.

General Procedures

The following experimental procedure was followed on the day of each test:

- A safety briefing was held for all personnel present in the building during experiments.
- Personnel involved in igniting the burner and extinguishment put on firefighter turnout gear and self-contained breathing apparatus (SCBA).
- Data collection was initiated, and recording was started with the standard and IR video cameras which were viewing the fire side of the motorcoach.
- The burner pilot (a propane torch with a long tube) was ignited with a butane lighter.

- With the pilot located at the natural gas burner, the natural gas valve was opened, and the initial target HRR fuel flow was set.
- The air valve was opened and the flow was adjusted for pre-mixed, blue, conical flames.
- The burner was placed next to the wheel rim so flames impinged on the wheel.
- A few minutes before tire ignition, tapes were changed for the video cameras already running, and recording was started with the others.
- The halogen lights were cycled off and on to briefly darken the motorcoach which provided a synchronizing event for the video recordings.
- The wheel was heated until the tire was fully ignited (sustained flames on the tire at the bottom of the tag axle wheel or between the drive axle tires). Target range for the pre-ignition heating period was 25 min to 40 min. The burner was maintained beyond intermittent ignition to ensure that the tire fire would progress and not self-extinguish.
- The natural gas valve and air valve were closed, and the burner was removed.
- For penetration and fire-hardening experiments, whether fire had penetrated into the interior compartment was determined through observation of the interior side of the flame impinged windows.
- For penetration and fire-hardening experiments, the fire was extinguished using a manned fire hose with water and foam (plus multiple water hoses if necessary) once fire penetration into the interior compartment was determined.
- For the tenability experiment, the fire was to be extinguished using multiple manned fire hoses (one with water and foam) once tenability thresholds were surpassed or once the fire HRR exceeded 6 MW or if significant smoke was observed escaping the exhaust hood and entering the high bay.
- Data collection was terminated after recording several minutes of post-extinguishment measurements.
- Clean-up operations commenced after surface temperatures decreased to below 50 °C, smoke had sufficiently cleared the test bay, and CO volume fractions were less than 50 µL/L in the motorcoach (determined by the fire test Safety Officer).

Extinguishment

For extinguishing each fire, a Task Force Tips PRO/pak Portable Foam System was employed. The PRO/pak automatically mixes foam into the water according to a dialed setting. The foam used was KnockDown from Kidde Fire Fighting/National Foam. The foam mixing range was 0.1 % to 1 %, and the 1 % setting was used. The hose for the foam plus water combination had a 2.5 cm (1 in) ID. Additional 3.8 cm (1.5 in) water hoses were attached to building stand pipes. A handheld water canister extinguisher was also used for directing small streams on spot fires.

A fixed sprinkler was installed in the roof of the motorcoach near the rear sampling station in case remote extinguishment of the interior fire was required. The exact location, shown in Figure 21, was 54.6 cm (21.5 in) forward of window post 2, 14 cm (5.5 in) toward the right side from the motorcoach centerline, and 8.4 cm (3.3 in) rearward of the ceiling hatch opening. The sprinkler consisted of a 19 mm (¾ in) ID pipe positioned over a 5 mm (3/16 in) thick, 32 mm x 19 mm (1 ¼ in x ¾ in) oval deflector plate held in place with two 5 mm (3/16 in) OD steel rods. The pipe was connected with a 19 mm (¾ in) hose to the LFL water supply, and a manual quarter turn ball valve was installed for control.

RESULTS AND DISCUSSION

Penetration Experiments

Event Timing

Both experiments initiated on each axle showed penetration of the fire into the passenger compartment through the long window between the axles. This finding is in contrast with research conducted by SP [17] when a non-combustible barrier was placed on the exterior above the tires and fire penetration through the windows did not occur. Table 11 lists the times and corresponding events for each experiment. The time referenced is when the burner was applied to the wheel. The maximum uncertainty (combined, expanded) in the times listed is approximately ± 3 s. Uncertainty in the timing is primarily due to the judgment of the project director as to when events occurred, communicating those events to the data acquisition system via a remote marker or to the operator verbally, and also to minor synchronization issues between the two computer data acquisition systems used. Table 12 lists the duration of the main periods of interest in these experiments: the period of heating before the tire was burning steadily, and the period between heating and penetration of the fire into the passenger compartment.

Table 11 Timing of events and observations during the penetration experiments. (uncertainty = ± 3 s)

Test 1 (Heated Tag Axle Wheel)		Test 2 (Heated Drive Axle Wheel)	
Time (s)	Event Description	Time (s)	Event Description
-807	Data recording initiated	-1636	Data recording initiated
0	Burner applied to wheel	0	Burner applied to wheel
189	Pool fire	452	Flare up of hub fluids
1014	Flare up	609	Cameras started
1188	Cameras started	760	Smoke from back of tire
1361	Flare up	789	Smoke on backside of bus
1860	Intermittent ignition	979	Smoke coming from inside wheel at the 12 o'clock (top) position
1918	Intermittent ignition at tire bottom	1185	Ignition in the back of outside tire
1972	Steady ignition at top of tire	1255	Sustained tire burning, burner removed, gas off
2170	Fender ignited	1278	Flames licking at outside molding
2177	Sustained tire burning, burner removed, gas off	1355	Melt dripping of fender plastic
2390	Smoke inside at bottom of array 6	1417	Glass cracking, flaming inside
2457	Window penetration, suppression started	1504	Flames along inside post 3
2469	Extinguishment	1582	Panes of glass breaking
		1603	Some flames on inside
		1618	Window penetration, suppression started
		1632	Suppression completed
		1712	Increased exhaust hood flow

Table 12 Duration of periods of heating and between heating and window penetration.

Period	Duration (s) (min:s)	
	Test 1 (Heated Tag Axle Wheel)	Test 2 (Heated Drive Axle Wheel)
Burner heating wheel to sustained tire burning	2177 (36:17)	1255 (20:55)
Burner removed to fire penetration of window	280 (4:40)	363 (6:03)

Sustained or established burning for the tag axle wheel fire was defined as continuous (versus intermittent) burning of the tire rubber at one or more locations in the bottom half of the tire (away from the top which received additional heat from buoyant convection). Sustained burning for the drive axle wheel fire was more difficult to determine since the flames were between the dual tires and mostly obscured. A consistent, non-intermittent flame plume proceeding from between the tires was considered sustained or sufficiently established burning for that experiment.

The periods of heating before sustained burning were quite different for each experiment with the experiment initiated on the tag axle wheel requiring about fifteen more minutes than the one initiated on the drive axle wheel. The likely reason for this is that the tag axle wheel had more conduits for heat loss than the drive axle wheel had. The outside of the tag axle wheel was convex and exposed to ambient air, while the outside of the drive axle wheel was concave and recessed (see Figure 5). This allowed the drive axle wheel to trap more heat than the tag axle wheel. The heat from the burner that did not go into the tag axle wheel was convected along the bottom of the shield and away, but for the drive axle wheel, it heated the upper portion of the wheel first before reaching the shield. Also, while the back of the tag axle wheel radiated and convected heat away, the drive axle wheel was connected to the second inner wheel, promoting overall heating of the dual tire system and blocking convective cooling on the backside of the outer wheel and tire. The rubber of the tires acts as an insulator as well, trapping heat between the tires and near their surfaces.

The period between heating and compartment penetration was about 1.5 min shorter for the tag axle experiment than for the drive axle experiment. While the time periods are both short and their difference could be due to random variation, there are some factors that could explain the distinction. The tag axle tire started burning on the outside and had access to air for more complete and hotter combustion. The drive axle tires started burning at the surfaces between the inner and outer tire, away from the outer surface of the outer tire. The narrow region between tires limited the flow of air and decreased the rate of fire growth. Also, the fire between the drive axle tires had to grow sufficiently to send a plume horizontally to spread outward and then upward onto the GRP fender and exterior panel. This extra path for fire spread took longer (363 s) than for the more direct path of the tag axle (280 s) up to the fender and panel.

Penetration was defined as fire entering the motorcoach by some path such as a hole created by the fire or evidence of sustained flame spread into the interior due to the tire fire. In these experiments, both tire fires resulted in compartment penetration by breaking through the windows. If the floor had been the pathway of fire spread, observation of a sustained and

growing fire in a region of the floor heated by the tire fire would have been required, but not necessarily a hole in the floor as occurred with the windows when they broke.

While breaking the windows was the path by which the fires penetrated into the passenger compartment, the windows did not break easily. The window design was two glass layers with a clear polymer laminate layer between them. The inner glass was a safety type which shattered, and the outer was not. It is noteworthy that the glazing layers often broke independently from each other with the fire impinging on the outside. For the drive axle experiment, glass layers sometimes fell in or out, but it took about 2 min from cracking of glass to the time that layers started falling away and another minute for any window areas to have both glass layers break off, thus creating a hole and path for fire entry. Some of the pieces of glass with burning laminate fell inside and burned on the floor. This was not considered fire penetration because the burning laminate did not create a sustained flame spread, although it is possible that the burning material could have ignited seat cushions if they had been installed. Also, material between the front most window and post 3 (most likely a window seal) burned during the second test but was not considered fire penetration since it may not have been self-sustaining based on the localized and limited nature of the fuel and flames.

Photographs

Hundreds of digital photographs were taken of the motorcoach before, during, and after the tire fire passenger compartment penetration experiments. Several photographs recorded during the experiments are included here to illustrate the evolution of the fires. Figure 32 through Figure 35 show the tag axle experiment, and Figure 36 to Figure 45 show the drive axle experiment. A select collection of additional photographs, including some taken after the experiments, is shown in Appendix B.



Figure 32 Tag axle wheel heating penetration experiment about 1 min after the burner was removed. The fender is already burning and the exterior panel is just igniting.



Figure 33 Tag axle wheel heating penetration experiment about 2 min after the burner was removed. The exterior panel is burning up to the windows.



Figure 34 Tag axle wheel heating penetration experiment just under 4 min after the burner was removed.



Figure 35 Tag axle wheel heating penetration experiment at fire penetration, about 4 min 40 s after burner removal.



Figure 36 Drive axle wheel heating penetration experiment about 1 min before burner was turned off.



Figure 37 Drive axle wheel heating penetration experiment just after burner was turned off.



Figure 38 Drive axle wheel heating penetration experiment about 30 s after burner was turned off.



Figure 39 Drive axle wheel heating penetration experiment showing fire spreading from the drive axle to the tag axle area of the fender.



Figure 40 Drive axle wheel heating penetration experiment about 3 min after the burner was removed showing a view of the fire plume from the interior.



Figure 41 Drive axle wheel heating penetration experiment showing large fire plumes on each tire.



Figure 42 Drive axle wheel heating penetration experiment showing the joined fire plumes within 2 min of fire penetration.



Figure 43 Drive axle wheel heating penetration experiment just under 5 min after burner removal.



Figure 44 Drive axle wheel heating penetration experiment at fire penetration, about 6 min 3 s after burner removal. Window breakage occurred on the more rearward window while the burning tire was fairly centered on post 3 between windows.



Figure 45 Drive axle wheel heating penetration experiment within a few seconds of fire penetration and at the very beginning of extinguishment.

Heat Release Rate

For the first test, the average LFL exhaust hood flow, 19.2 m³/s (40 600 ft³/min), was selected close to the maximum flow for one of two exhaust trains since the potential size of the tire/motorcoach fire was unknown. Since the hood flow proved more than adequate for the first test, the setting was maintained approximately the same for the second at 20.1 m³/s (42500 ft³/min). The peak heat release rates were 1162 kW and 1465 kW for the first and second tests, respectively. Figure 46 and Figure 47 show the HRRs plotted versus time for the two experiments. The time of window penetration is marked with a vertical line. Suppression was initiated within 5 s of penetration and is indicated by the sudden drop in HRR.

The uncertainty of the HRR measurement for the period immediately preceding each peak was $\pm 9\%$. The peak values were also attenuated by about 1 % due to the time response of the calorimetry system to transients. [42] Taking time response into account, the revised values for the two tests were 1175 kW \pm 107 kW and 1480 kW \pm 135 kW, respectively. The rates of increase of each fire were between 300 kW/min and 400 kW/min during the final 2 min of each test.

The natural gas burner HRR was calculated using measurements of the gas flow, temperature, and pressure and a chemical analysis of the natural gas. The calculated average values were 61.7 kW for the first test and 60.3 kW for the second. These values each have uncertainties of about $\pm 2.5\%$. [42]

For the first test, the total heat released by the burner and motorcoach materials was 323 MJ, which consisted of 138 MJ (43 %) from the burner and 185 MJ (57 %) from the bus materials. For the second test, the total heat released by the burner and motorcoach materials was 341 MJ, which consisted of 77 MJ (32 %) from the burner and 264 MJ (77 %) from the bus materials. The total heat released during each test was similar, but the drive axle test required much less heating (56 %) for the reasons described in the previous section on event timing. During the drive axle test (#2), 43 % more bus material was burned than in the tag axle test (#1). The drive axle tire fire actually spread to the tag axle tire causing two plumes to merge and involving more of the exterior panel than the single plume from the tag axle test. Also, the tires and exterior panels burned longer before penetration during the drive axle test.

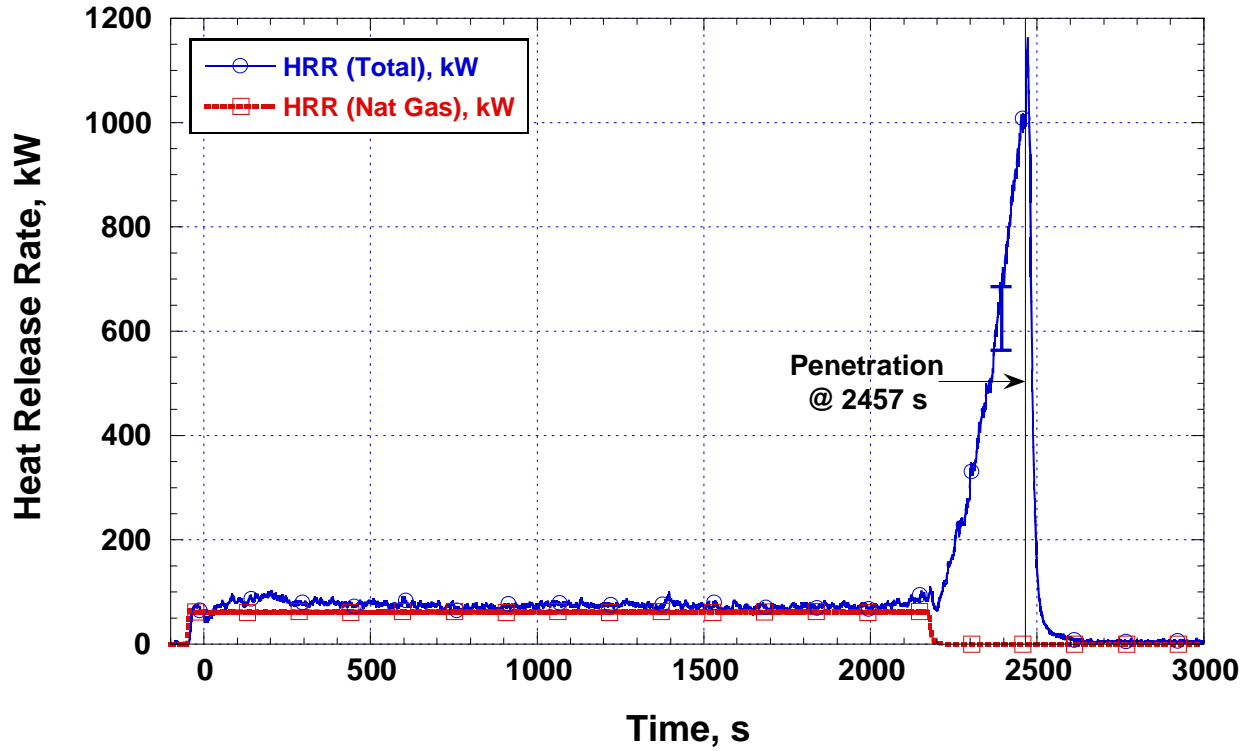


Figure 46 Heat release rate plotted versus time for test 1, the heated tag axle wheel passenger compartment penetration experiment.

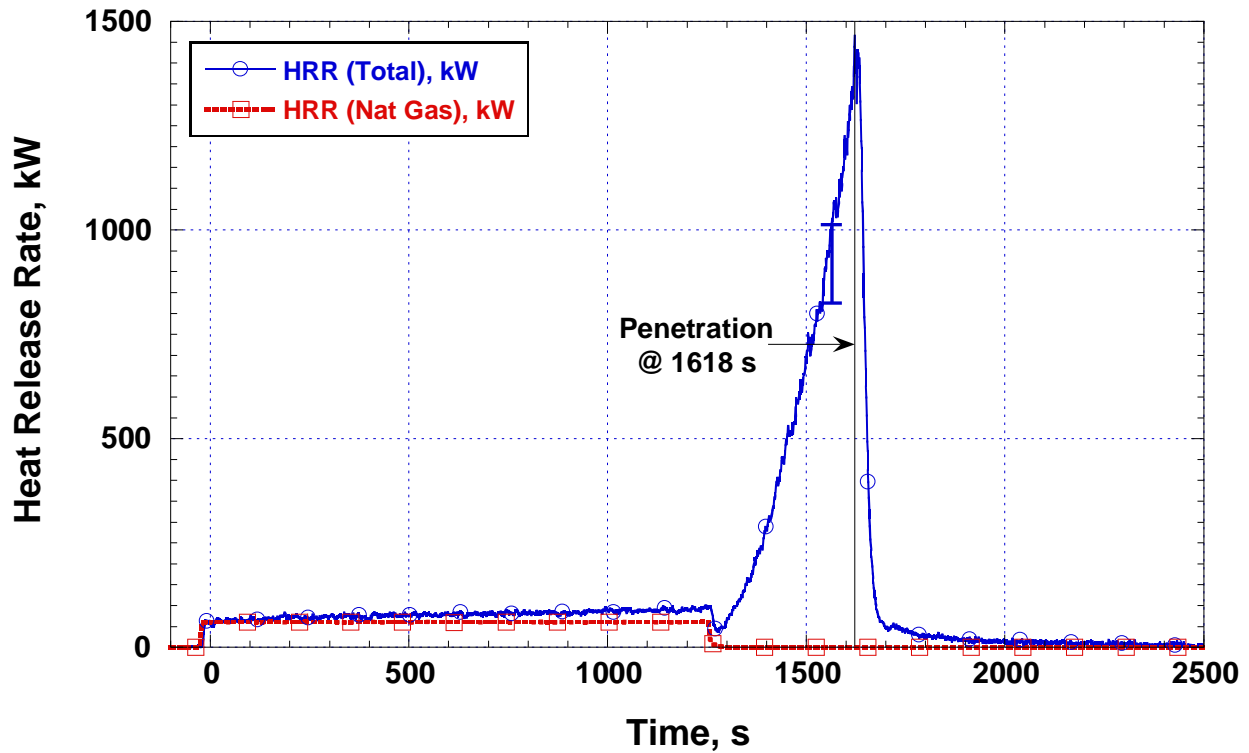


Figure 47 Heat release rate plotted versus time for test 2, the heated drive axle wheel passenger compartment penetration experiment.

Wheel, Tire, and Wheel Well Temperatures

For thermocouples on surfaces exposed to heating by the burner, the measured temperatures have approximate uncertainties of ± 10 °C. For gas temperatures in this and following sections, thermocouples impinged by fire may have recorded temperatures as much as 10 % (90 °C) low for a 600 °C reading and 20 % (220 °C) low for an 850 °C reading. Thermocouples located in relatively cool areas but with optical views of the fire plume may have measured temperatures higher than the actual surrounding gas temperatures due to heating by thermal radiation. The extent of this temperature error depends on the temperature of the plume and the thermocouple's view factor of the plume, but the magnitude of error could be tens of degrees Celsius.

Figure 48 and Figure 49 are plots of temperature versus time for the wheel and tire thermocouples on the right side of the motorcoach. Figure 15 shows the labeling scheme used in the plot legends, and Appendix A provides more detailed location descriptions for these and subsequent plots. For the heated tag axle wheel experiment, the wheel temperatures only led the tire temperatures by about 40 °C. As shown in Table 11, some intermittent ignition of the tire was occurring at 1860 s. By that point, the tire temperatures at the top and bottom positions had exceeded 360 °C. At that same time, the maximum wheel temperatures had just surpassed 400 °C. For the heated drive axle wheel experiment, the wheel temperatures led the tire temperatures by 100 °C to 150 °C. This is easily explained by the fact that the tire temperatures were measured on the outside interface between the tire and wheel rim, but wheel thermocouples were located on the inside surface of the wheel between the outer and inner wheels. Also, the heat from the burner was focused at the inside surface of the wheel which preferentially heated up the inside parts of the tire as well. At the time when flames were seen rising between the tires, the wheel temperatures all exceeded 420 °C. Because a lot of smoke was visible and some wheel temperatures exceeded 400 °C about 7 min prior to visible flames, it's likely that a smoldering or small flaming fire existed between the tires well before flames were seen.

Wheel well gas temperature plots are shown in Figure 50 and Figure 51. The heated tag axle wheel experiment produced the highest temperatures (850 °C) directly over the rear tire and the second highest temperatures (650 °C) directly behind and between the tag and drive axle tires. For the heated drive axle wheel experiment, all but the front most temperature exceeded (900 °C). Far (driver's) side wheel well temperatures were rising, but were below 300 °C at the time of penetration. For the minute prior to penetration, the far side wheel well temperatures rose at about 20 °C/min for the tag axle test and between 40 °C/min and 60 °C/min for the drive axle test.

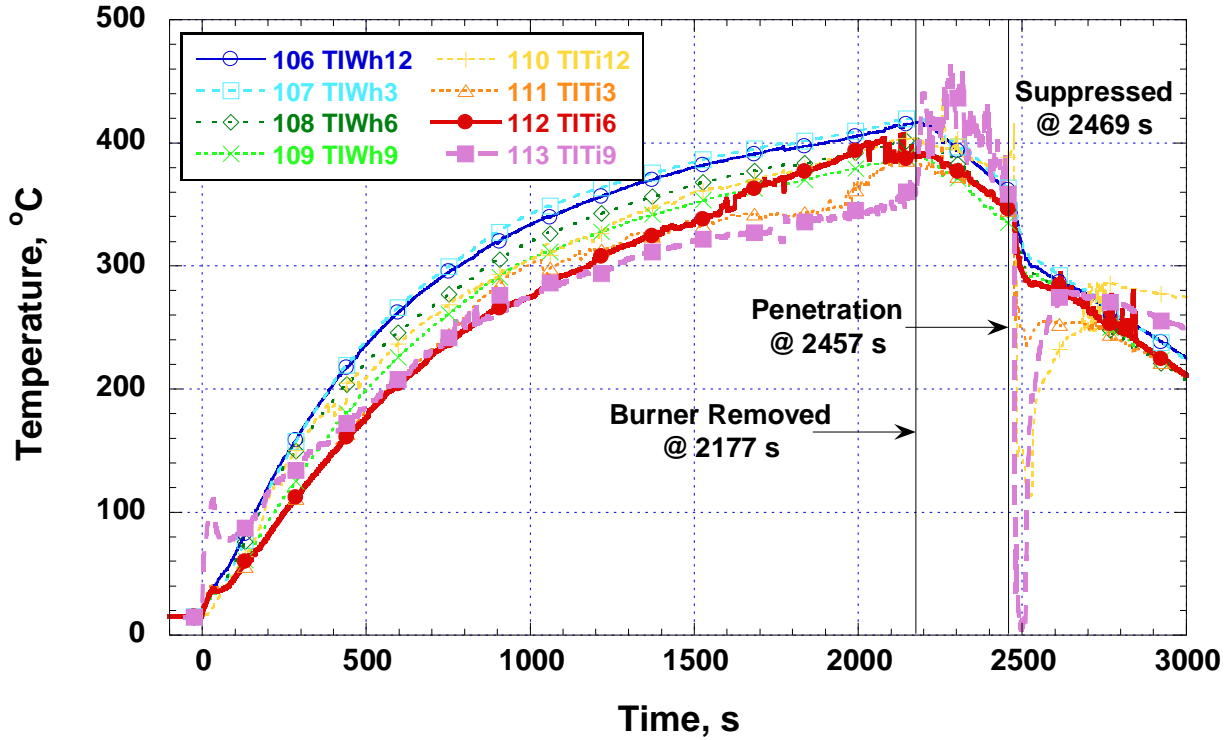


Figure 48 A plot of test 1 (tag axle) temperatures versus time for the heated wheel (Wh) and tire (Ti). Numbers in the labels represent 12, 3, 6, and 9 o'clock positions (0°, 90°, 180°, and 270° from top).

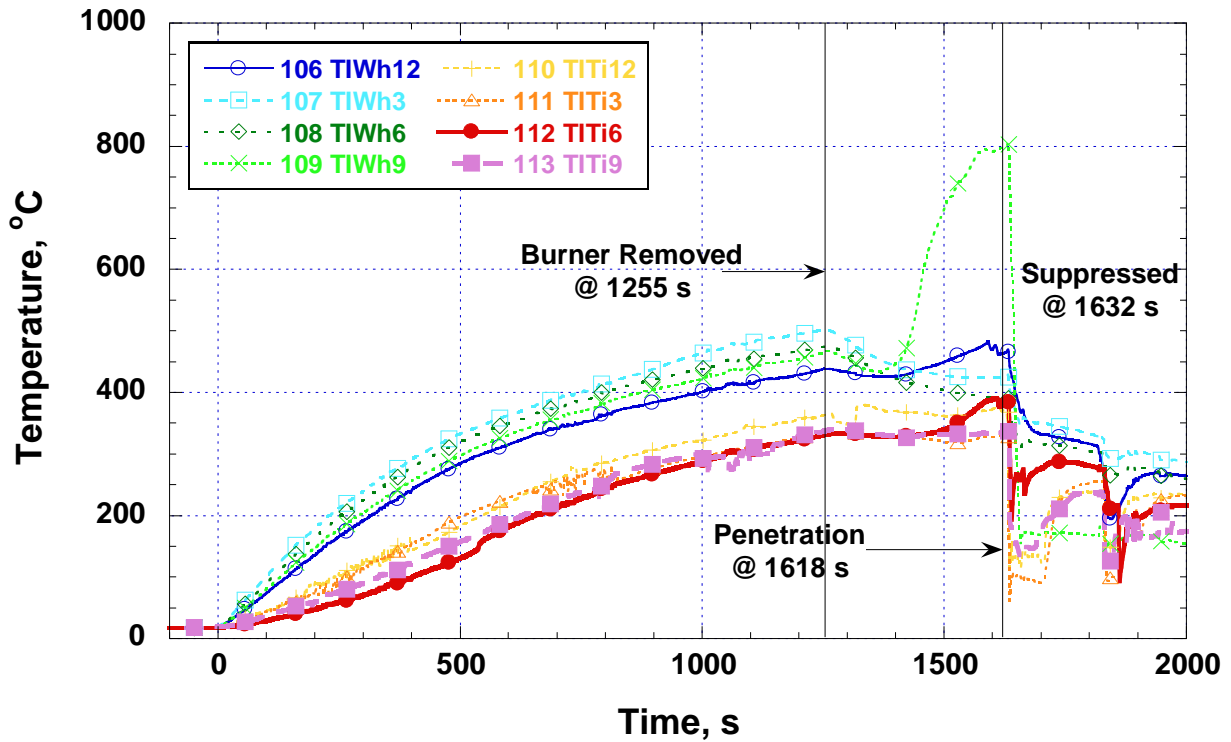


Figure 49 A plot of test 2 (drive axle) temperatures versus time for the heated wheel (Wh) and tire (Ti). Numbers in the labels represent 12, 3, 6, and 9 o'clock positions (0°, 90°, 180°, and 270° from top).

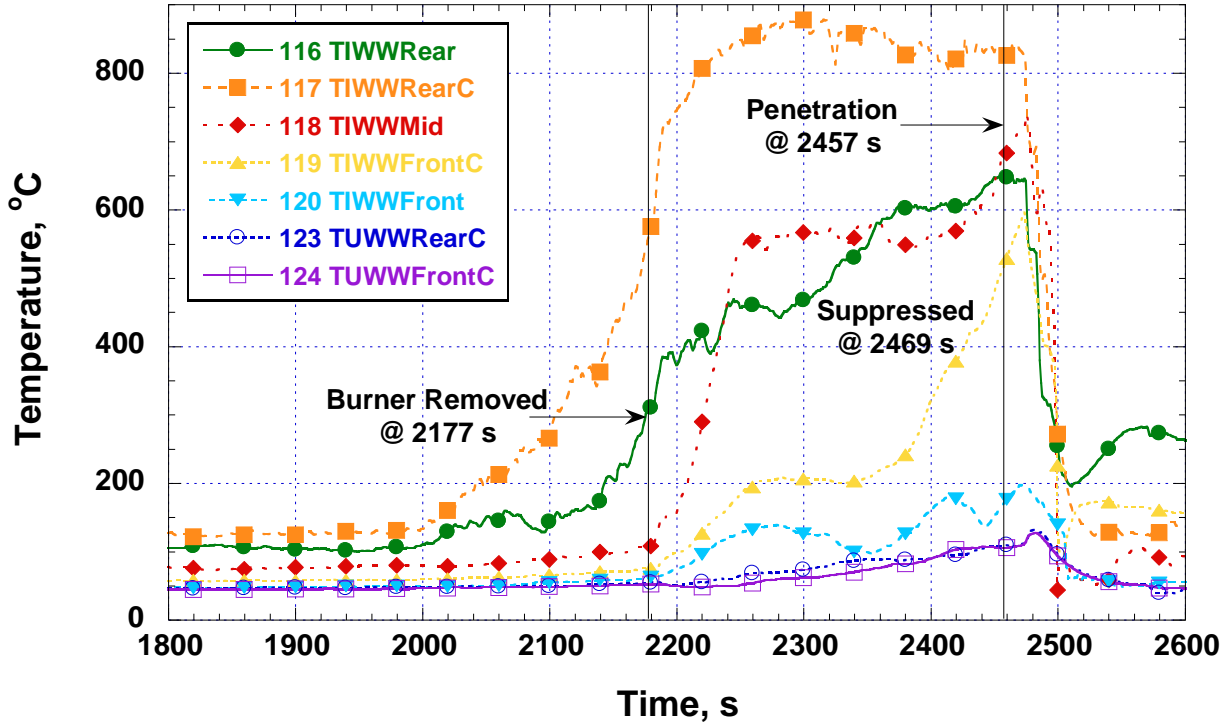


Figure 50 A plot of test 1 (tag axle) temperatures versus time for the wheel wells. I and U represent ignited and unignited sides, respectively.

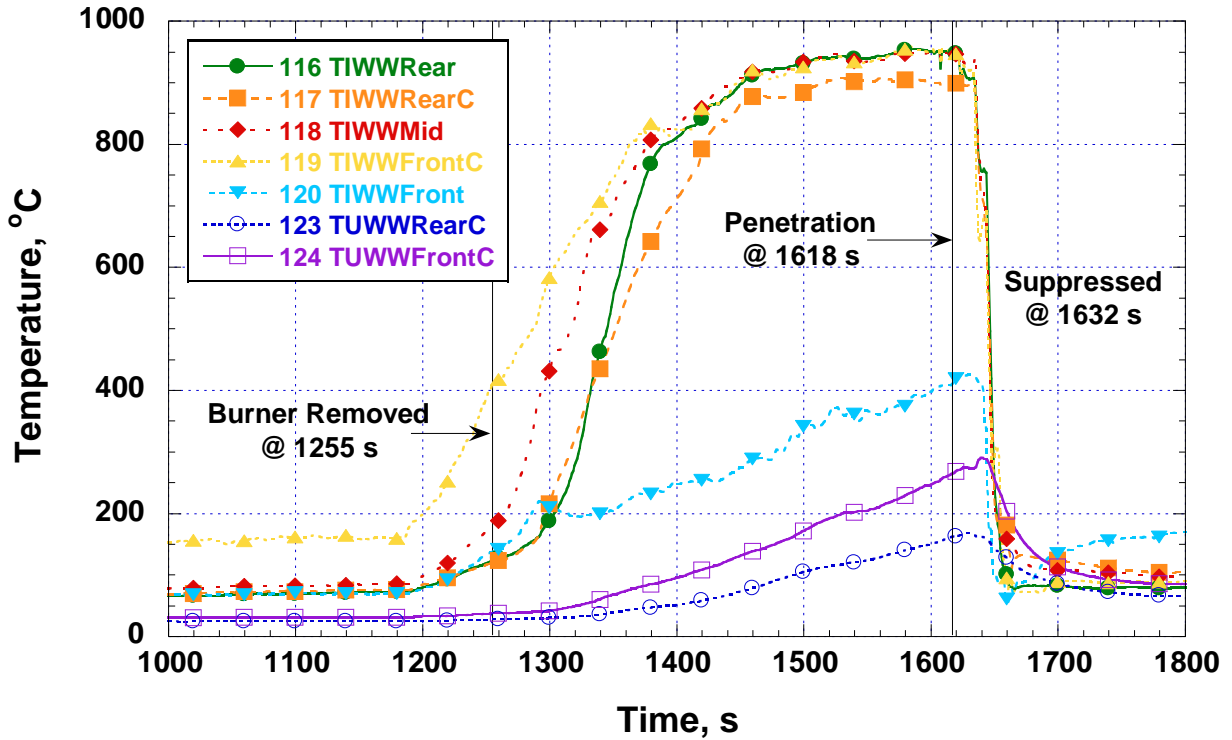


Figure 51 A plot of test 2 (drive axle) temperatures versus time for the wheel wells. I and U represent ignited and unignited sides, respectively.

Window and Panel Temperatures

Figure 52 and Figure 53 are plots from both experiments showing temperature versus time for the exterior thermocouples located over the GRP paneling just below the window line. Refer to Figure 16 for the exterior thermocouple locations and Figure 17 for the interior locations. The plots show that before penetration for both experiments, the temperatures in columns 5 to 9 were much higher than those for columns 1 to 4 and 10 to 12 with the exception of column 7 for test 2 which had a lower temperature. For both tests, the temperatures for columns 5 to 9 ranged from 600 °C to 850 °C except for test 2 column 7 which had a temperature of 400 °C at penetration. Column 7 is located just forward of the midpoint between the two axles so the separate fire plumes apparently did not affect the space between the plumes as severely as they did the space directly above them.

Figure 54 and Figure 55 are plots from both experiments showing temperature versus time for the highest exterior thermocouples located near the tops of the windows. For test 1, columns 5 to 9 are again the hottest. For test 2, temperatures in columns 8 and 9 are high early with columns 5 and 6 (over the tag axle tire) lagging behind by about 1.5 min and 3 min, respectively. As with the lowest position on the panel, column 7's temperature lags even farther behind since it is in between the main plumes.

Figure 56 and Figure 57 are plots from both experiments showing temperature versus time for the lowest interior thermocouples located about 3 cm from the bottom of the windows. For test 1, the column 6 thermocouple approached 200 °C for about 30 s and briefly exceeded 600 °C at penetration while the other interior temperatures remained below 100 °C. This indicates that the windows acted as somewhat effective thermal barriers until actual penetration, which occurred near column 6. For test 2, column 8 temperatures rose steadily to 200 °C for the 3 min prior to penetration and then quickly exceed 500 °C along with the column 9 temperature. Again, except when breakthrough occurred, the temperatures remained relatively low.

Figure 58 and Figure 59 are plots from both experiments showing temperature versus time for the hottest columns of interior TCs, column 6 and column 8 for test 1 and test 2, respectively. T3 is the lowest position and T0 is above the window. For test 1, column 6 temperature in position T3 rises from 60 °C to 200 °C in the 25 s prior to penetration. T1 and T2 rise from about 45 °C to about 70 °C in the 25 s prior to penetration. For test 2, column 8 temperatures except for position T0 rise from about 200 °C to about 400 °C in the 30 s before penetration. Both plots show a rapid degradation of the windows in the 30 s prior to penetration, when temperature changes inside the window accelerate dramatically.

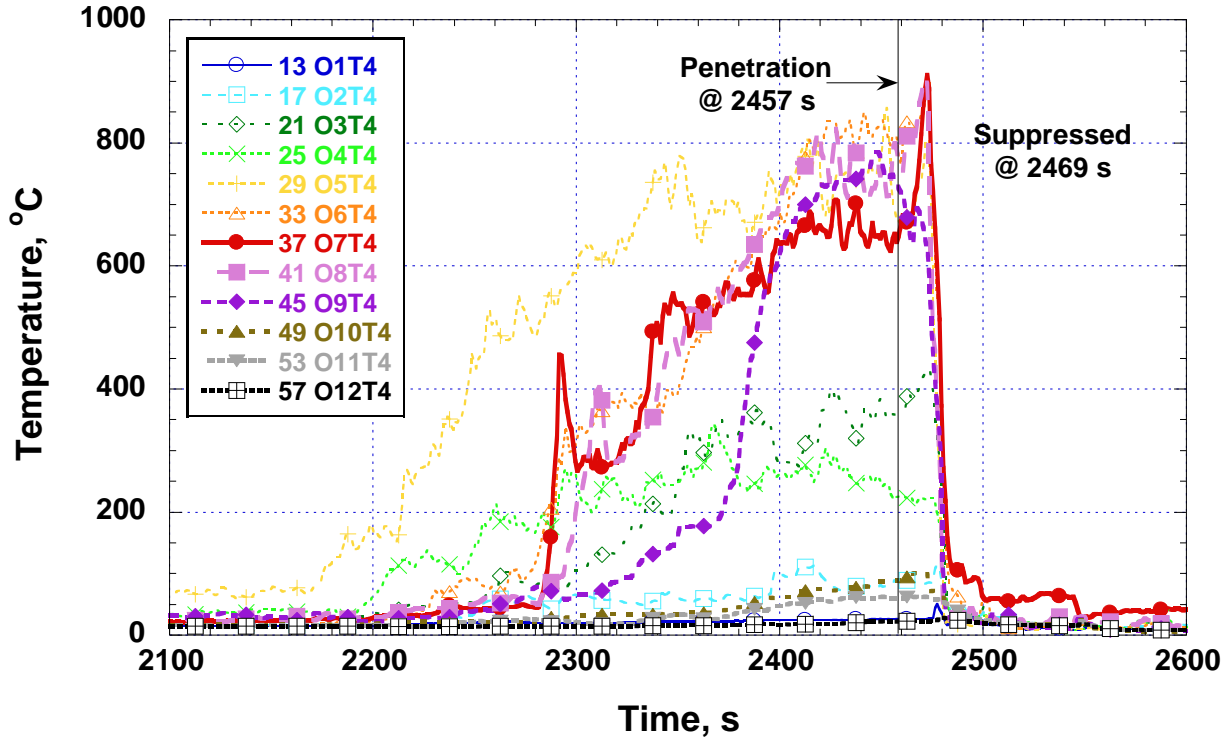


Figure 52 A plot of test 1 (tag axle) temperatures versus time for the lowest row of exterior TCs located below the window line 1 cm from the exterior GRP panel. See Figure 16 for labeling system.

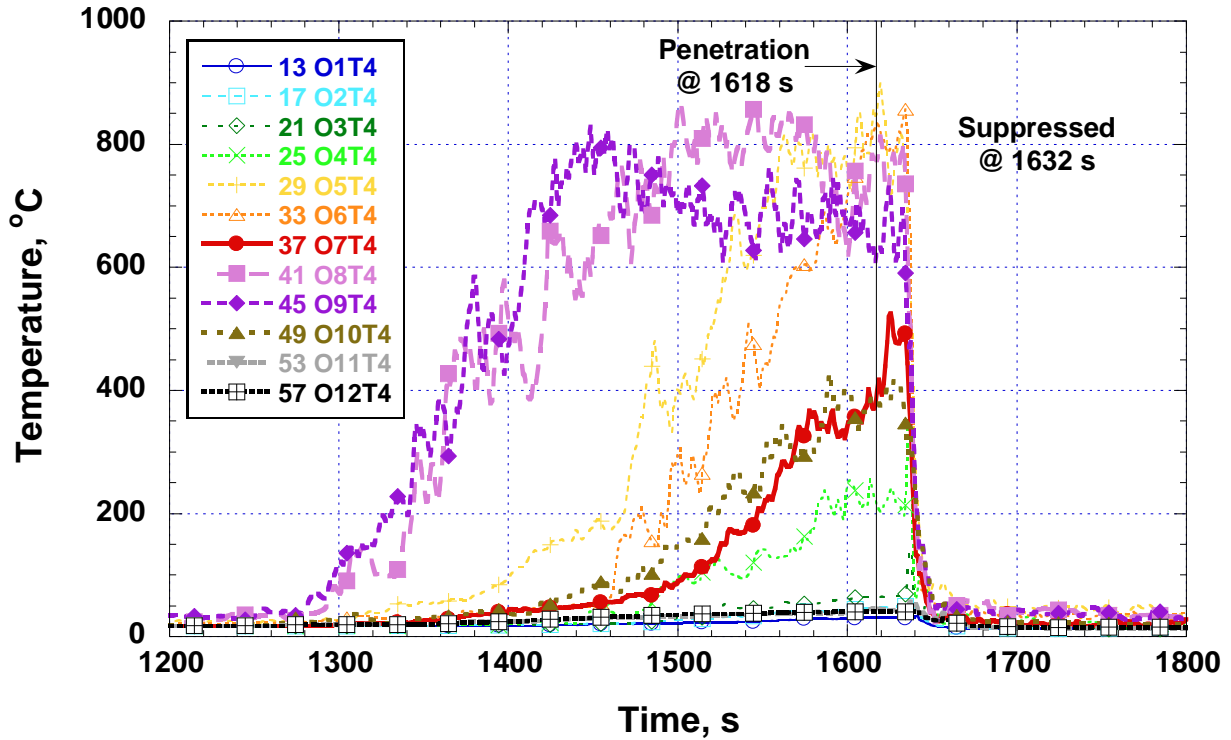


Figure 53 A plot of test 2 (drive axle) temperatures versus time for the lowest row of exterior TCs located below the window line 1 cm from the exterior GRP panel. See Figure 16 for labeling system.

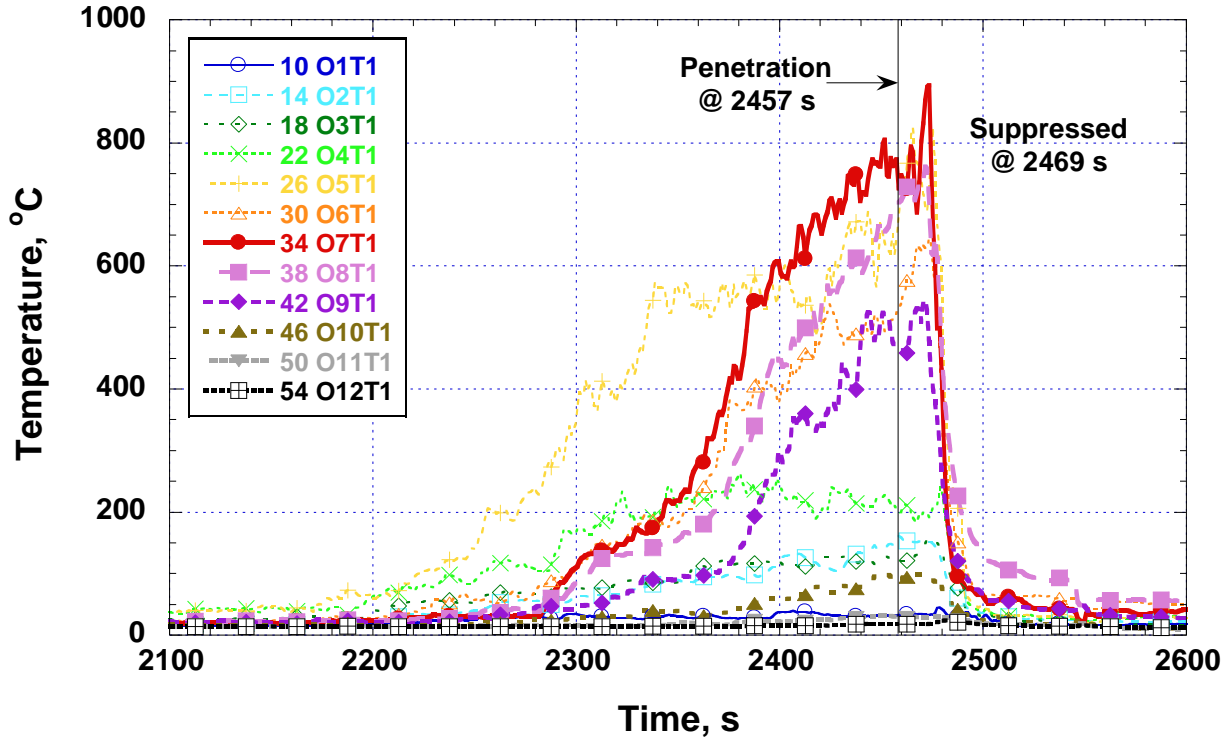


Figure 54 A plot of test 1 (tag axle) temperatures versus time for the highest row of exterior TCs located 1 cm from window surfaces and about 10 cm from the top of the windows. Figure 16 shows labeling.

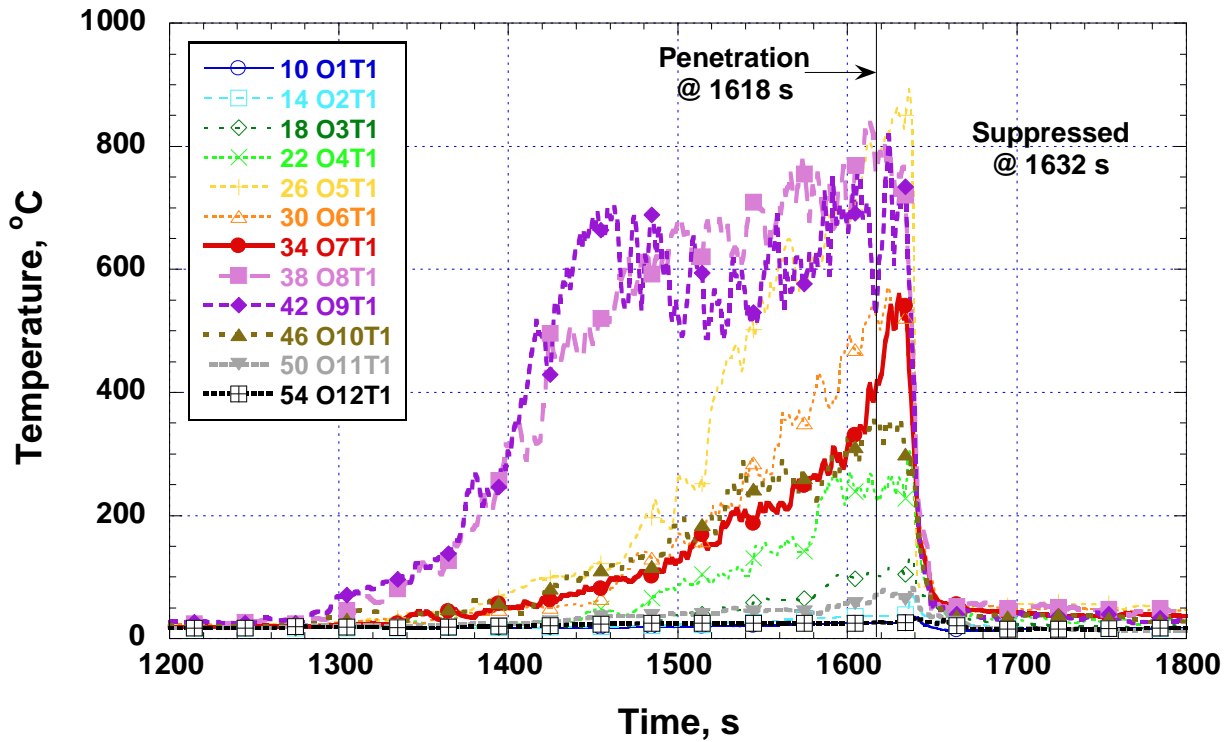


Figure 55 A plot of test 2 (drive axle) temperatures versus time for the highest row of exterior TCs located 1 cm from window surfaces and about 10 cm from the top of the windows. Figure 16 shows labeling.

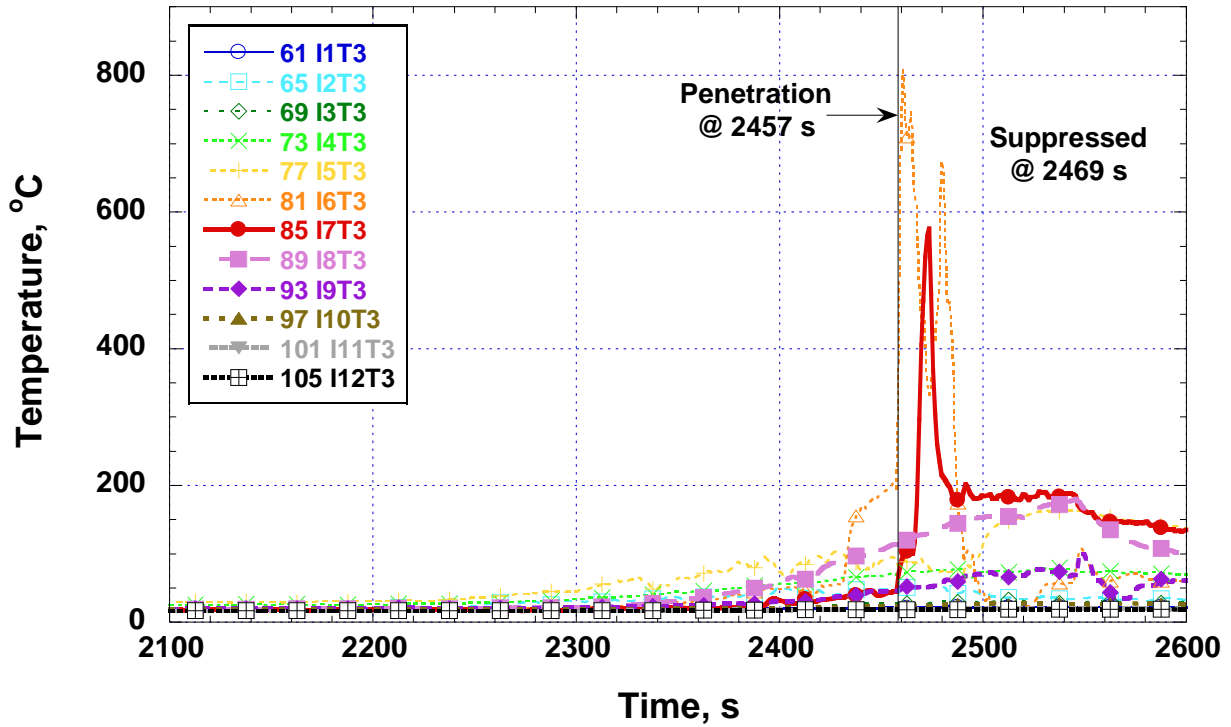


Figure 56 A plot of test 1 (tag axle) temperatures versus time for the lowest row of interior TCs, 1 cm from window surfaces and about 3 cm from the bottom of the windows. Figure 17 shows labeling.

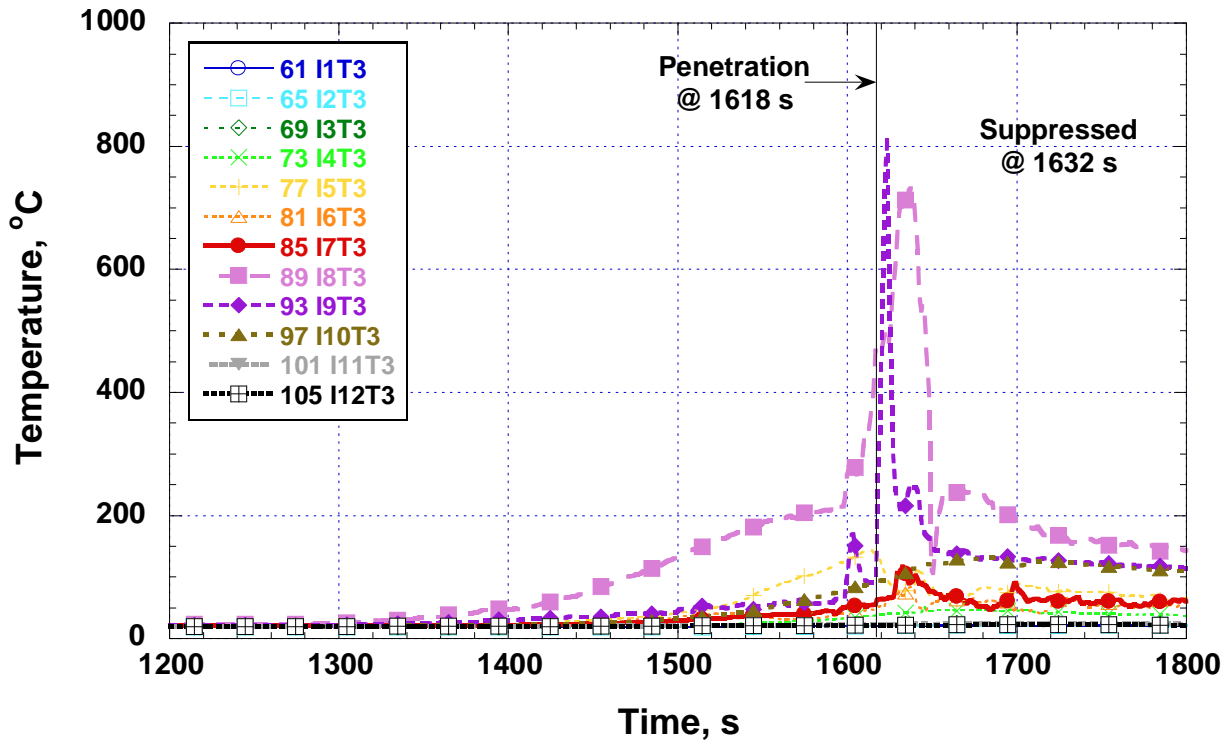


Figure 57 A plot of test 2 (drive axle) temperatures versus time for the lowest row of interior TCs, 1 cm from window surfaces and about 3 cm from the bottom of the windows. Figure 17 shows labeling.

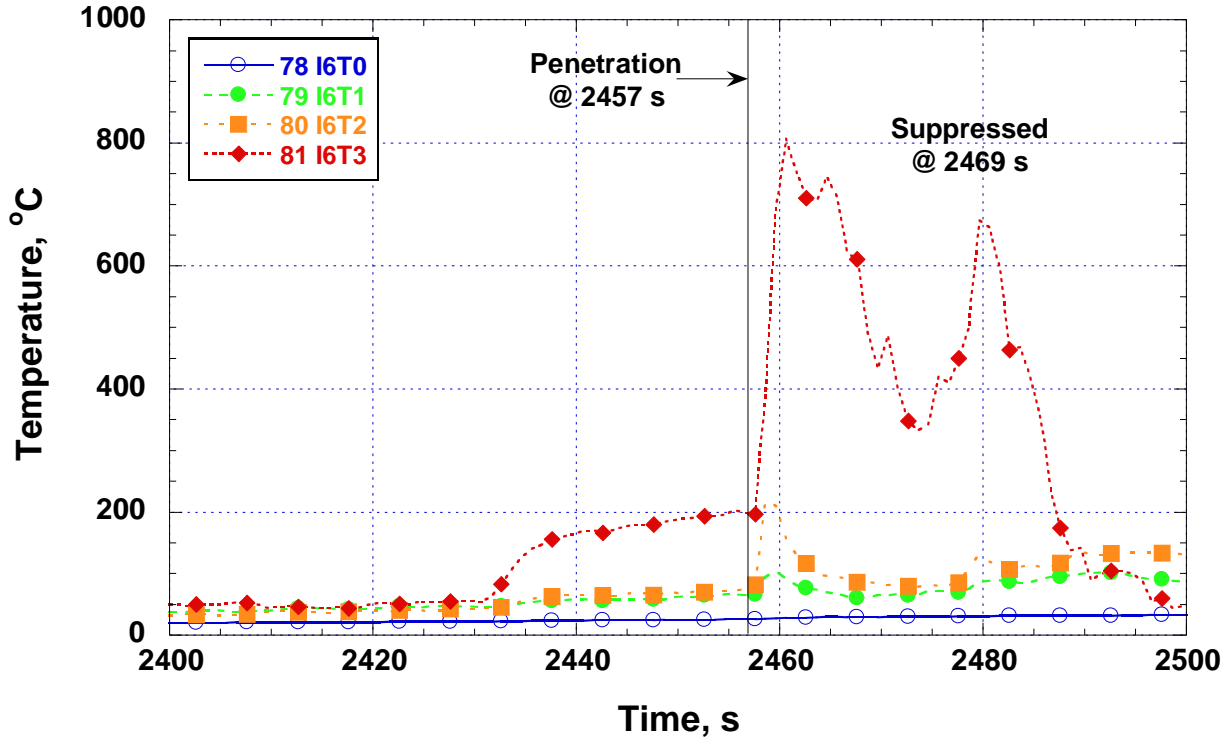


Figure 58 A plot of test 1 (tag axle) temperatures versus time for the hottest column of interior TCs, array 6, 1 cm from window. T0 was located above the window. See Figure 17 for labeling system.

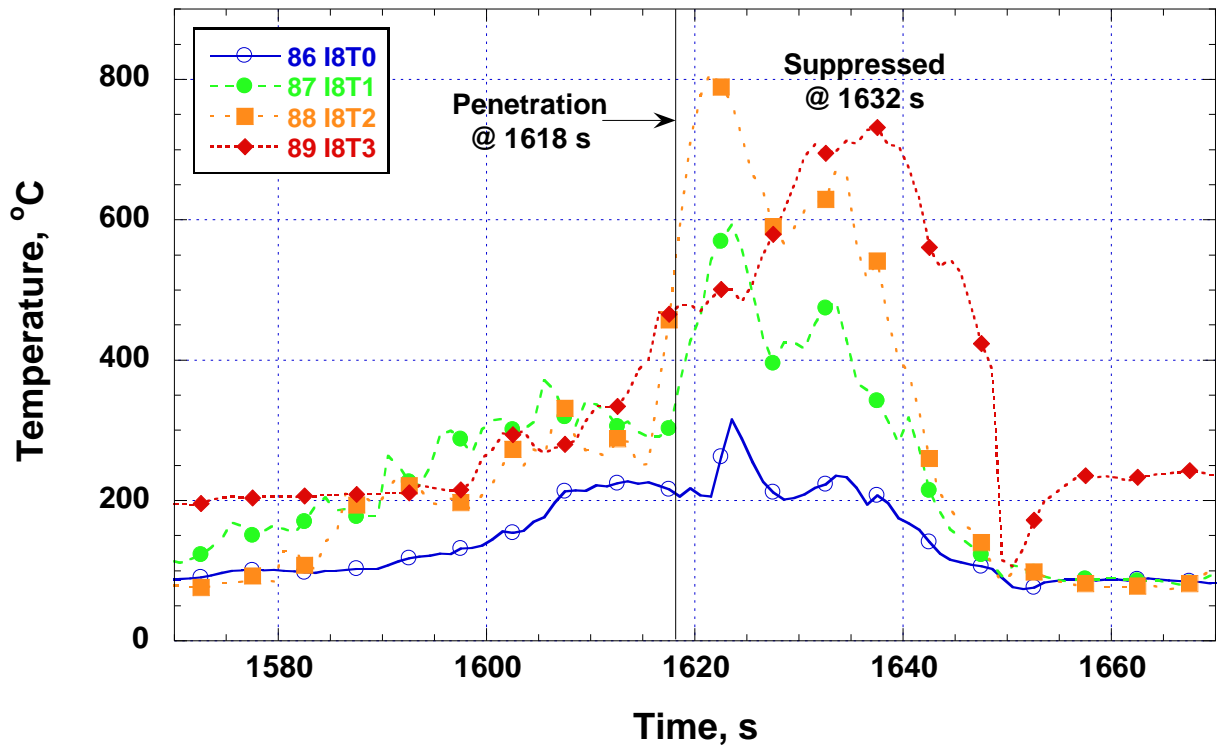


Figure 59 A plot of test 2 (drive axle) temperatures versus time for the hottest column of interior TCs, array 8, 1 cm from window. T0 was located above the window. See Figure 17 for labeling system.

Floor, Lavatory, and Central Tunnel Temperatures

Floor, lavatory floor, and central tunnel temperatures were monitored because the path of the fire penetration into the passenger compartment was unknown, and the floor was believed to have a significant possibility of being that path. The central tunnel runs under the central aisle and contains tubing and wiring harnesses. Refer to Table 8 and Figure 18 to review locations of these measurements. Figure 60 and Figure 61 show the temperatures of thermocouples along the floor by the right side wall. All of the temperatures exhibited barely any impact from the nearby fire and remained near the ambient starting temperatures. This revealed that the floor structure for this particular motorcoach was insulated from the tire fire's heat. Inspection of the floor design showed between 15 cm and 20 cm of fiberglass thermal insulation under the floor in the vicinity of the fire. Figure 61 does show a sharp rise in temperature just before test 2 penetration midway between the tires, but it is only a rise of about 15 °C and may be related to a piece of glass with burning laminate or other debris that fell from the window.

The lavatory floor temperatures shown in Figure 62 and Figure 63 only rose about 1 °C during each test. The floor area near the lavatory is similarly protected from heating from below as the floor areas near the motorcoach walls.

The central tunnel plots of temperature in Figure 64 and Figure 65 show some heating. The test 1 front position rose 7 °C, but the change occurred after penetration and extinguishment. The test 2 front position rose over 25 °C prior to penetration and the center position rose about 15 °C after penetration.

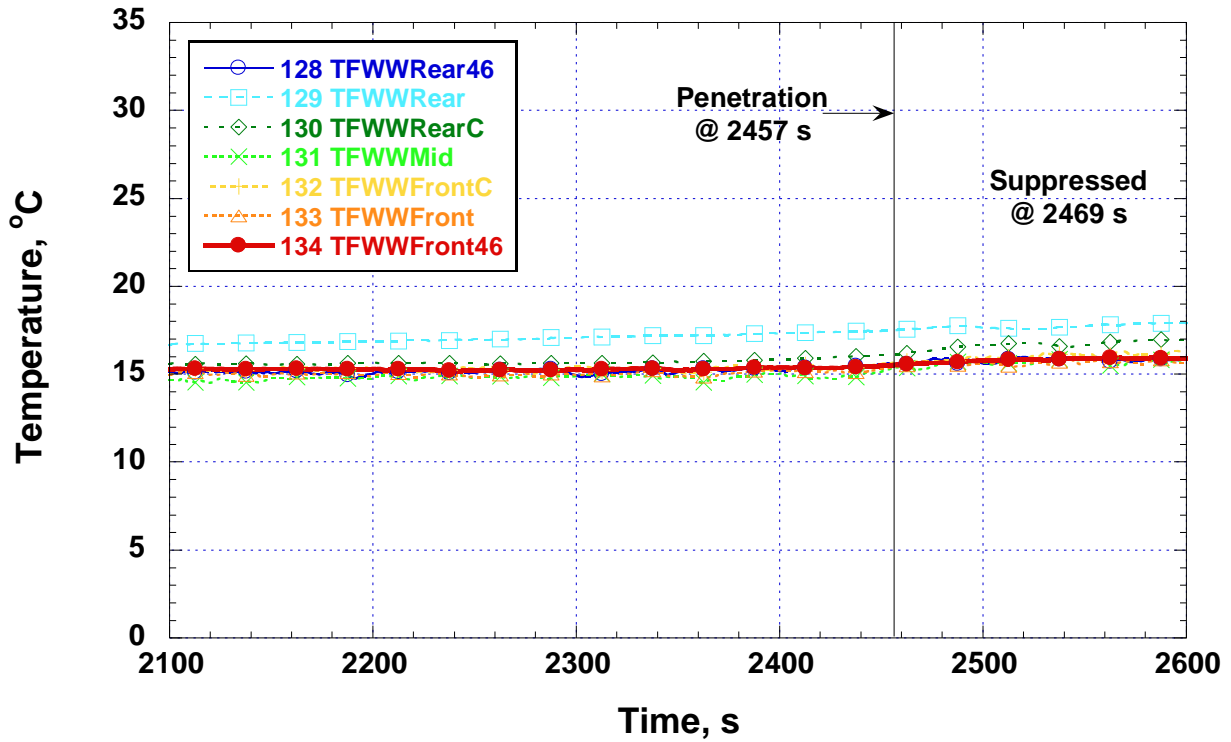


Figure 60 A plot of test 1 (tag axle) temperatures versus time for TCs on the interior floor at the bottom of the right side wall. Table 8 and Figure 18 describe thermocouple locations.

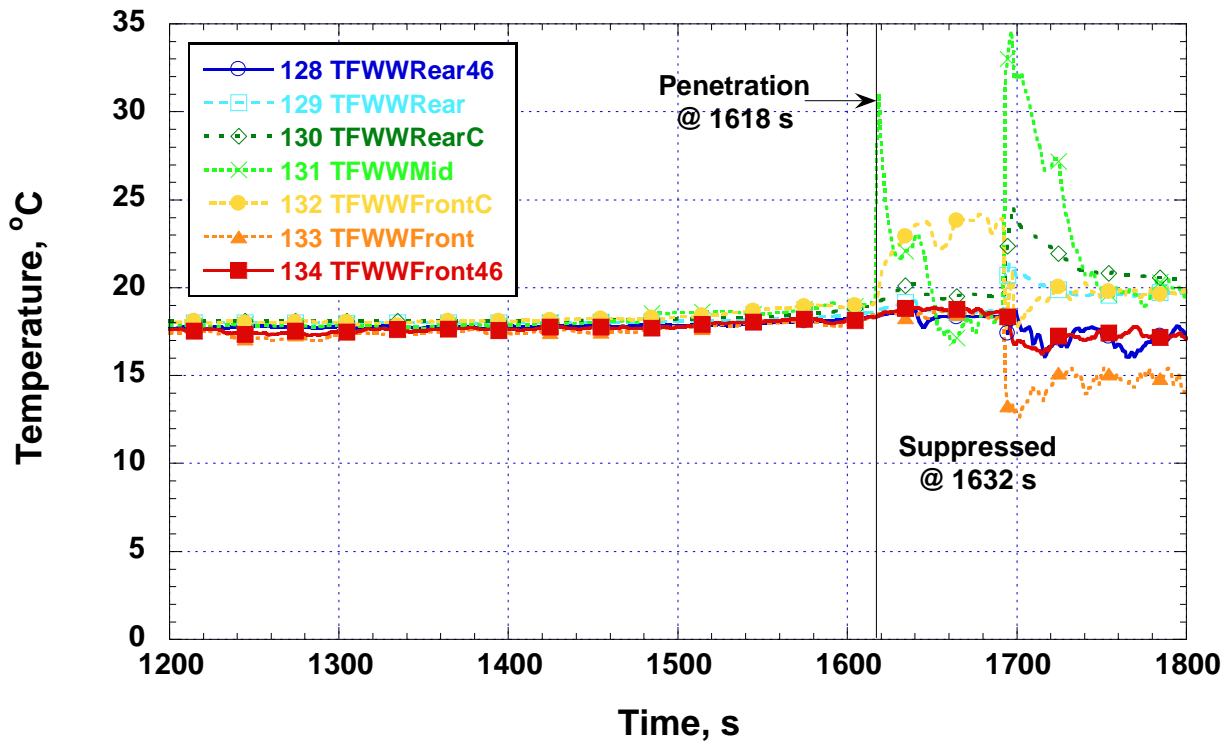


Figure 61 A plot of test 2 (drive axle) temperatures versus time for TCs on the interior floor at the bottom of the right side wall. Table 8 and Figure 18 describe thermocouple locations.

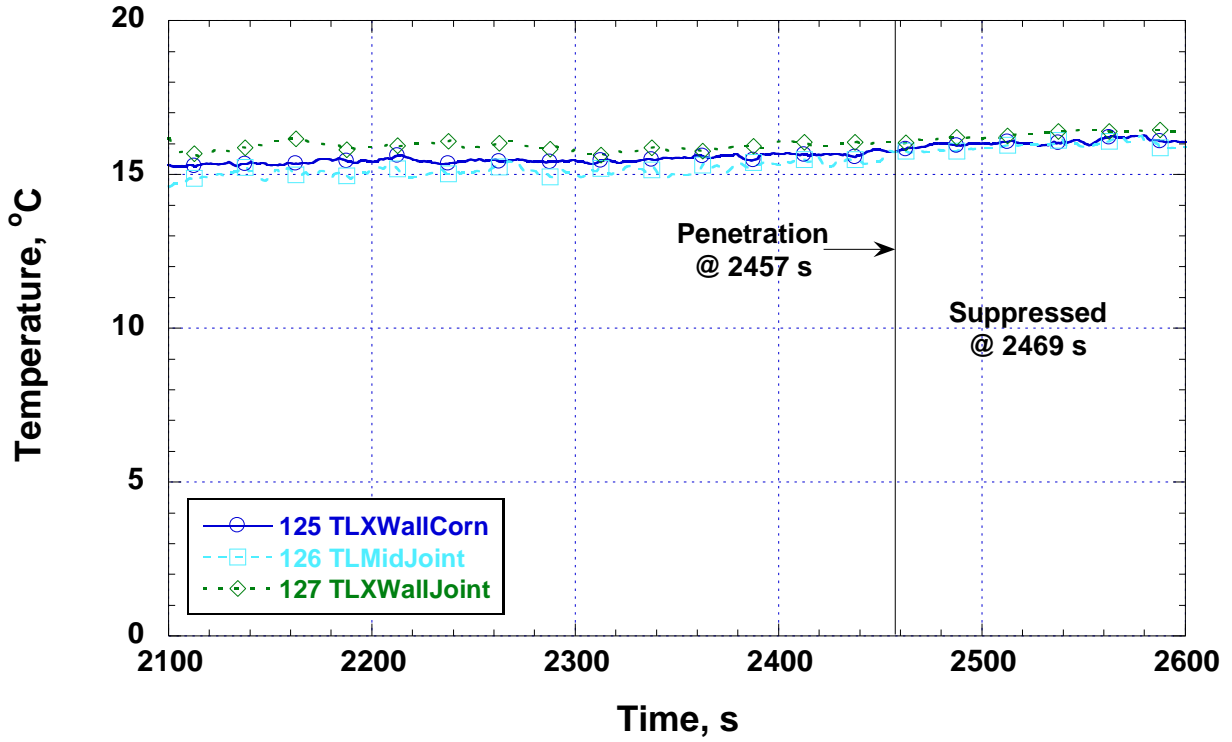


Figure 62 A plot of test 1 (tag axle) temperatures versus time for TCs on the interior floor where the lavatory walls join the exterior wall and floor in the middle of the coach. See Table 8 and Figure 18.

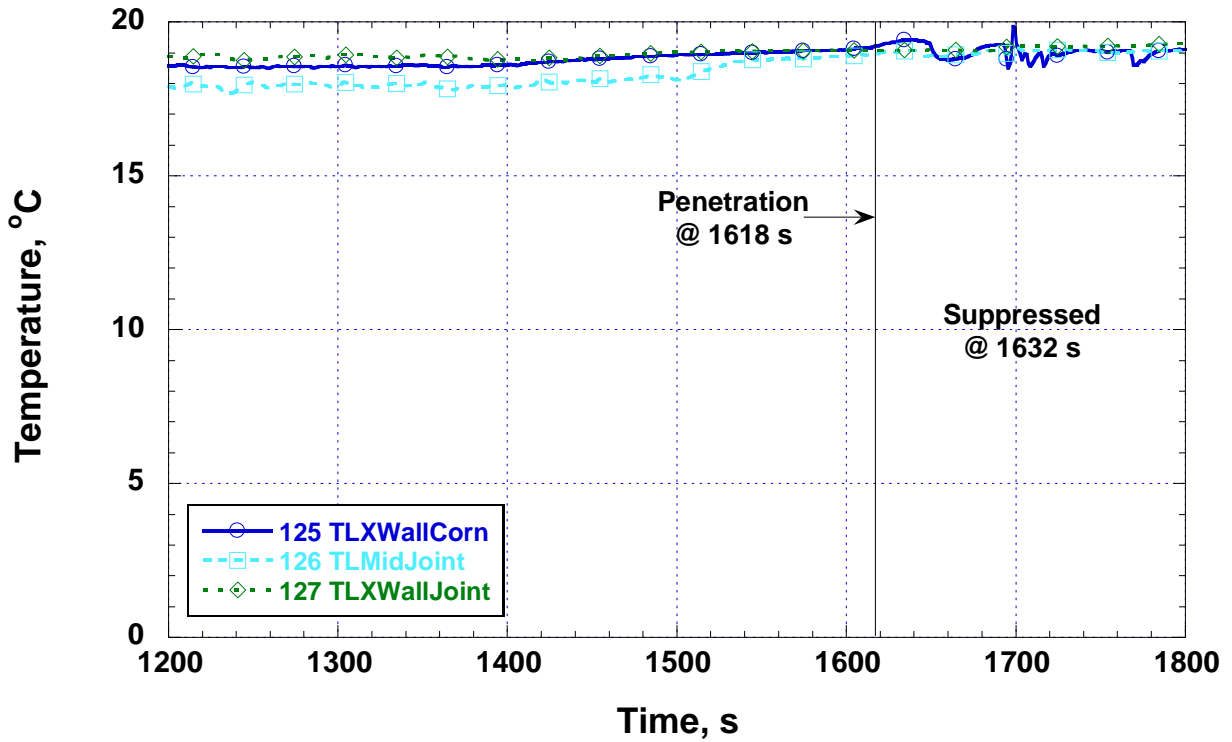


Figure 63 A plot of test 2 (drive axle) temperatures versus time for TCs on the interior floor where the lavatory walls join the exterior wall and floor in the middle of the coach. See Table 8 and Figure 18.

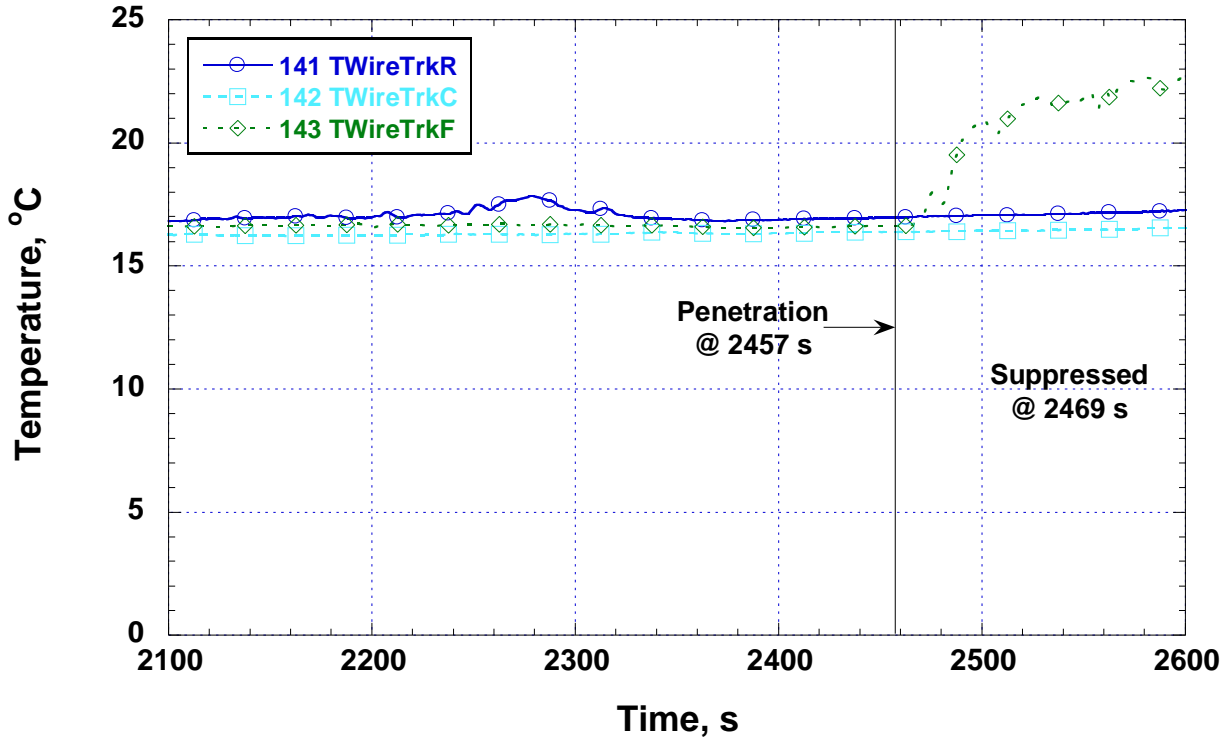


Figure 64 A plot of test 1 (tag axle) temperatures versus time for TCs inside the central tunnel for wires under the interior floor along the centerline of the coach. R, C, and F represent rear, center, and front, respectively, of the test section. Table 8 and Figure 18 describe thermocouple locations.

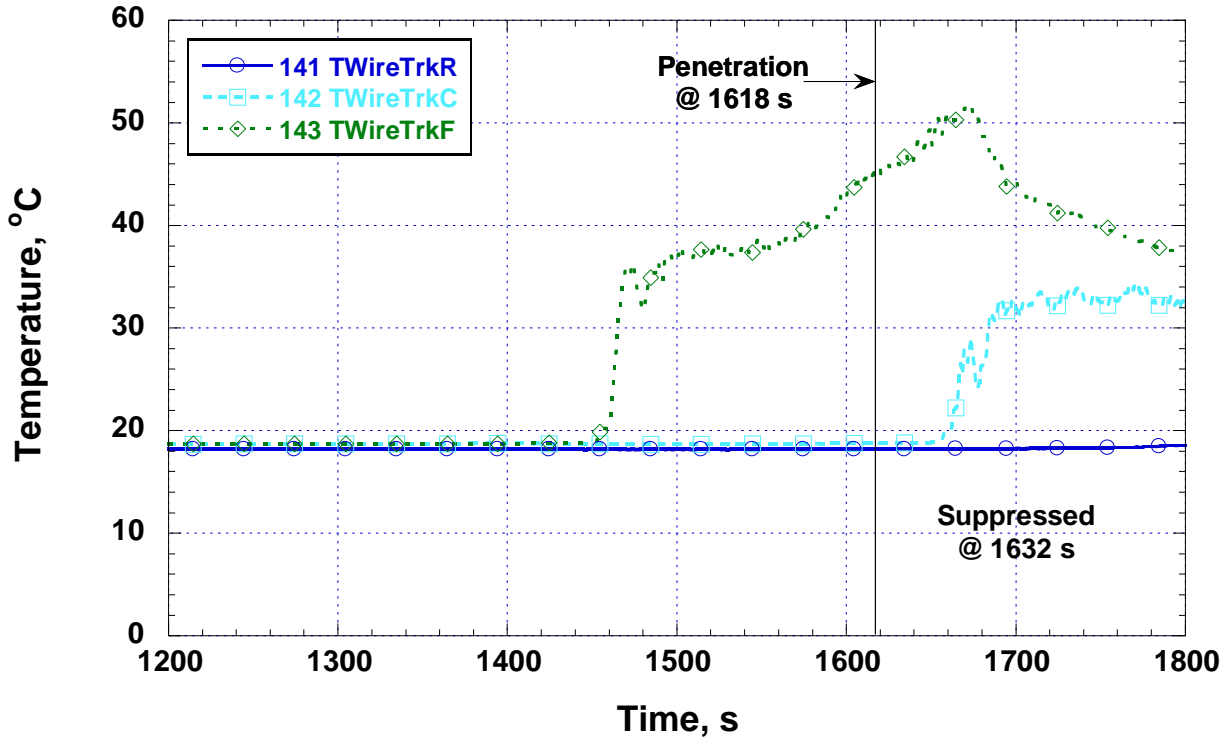


Figure 65 A plot of test 2 (drive axle) temperatures versus time for TCs inside the central tunnel for wires under the interior floor along the centerline of the coach. R, C, and F represent rear, center, and front, respectively, of the test section. Table 8 and Figure 18 describe thermocouple locations.

Axle Temperatures

Possible spread of fire along the axles and upward through the floor or to the far side tires and panels was a concern that prompted monitoring of these regions. Figure 66 and Figure 67 are plots of temperature for test 1 and 2, respectively, for the thermocouples located above the two axles. In Figure 66, for the tag axle wheel heating test, both of the right (passenger) side thermocouples over each axle showed significant heating with the tag axle at a maximum temperature of 700 °C and the drive axle maximum at 450 °C. It is surprising that the tag axle right side temperature reached its maximum over 2 min prior to penetration and then dropped down to 350 °C. One possible reason for this is that while the tire continued to burn and flames spread upward to the exterior panel, the fender was consumed more quickly, and its contribution to the fire decreased which provided less hot gases in lower areas such as along the axle. For test 1, the center and driver's (left) side axle temperatures barely exceeded 100 °C before window penetration.

For test 2, Figure 67 shows the drive axle right (passenger) side and center thermocouples rising to 950 °C and 550 °C, respectively. Even the drive axle driver's side thermocouple rose to 300 °C before penetration which is significant in that temperatures over 400 °C generally will ignite combustible materials such as the tire and GRP panels. While right side and center position axle temperatures greater than 550 °C were significant for causing ignition of nearby combustible materials, the interior floor and central tunnel temperatures showed very little thermal penetration. The far (left side) position rose past 300 °C at about 50 °C /min, but it is unknown whether this rate would have continued and whether or not combustible materials would have eventually ignited if the fire were allowed to continue.

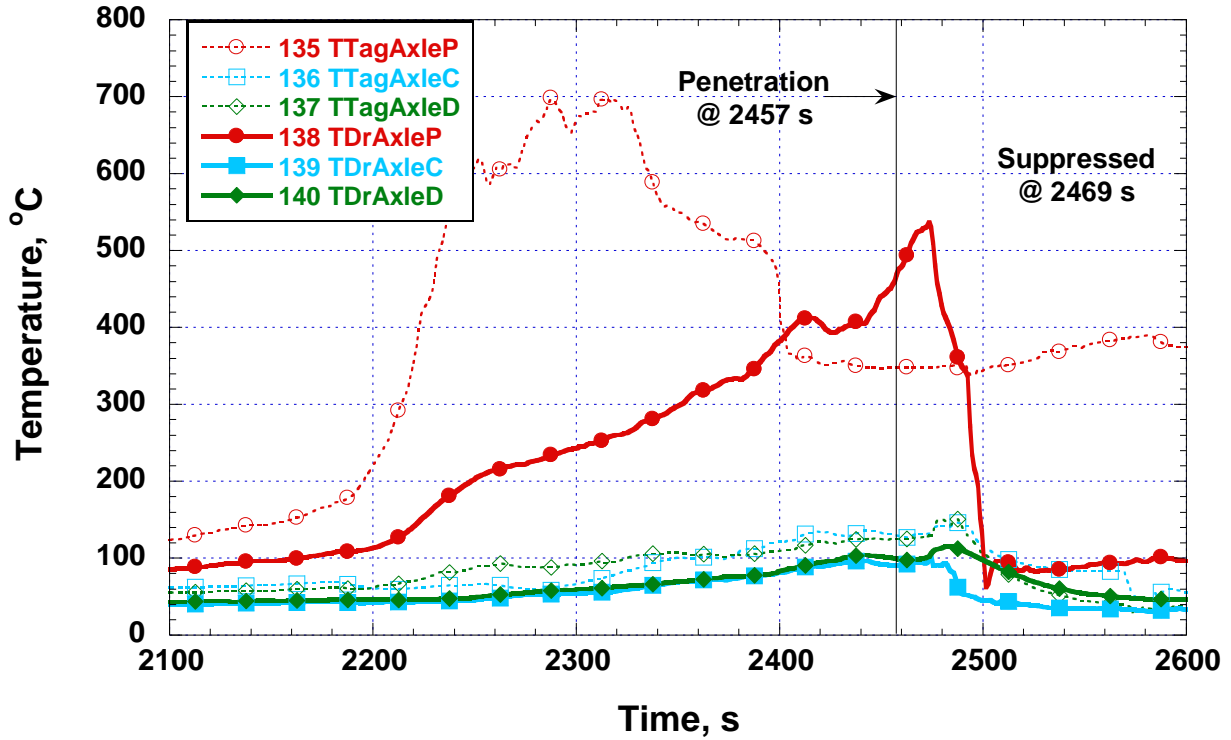


Figure 66 A plot of test 1 (tag axle) temperatures versus time for TCs above the two axles. P, C, and D represent passenger (right) side, center, and driver (left) side, respectively.

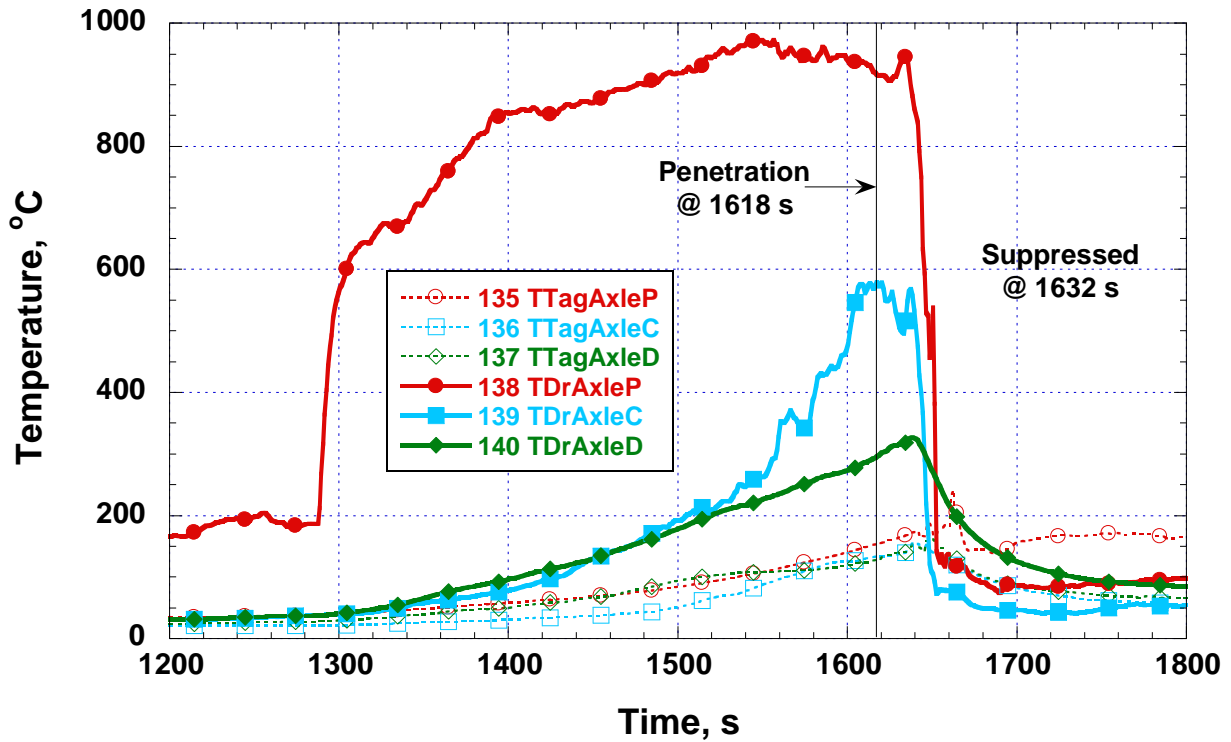


Figure 67 A plot of test 2 (drive axle) temperatures versus time for TCs above the two axles. P, C, and D represent passenger (right) side, center, and driver (left) side, respectively.

Heat Fluxes

Table 9 lists the locations and orientations of the heat flux gauges corresponding to the following results. Figure 68 and Figure 69 show the heat flux measurements for test 1 (tag axle wheel heating) and test 2 (drive axle wheel heating), respectively. For test 1, only the seat position heat flux rose significantly to about 1.5 kW/m^2 before penetration. After penetration, despite extinguishment activities, the heat flux increased to about 4 kW/m^2 , probably due to the impact of the penetrating fire plume quickly heating the interior even for just the brief period. The other fluxes in test 1 remained below 0.4 kW/m^2 before penetration. At the time of penetration, the accumulated thermal radiation at the seat location was about 16 % of an incapacitating dose. This type of analysis is described in the Thermal Tenability Analysis section.

For test 2, the seat position heat flux rose to about 3 kW/m^2 before penetration and the front side facing gauge rose to 1.5 kW/m^2 . The other fluxes remained below 0.5 kW/m^2 . At the time of penetration, the accumulated thermal radiation at the seat location was about 68 % of an incapacitating dose. About 2 s before penetration, the radiative heat flux passed the 2.5 kW/m^2 tenability limit for exposure of skin to radiant heat.

The heat flux required for piloted ignition of materials such as fabric covered seat cushions is typically greater than 6 kW/m^2 . [46] The situation in these experiments was unpiloted which requires much greater heat flux for ignition so the thermal radiation through the windows was not nearly enough to ignite combustible materials inside. At the stages of growth of the tire/motorcoach fires upon window penetration, the heat fluxes were not sufficient alone to ignite the seat material before or after the window breakage. Without extinguishment, additional glass breakage and further fire growth would have allowed greater heat fluxes on the interior materials as well as direct impingement of hot gases and flames leading to ignition by thermal radiation alone or piloted.

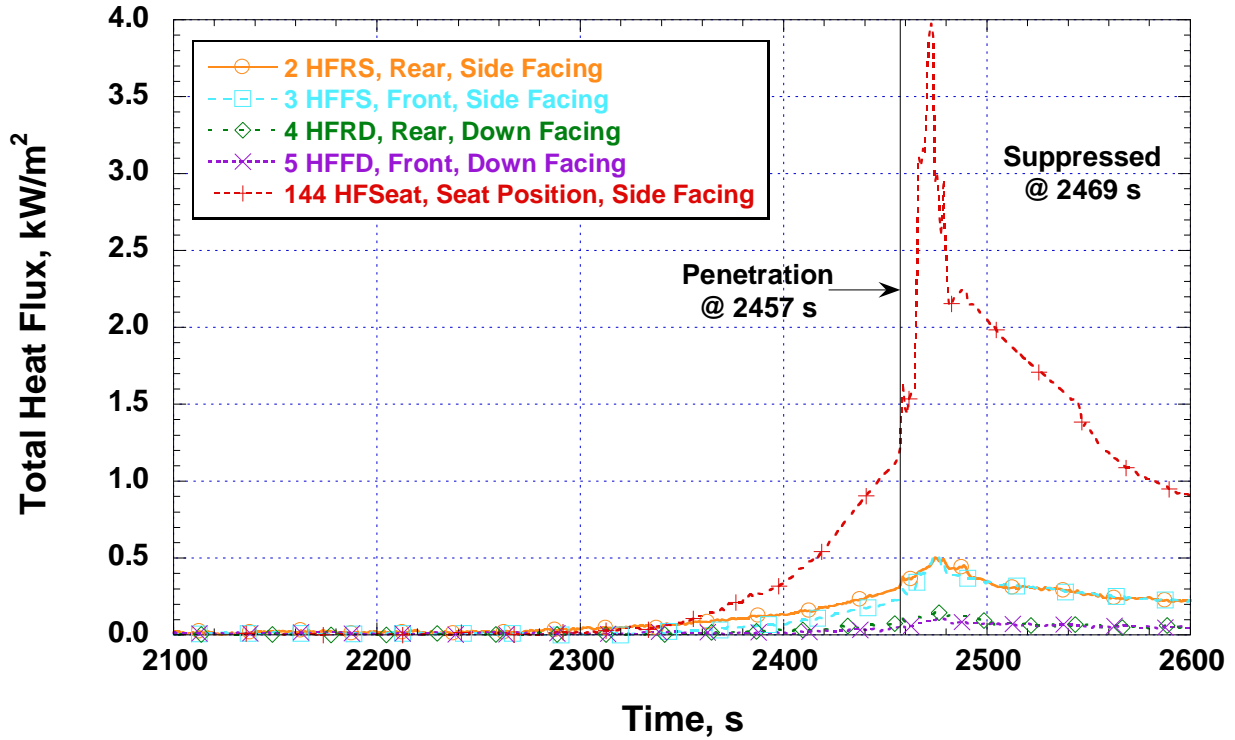


Figure 68 A plot of test 1 (tag axle) total heat flux versus time for the 5 heat flux gauges in the passenger compartment. Table 9 provides additional descriptions of the locations.

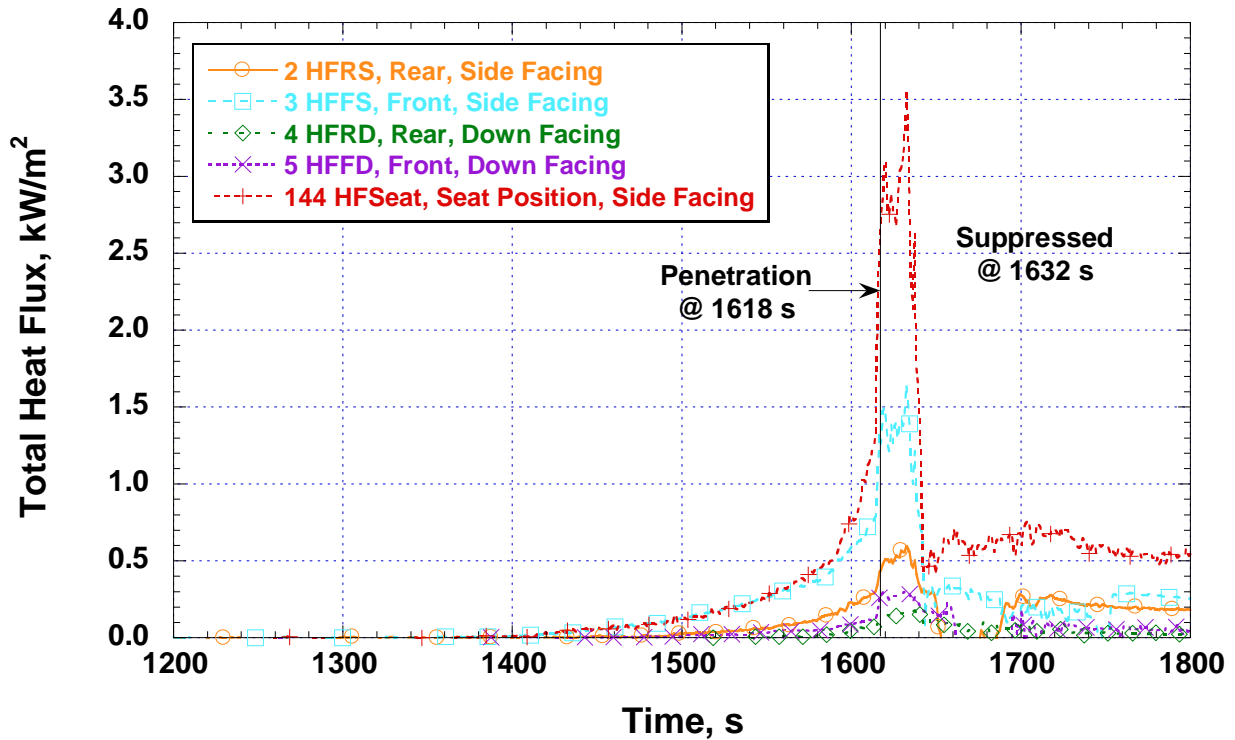


Figure 69 A plot of test 2 (drive axle) total heat flux versus time for the 5 heat flux gauges in the passenger compartment. Table 9 provides additional descriptions of the locations.

Fire-hardening Experiments

Event Timing

The times of events during the fire-hardening experiments are listed in Table 13. The time referenced is when the burner was applied to the wheel. The times have uncertainties of about ± 3 s primarily due to the judgment of the project director as to when events occurred, communicating those events to the data acquisition system via a remote marker or to the operator verbally, and also to minor synchronization issues between the two computer data acquisition systems used.

Table 13 Timing of events and observations during the fire-hardening experiments. (uncertainty = ± 3 s)

Test 3 (Steel Panel)		Test 4 (Intumescent Coating)		Test 5 (Deflector)	
Time (s)	Event Description	Time (s)	Event Description	Time (s)	Event Description
-942	Data recording initiated	-662	Data recording initiated	-2078	Data recording initiated
0	Burner placed on wheel	0	Burner placed on wheel ¹	0	Burner placed on wheel ²
774	Smoke from tire well	937	Smoke from tire	409	Smoke above wheel well
1237	Substantial visible smoke	2807	Ignition at 9, 12, and 6 o'clock	1926	Ignition of tire
1641	Sustained ignition at bottom of tire at 6 and 9	2848	Gas off, burner removed	1990	Fender ignited
1680	Ignition at top of tire	2864	Shield removed	2015	Burner removed
1705	Removed burner	2897	Flames on fender	2165	Shield removed
1740	Shield removed	3174	Flames on fender at 10 o'clock relative to tire	2158	Fender over front (drive axle) wheel burning
2016	Smoke from far side	3244	Flames to top of fender	2265	Fender was sagging
2414	Flames on outside of stainless steel plate	3538	Ignition of whole fender bottom over tire	2454	Front part of fender fell off
3197	Mud flap fell off	3563	Pieces of fender coming off	2516	Glass breakage
3462	Smoke through seam in floor near heat flux	3796	Flames coming out of the front (drive) wheel well, fender edge ignited	2563	Entire fender fell off
3977	Dual tire (outermost) started burning	3929	Dual tire (outermost) ignition	2603	Window penetration, extinguishment started
4169	Extinguishment started	4728	Window breakage		
		4794	Window penetration, extinguishment started		

¹ Some burner nozzles had to be relit multiple times between 1722 s and 2548 s.

² Some burner nozzles had to be relit multiple times between 397 s and 1841 s.

Table 14 summarizes the key periods for the 5 experiments initiated at the tag axle wheel. It is notable that the periods for heating the tag axle wheel before sustained tire burning varied widely (between 28 min and 48 min), mainly due to intermittent blowoff of some burner torches. This will be discussed further under the topic of repeatability. Tests 3, 4, and 5 listed in the table were the fire-hardening experiments. The shortest duration between burner removal and window penetration (9 min 48 s) was for test 5, the deflector experiment. The longest duration (41 min 4 s) was for test 3, the steel fender/panel experiment, although this experiment was stopped (through fire suppression) before window penetration occurred after 600 °C temperatures were measured behind the panel which threatened to ignite the paper-covered foam wall insulation. Test 4, the experiment using the intumescent coating for the panel and fender, exhibited a duration from burner removal to window penetration of 32 min 26 s. Throughout the experiment, the coating remained intact over much of the fender and nearly all of the panel, but along the bottom edge of the fender, the coating degraded sufficiently to allow some flame spread upward over the fender.

Table 14 Duration of periods of heating and between heating and penetration for the tag axle experiments with and without fire-hardening.

Test Details					
Test Number	1	3	4	5	6
Axle of Heated Wheel	Tag	Tag	Tag	Tag	Tag
Fire-hardening/Protection	None	Metal	Coating	Deflector	None
Period	Duration (s) (min:s)				
Burner heating wheel to sustained tire burning	2177 36:17	1705 28:25	2848 47:28	2015 33:35	2210 36:50
Burner stopped to fire penetration of window	280 4:40	2464* 41:04*	1946 32:26	588 9:48	679 11:19

*This test was stopped to prevent damage due to 600 °C temperatures behind the side panel and not fire penetration.

Photographs

Hundreds of digital photographs were taken of the motorcoach before, during, and after the tire fire passenger compartment fire-hardening experiments. Several photographs taken during the experiments are included here to illustrate the evolution of the fires. Figure 70 and Figure 71 show the steel exterior panel experiment, Figure 72 through Figure 75 show the intumescent coating experiment, and Figure 76 through Figure 78 show the steel deflector experiment. A select collection of additional photographs, including some taken before and after the experiments, is shown in Appendix B.



Figure 70 Steel exterior panel fire-hardening experiment about 8 min after burner removal.



Figure 71 Steel exterior panel fire-hardening experiment about 39 min after burner removal.



Figure 72 Intumescent coating fire-hardening experiment about 4 min after burner removal.



Figure 73 Intumescent coating fire-hardening experiment about 6 min after burner removal.



Figure 74 Intumescent coating fire-hardening experiment about 19 min after burner removal.



Figure 75 Intumescent coating fire-hardening experiment about 28 min after burner removal.



Figure 76 Steel deflector fire-hardening experiment about 1 min after burner removal.



Figure 77 Steel deflector fire-hardening experiment about 2 min after burner removal.



Figure 78 Steel deflector fire-hardening experiment about 8 min after burner removal.

Heat Release Rate

Figure 79 shows the plot of HRR versus the start of heating time for the first fire-hardening experiment which used stainless steel sheet metal in place of the exterior side panel and fender. The nominal peak HRR was 387 kW. Taking into account the $\pm 8.1\%$ uncertainty in the measurement and the 1% attenuation due to transients (discussed in the previous HRR section), the revised HRR peak was $391 \text{ kW} \pm 32 \text{ kW}$.

Figure 80 shows the plot of HRR versus the start of heating time for the second fire-hardening experiment which used an intumescent coating on the exterior side panel and fender. The nominal peak HRR was 1033 kW. Taking into account the $\pm 8.1\%$ uncertainty in the measurement and the 1% attenuation due to transients, the revised HRR peak was $1043 \text{ kW} \pm 85 \text{ kW}$.

Figure 81 shows the plot of HRR versus the start of heating time for the third fire-hardening experiment which used a stainless steel deflector between the exterior side panel and fender. The nominal peak HRR was 1125 kW. Taking into account the $\pm 8.1\%$ uncertainty in the measurement and the 1% attenuation due to transients, the revised HRR peak was $1136 \text{ kW} \pm 92 \text{ kW}$.

The average HRRs for the wheel burner were 61.2 kW, 60.9 kW, and 59.1 kW for the steel panel, coated panel, and deflector experiments, respectively. The natural gas burner HRR uncertainties were about $\pm 2.5\%$.

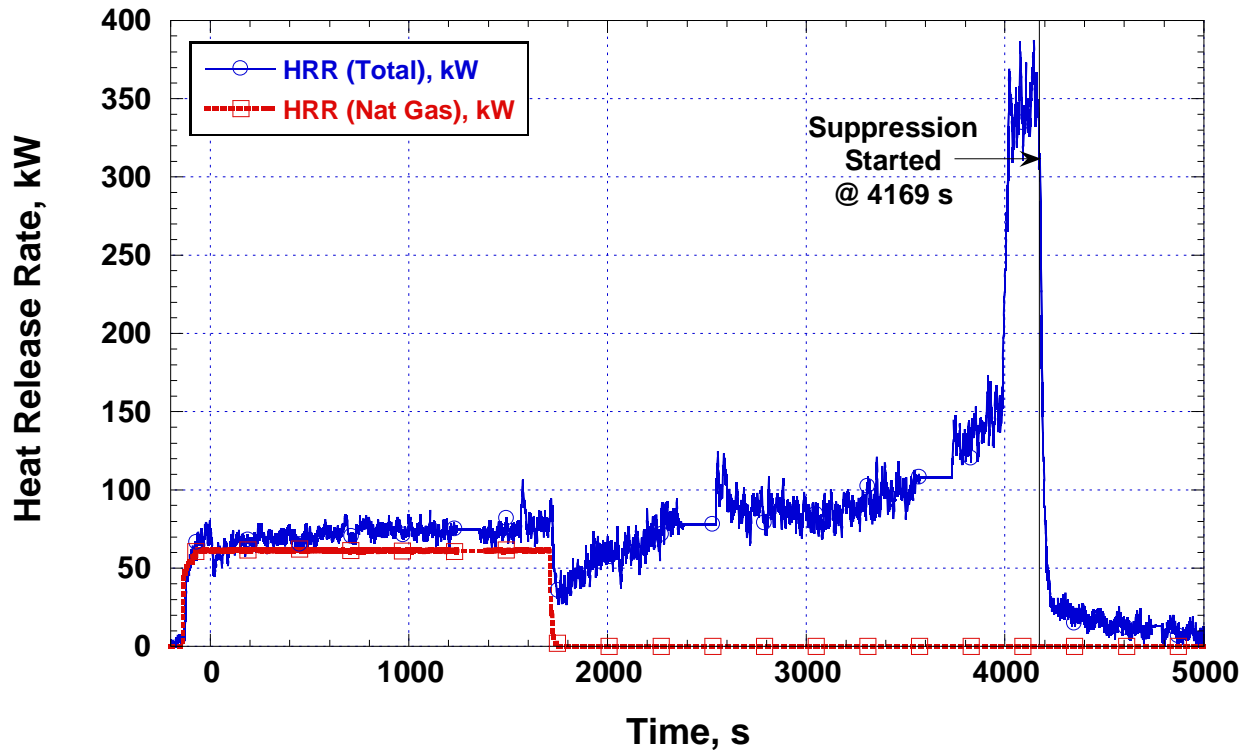


Figure 79 Heat release rate plotted versus time for test 3, the metal panel/fender experiment.

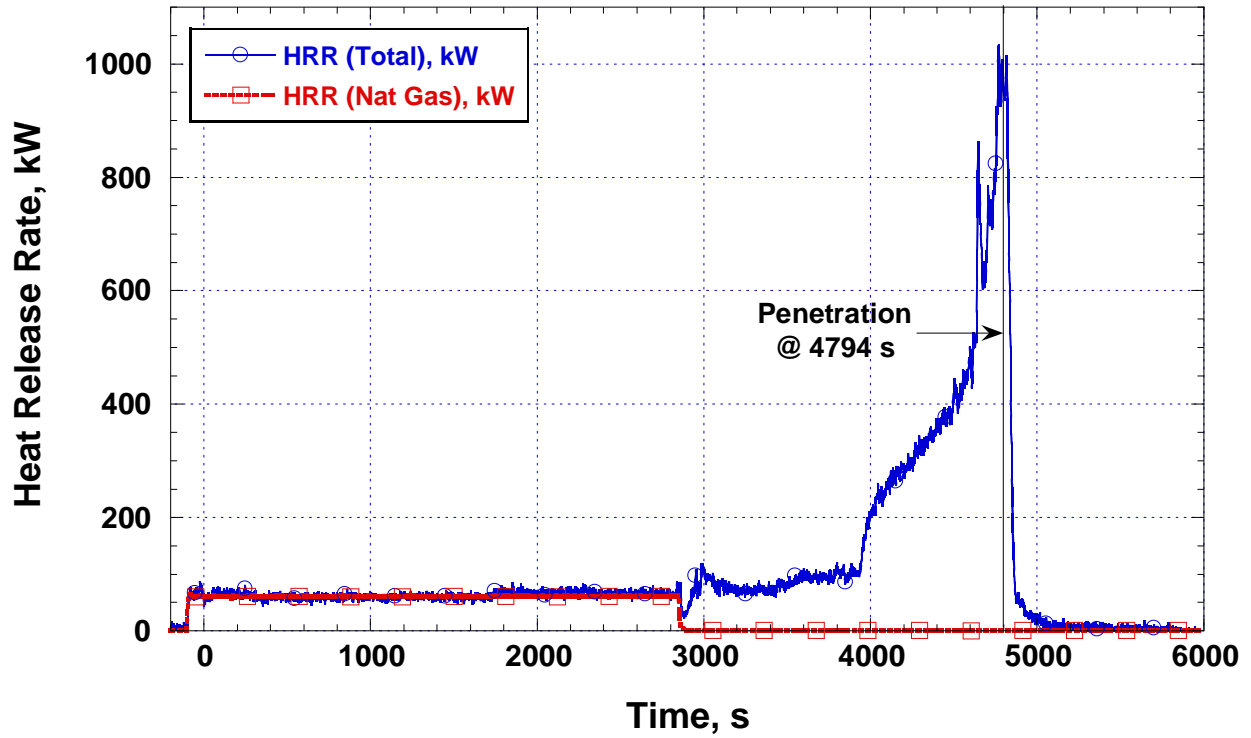


Figure 80 Heat release rate plotted versus time for test 4, the coated panel/fender experiment.

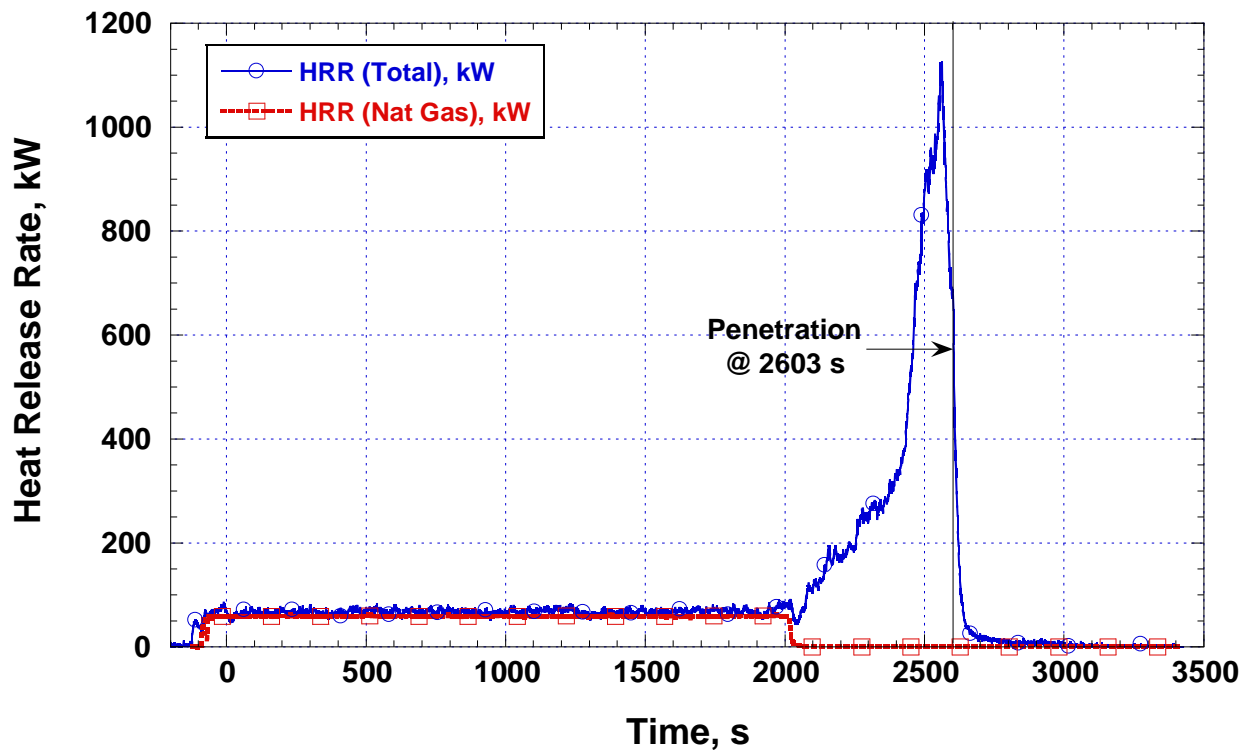


Figure 81 Heat release rate plotted versus time for test 5, the steel deflector experiment.

ABS Sensor

For the fire-hardening and tenability experiments, the ABS sensor was monitored to determine if its output changed with temperature even though it wasn't being used with rotating metal (the motorcoach wheels weren't rolling). The battery voltage did tend to decrease with temperature rise for each experiment, although the amount varied. Figure 82 shows a plot of the best performance of an ABS sensor and accompanying thermocouple which was used during the steel panel fire-hardening experiment. The battery voltage decreased with temperature rise and the rate of decrease correlated with the rate of temperature change. When the fire was suppressed and the temperature started to decrease, the battery voltage started to increase again. From about 2100 s (when the temperature exceeded 30 °C) until suppression started, the average slope of the voltage change with respect to the temperature change was $-71\mu\text{V}/^\circ\text{C}$.

While the result from the steel panel experiment showed a correlation between temperature and ABS voltage, the results of other experiments were more difficult to interpret. Figure 83 shows the data from the intumescent coating experiment. The sensor minimum lagged the temperature peak by 5 min, and the thermocouple had a malfunction where it measured an impossible negative temperature for most of the experiment.

From the deflector experiment results shown in Figure 84, it is not clear whether the sensor voltage followed the temperature rise or if the sensor minimum lagged the temperature peak by 16 min. If the sensor voltage trend was the same as the temperature trend, this was the opposite correlation from that seen in the other experiments. The temperature peaked about 500 s before suppression which may have been a partial thermocouple malfunction. Also, the ABS sensor output varied over a range of just 0.4 mV.

Although the tenability experiment was not one of the fire hardening tests, its ABS results are presented here. Figure 85 shows that the temperature peak lagged 15 min behind the sensor minimum. The thermocouple seemed to malfunction about 500 s before suppression since it peaked early and then decreased to impossible negative temperatures.

The time lags experienced may be due to the difficulty in deploying the ABS sensor and thermocouple such that they experienced the same thermal impact by combinations of radiation, convection, and conduction. The impact of the harsh environment on the thermocouple leads led to their malfunction in all but the steel hardened experiment. The maximum signal change by the battery was less than 4 mV out of the total of 9.5 V, which may be a difficult voltage change to sense in a less controlled environment. It's not known if the ABS sensor output would track temperature better if it were used in its typical installation with a cyclical stimulus. The ABS sensor for a rolling motorcoach with a bearing, brake, or tire problem that could lead to a tire fire upon stopping could experience a very different environment than that produced in these experiments.

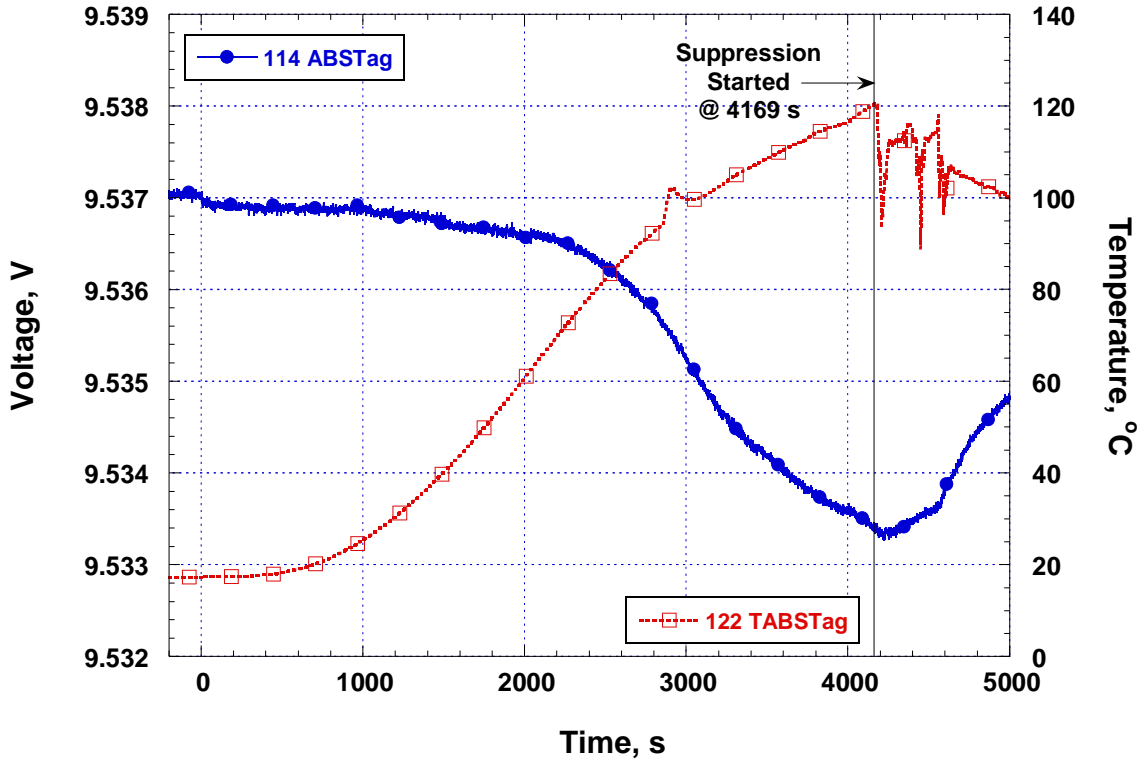


Figure 82 ABS sensor voltage (left axis) and ABS temperature (right axis) plotted versus time for test 3, the steel panel test.

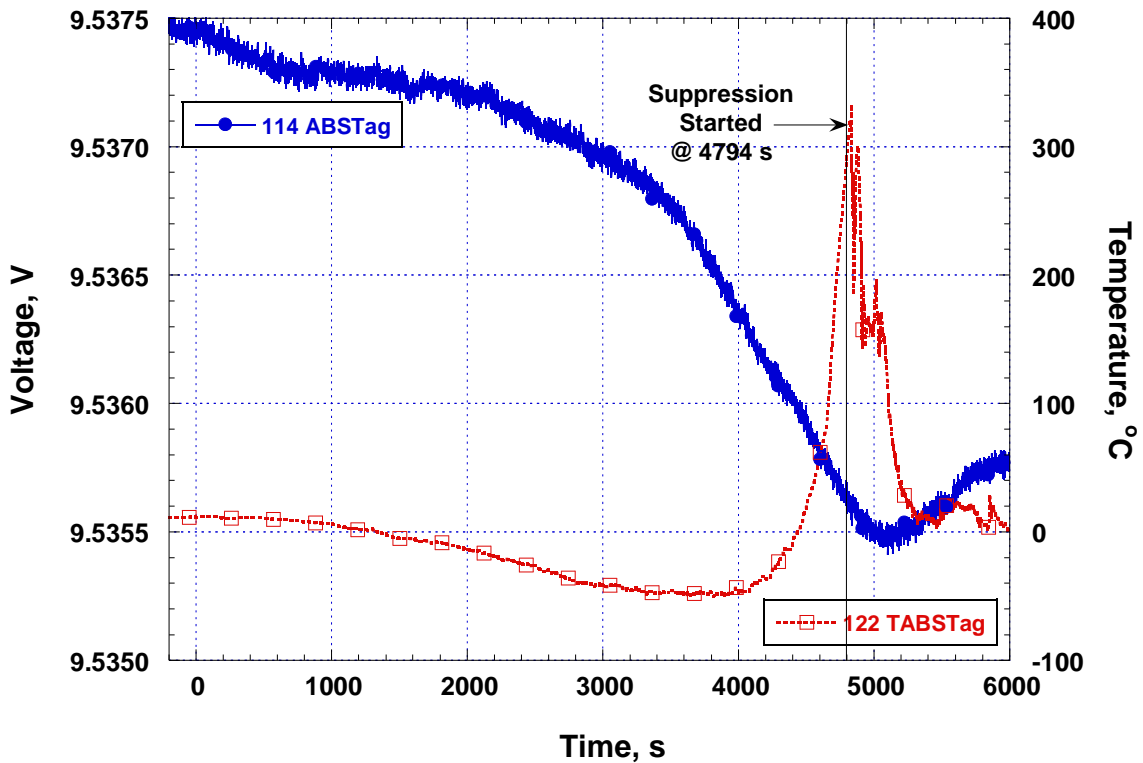


Figure 83 ABS sensor voltage (left axis) and ABS temperature (right axis) plotted versus time for test 4, the intumescent coating test.

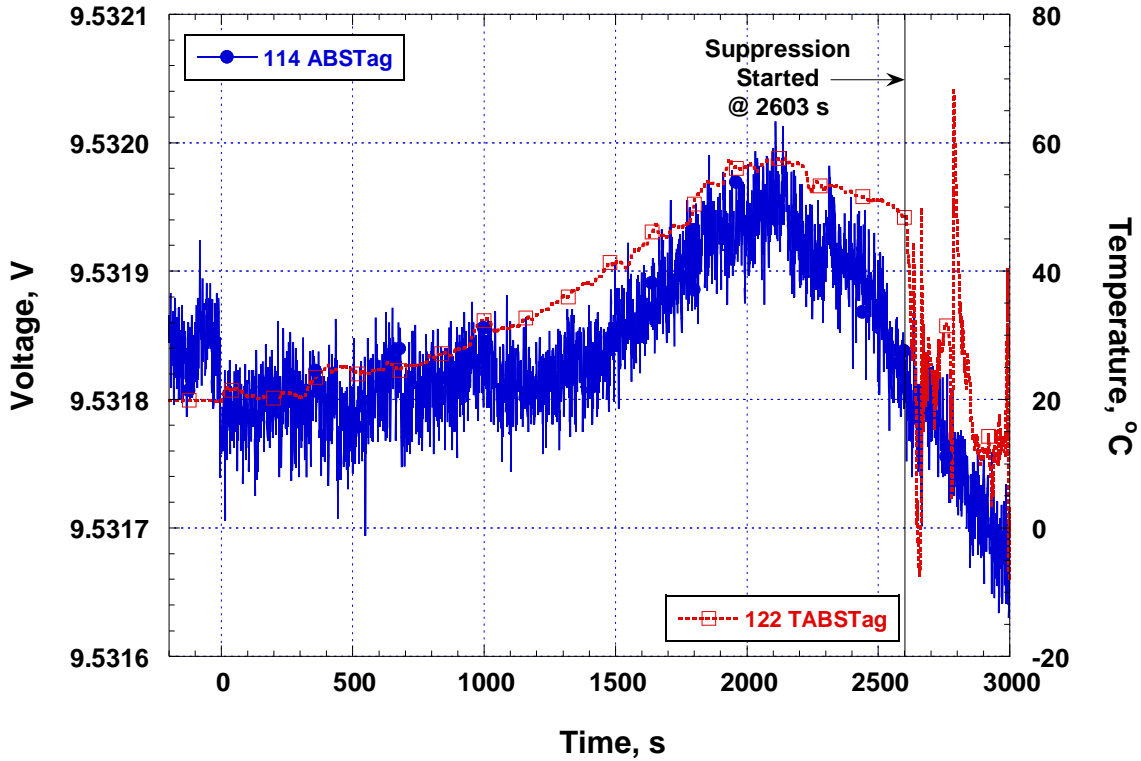


Figure 84 ABS sensor voltage (left axis) and ABS temperature (right axis) plotted versus time for test 5, the steel deflector test.

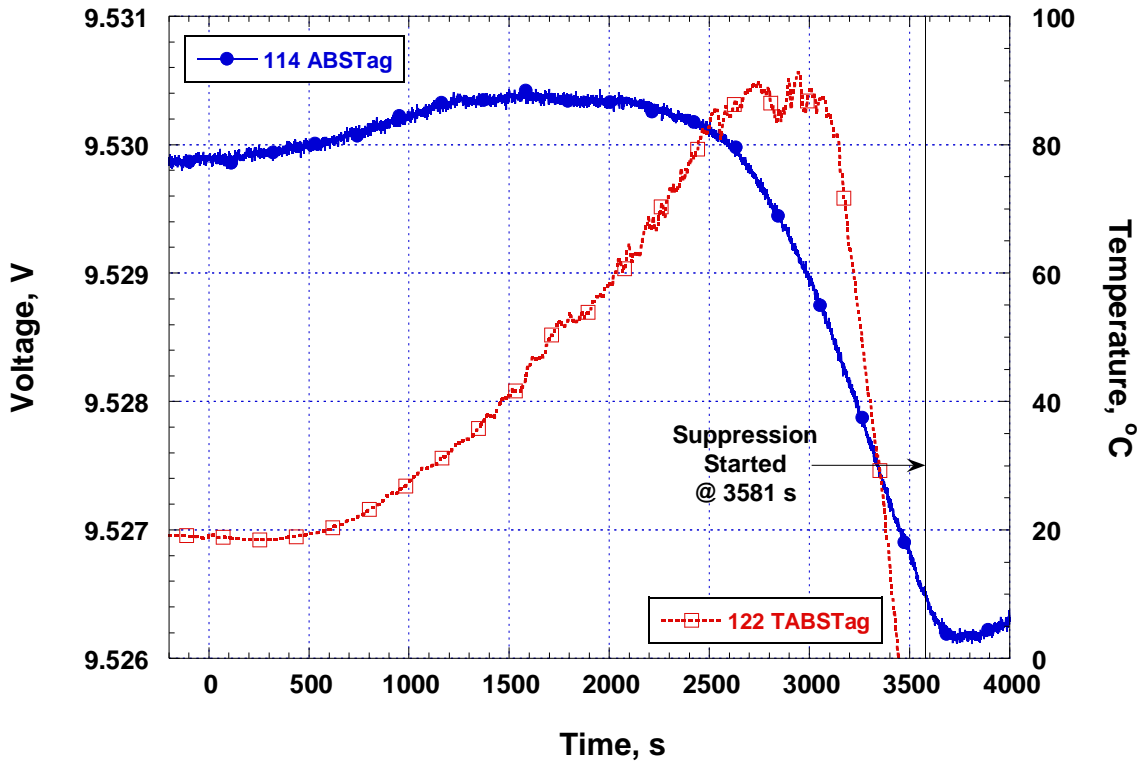


Figure 85 ABS sensor voltage (left axis) and ABS temperature (right axis) plotted versus time for test 6, the tenability test.

Extinguishment

Extinguishment of the penetration experiment fires was quickly achieved using the combination of water and foam. The majority of the flames in each case were doused in less than 10 s. While water/foam flows were not measured at the time of the experiments, recreations of the extinguishing flow provided some insights as to how much water and foam were required. The combined water and foam flow rate was bracketed between 0.61 kg/s (9.7 gal/min) and 0.74 kg/s (11.7 gal/min) with an uncertainty of about 15 %. Most of the mass flow was water. The total amount of water and foam used over 10 s would have been between 6.1 L (1.6 gal) and 7.4 L (2.0 gal) which is a remarkably low amount.

Tenability Experiment*Event Timing*

The time of events during the tenability experiment are listed in Table 15. The times have uncertainties of about ± 3 s. Table 14 lists the duration of heating before the burner was removed and the time from burner removal to window penetration by the fire. Table 14 also provides a comparison of timing between the tenability experiment and the other experiments initiated on the tag axle.

Table 15 Timing of events and observations during the tenability experiment. (uncertainty = ± 3 s)

Test 6 (Tenability)	
Time (s)	Event Description
-3450	Data recording initiated
0	Burner placed on wheel
720	Starting to see smoke from top of tire?
1462	Cameras started
1800	Started FTIR
1832	A lot of smoke coming from under the back of the bus
2111	Small flame at 7 o'clock on the tire
2201	Tire ignited
2210	Burner removed
2232	Shield removed
2400	Fender ignited
2648	Glass broke
2861	Glass fell out and front of fender fell
2889	Flames in interior
2998	Seats on fire
3581	Suppression
3606	Opened damper 2
4660	Visible flame in wheel well-suppressed

The burner heating times required to generate sustained tire fires for the tenability experiment and the first tag axle penetration experiment were very similar. The time for penetration for the tenability experiment was significantly longer (6 min 39 s) than for the first tag axle experiment. Only after flames penetrated the window during the tenability experiment could the interior materials ignite. It still took nearly 2 min after window penetration for the seats to ignite. After the seats ignited, fire growth was gradual over the next 7 min until the final 2 min (prior to suppression) when the fire growth, temperatures, and toxic gases ramped up quickly.

Photographs

Dozens of digital photographs were taken of the motorcoach before, during, and after the tire fire passenger compartment tenability experiment. A few photographs recorded during the experiments are included in Figure 86 through Figure 88 to illustrate the evolution of the fire. A select collection of additional photographs, including some taken after the experiment, is shown in Appendix B.



Figure 86 Tenability experiment about 12 min after burner removal.



Figure 87 Tenability experiment passenger compartment about 15 min after burner removal.



Figure 88 Tenability experiment almost 20 min after burner removal.

Repeatability

The tire fires for the first passenger compartment penetration experiment and the tenability experiment were both initiated on the tag axle wheel which provides an opportunity to examine the repeatability of the motorcoach tire fire experiments. The times to penetration after removing the burner were 4 min 40 s and 11 min 19 s for the two experiments, respectively. This is a large range of results. The fire-hardening experiment with the deflector, which was assumed to delay penetration by some period of time, experienced window penetration by fire at 9 min 48 s, which was 5 min 8 s longer than the first tag axle experiment, but 1 min 31 s shorter than the tenability experiment. Determination of the benefit of the deflector is not possible given these results with the fire-hardened penetration time in between the penetration times of the two experiments which were not fire-hardened.

The wheel heating times listed in Table 14 and Table 15 varied widely as well. Figure 89 shows a graphic comparison of the average tag axle wheel temperatures and times that the burner was removed for the five experiments initiated on the tag axle. The heating times before the tire was deemed fully ignited ranged from 28 min 25 s to 47 min 28 s. The average temperatures upon burner removal ranged from 396 °C to 469 °C. The heating period was sensitive to how much the flames were touching the wheel and whether the pre-mixed flame was subject to blowoff due to quenching from being too close to the wheel and an unstable combination of air and gas flows. When the burner torches experienced blowoff, there were many periods of tens of seconds when local heating at those torch locations was stopped. It was also a judgment call of the experiment's director as to when the tire was sufficiently ignited and the burner should be removed. This partly subjective decision also contributed to variations in the heating times and the penetration times for the four experiments for which flames entered the motorcoach.

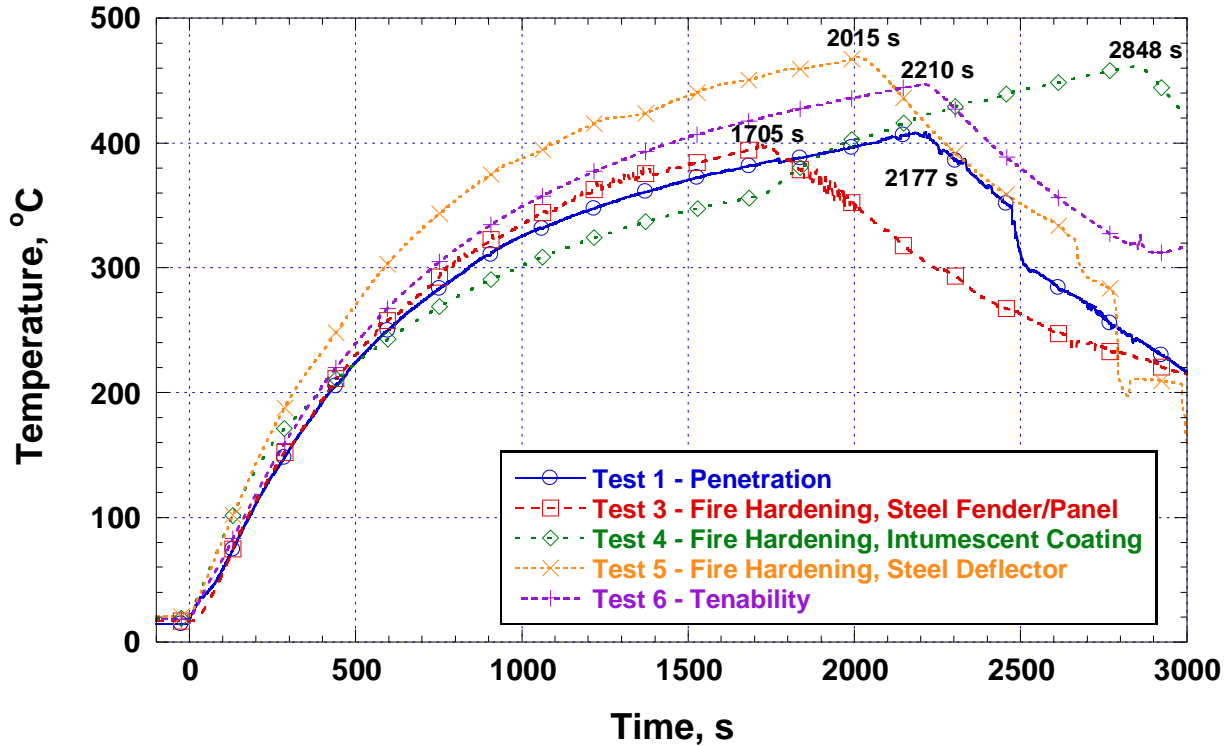


Figure 89 Comparison of average tag axle wheel temperatures plotted versus time for the experiments initiated on the tag axle wheel.

Heat Release Rate

Figure 90 shows the plot of HRR versus the start of heating time for the tenability experiment which required both the 9 m × 12 m and 6 m × 6 m exhaust hoods to capture the effluent. The nominal peak HRR was 5578 kW. Taking into account the ± 8.9 % uncertainty in the measurement and the 1 % attenuation due to transients, the revised HRR peak was 5633 kW ± 501 kW.

The average HRR for the wheel burner was 60.8 kW for the tenability experiment. The natural gas burner HRR uncertainty was about ± 2.5 %.

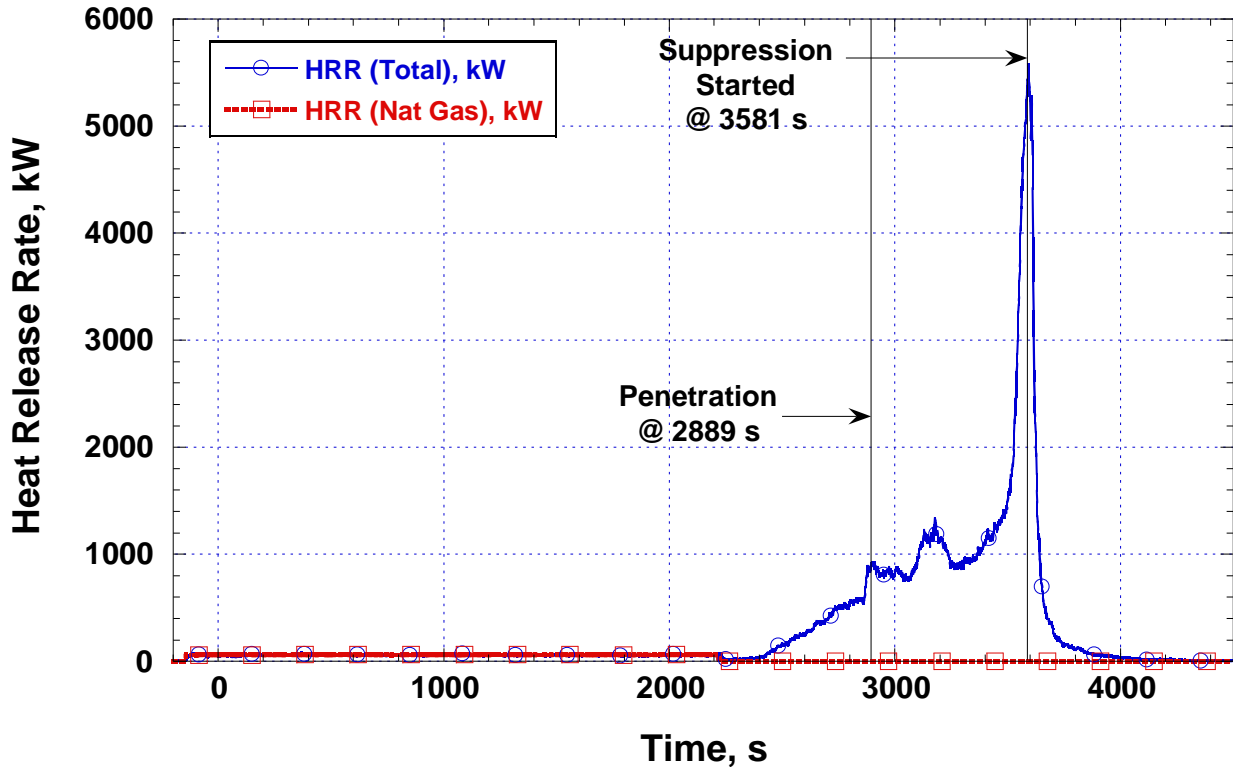


Figure 90 Heat release rate plotted versus time for test 6, the tenability experiment.

Interior Gas Temperatures

Figure 91 shows the thermocouple array temperatures for the tenability experiment plotted versus time for the 3 min before suppression. By 100 s prior to suppression, all of the temperatures at or above 1.2 m from the floor exceeded 100 °C. The thermocouples at 30 cm from the floor at the middle and front arrays had maximum temperatures before extinguishment of 54 °C and 34 °C, respectively. The 60 cm height temperatures were 133 °C and 172 °C, respectively. These peaks occurred at or within several seconds of extinguishment. This indicates that even the most tenable location, near the floor, was becoming untenable at the end of the experiment.

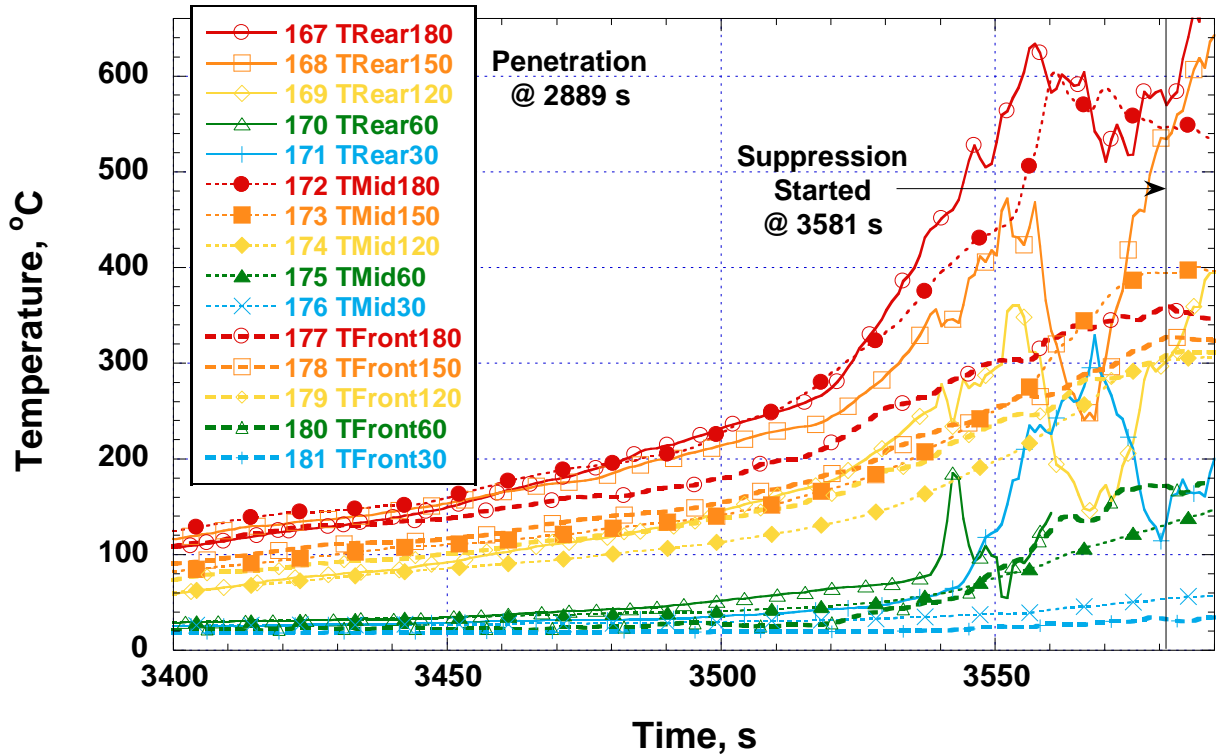


Figure 91 A plot of test 6 (tenability) interior rear, middle, and front gas temperatures versus time. Numbers 30 through 180 represent distance from the floor in centimeters.

Heat Fluxes

Figure 92 shows the heat flux results for the tenability experiment plotted versus time for the 4 min 40 s before suppression. The threshold for flashover, when all fuels may simultaneously ignite in an enclosure, is often defined at 20 kW/m^2 . [47] The times when the heat flux gauges reached this level were 3515 s for the 6 m gauge, 3519 s for the 1 m gauge, 3536 s for the 4 m gauge, 3539 s for the 3 m gauge, and 3554 s for the 2 m gauge. All of the rear measurement locations exceeded the flashover condition within 40 s of each other.

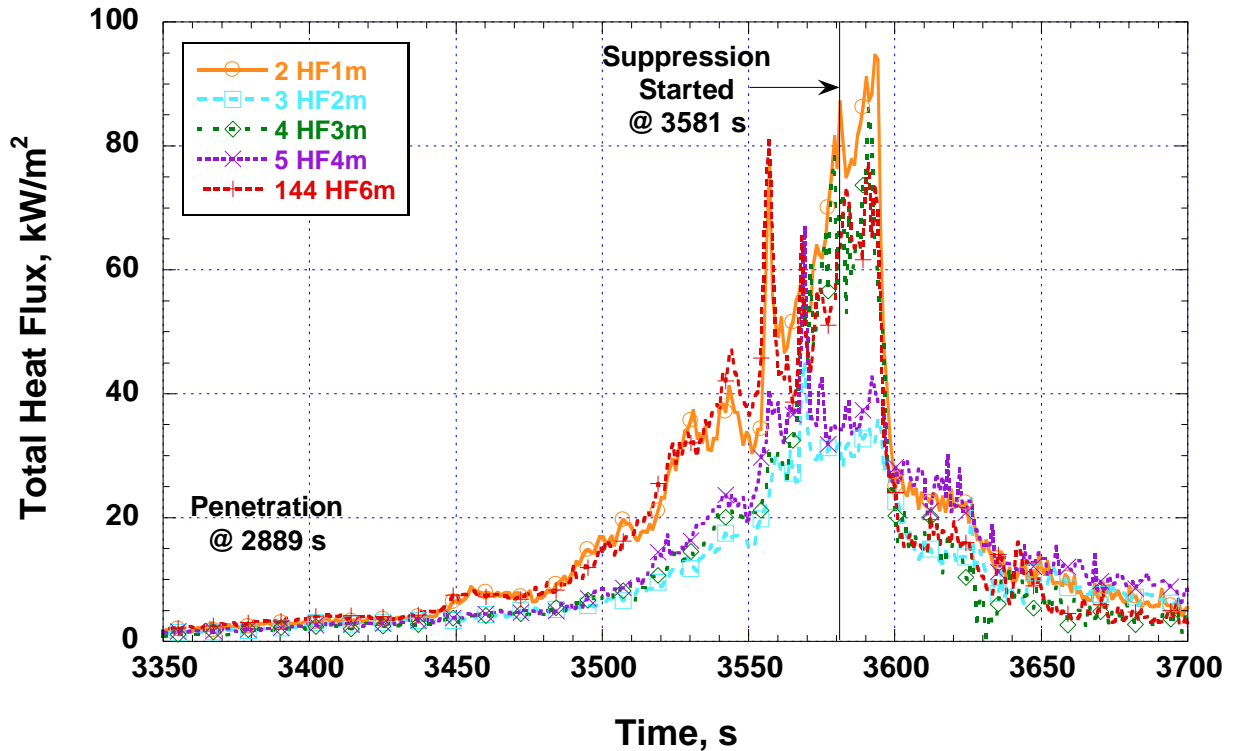


Figure 92 A plot of test 6 (tenability) total heat flux versus time for the 5 heat flux gauges in the passenger compartment. Table 10 provides additional descriptions of the locations.

Thermal Tenability Analysis

ISO 13571 [6] is an international standard which provides guidance for calculating incapacitation and time for escape from the life-threatening components of fires. This standard was used to analyze the thermal and chemical species volume fraction data from the tenability experiment. The standard uses fractional effective dose (FED) and fractional effective concentration (FEC) analyses. FED is the ratio of the exposure dose for an asphyxiant toxicant to that exposure dose of the asphyxiant expected to produce a specified effect on an exposed subject of average susceptibility. FEC is the ratio of the concentration of an irritant to that expected to produce a specified effect on an exposed subject of average susceptibility. The specified effect is usually incapacitation which would prevent escape; death would typically follow.

Thermal phenomena such as high temperature convective heat transfer and radiative heat flux are treated as asphyxiant toxicants and use the same FED definition as toxic gases. In this analysis, the response of the total heat flux gauges was assumed to be due to thermal radiation only and not convection. For heat flux, while the tenability limit for exposure of skin to radiant heat is 2.5 kW/m^2 , the FED takes into account accumulated exposure. Equation (1) defines the time in minutes, t_{rad} , to second degree burning of skin due to radiant heat, q in kW/m^2 . It has a 25 % uncertainty (specified in the standard) associated with it.

$$t_{\text{rad}} = 6.9q^{-1.56} \quad (1)$$

The reciprocal of t_{rad} is the FED for radiant heat. Figure 93 is a plot of the FEDs for the five total heat flux gauges plotted versus time from burner removal. The FED value of 1 reflects the tenability threshold. According to this analysis, the times for untenable conditions were 3226 s for the 1 m gauge, 3339 s for 6 m, 3379 s for 4 m, 3400 s for 3 m, and 3411 s for 2 m. Therefore, due to thermal radiation alone, the rear of the motorcoach started to become untenable 5 min 37 s after penetration and became completely untenable within an additional 3 min.

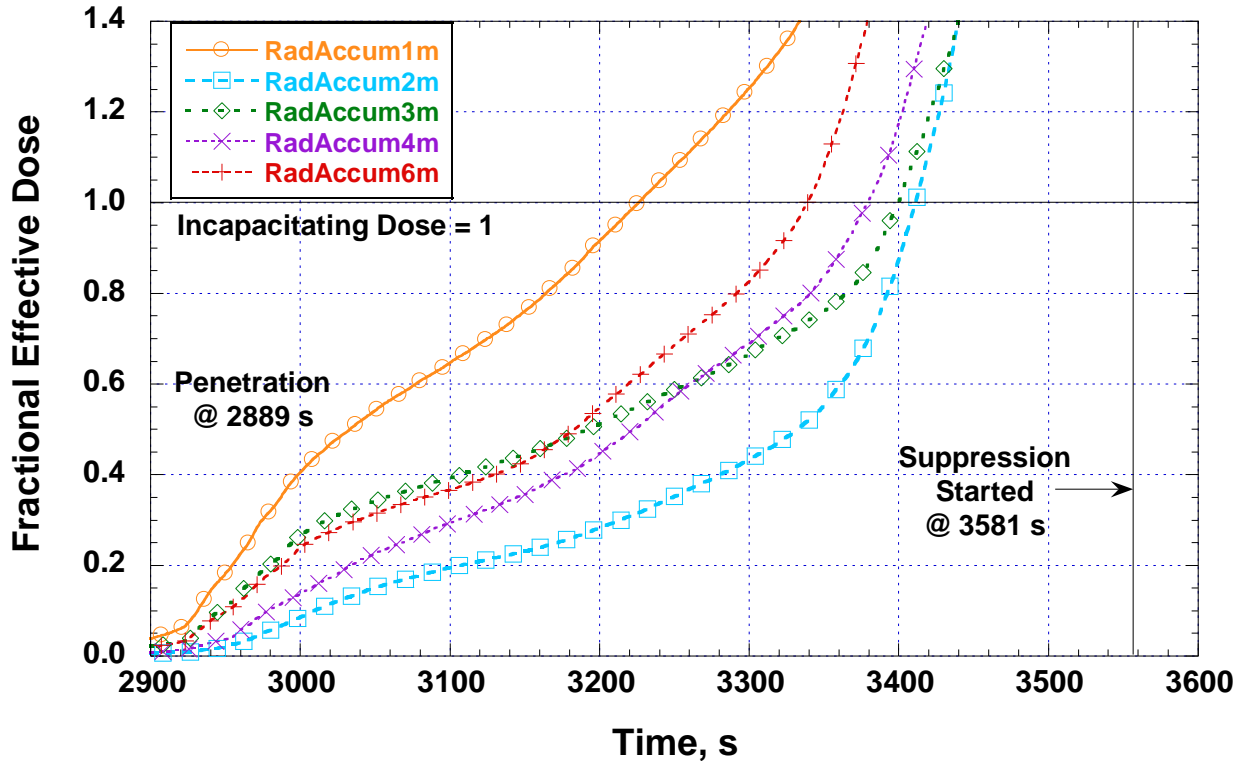


Figure 93 Fractional effective doses from thermal radiation plotted versus time for the six heat flux gauges located 1m, 2 m, 3 m, 4 m, and 6 m from the rear (lavatory door) of the motorcoach.

For thermal convection due to high temperatures, the time in minutes to experiencing pain is expressed in equation (2) for fully clothed persons and equation (3) for lightly clothed or unclothed persons. The equations have 25 % uncertainty (specified in the standard). The reciprocal of t_{conv} is the FED for accumulated exposure.

$$t_{\text{conv}} = (4.1 \times 10^8) T^{-3.61} \quad (2)$$

$$t_{\text{conv}} = (5 \times 10^7) T^{-3.4} \quad (3)$$

Figure 94 is a plot of the FEDs for thermal convection plotted versus time from burner removal. The FED value of 1 reflects the tenability threshold. According to this analysis, the times for untenable conditions for fully clothed passengers would be 3530 s at the rear station, 3564 s at the middle, and 3565 s at the front. For lightly clothed passengers, the times would be 3484 s at the rear station, 3537 s at the middle, and 3526 s at the front. From these times, the rear of the motorcoach became untenable 10 min 41 s after penetration for fully clothed persons and 9 min

55 s for lightly clothed persons. For the middle station, the times from penetration were 11 min 15 s and 10 min 48 s, and for the front, the times were 11 min 16 s and 10 min 37 s. In summary, from thermal convection alone and for any clothing type, the motorcoach began to be untenable in the rear just under 10 min after penetration and the whole motorcoach became untenable by 11 min 16 s.

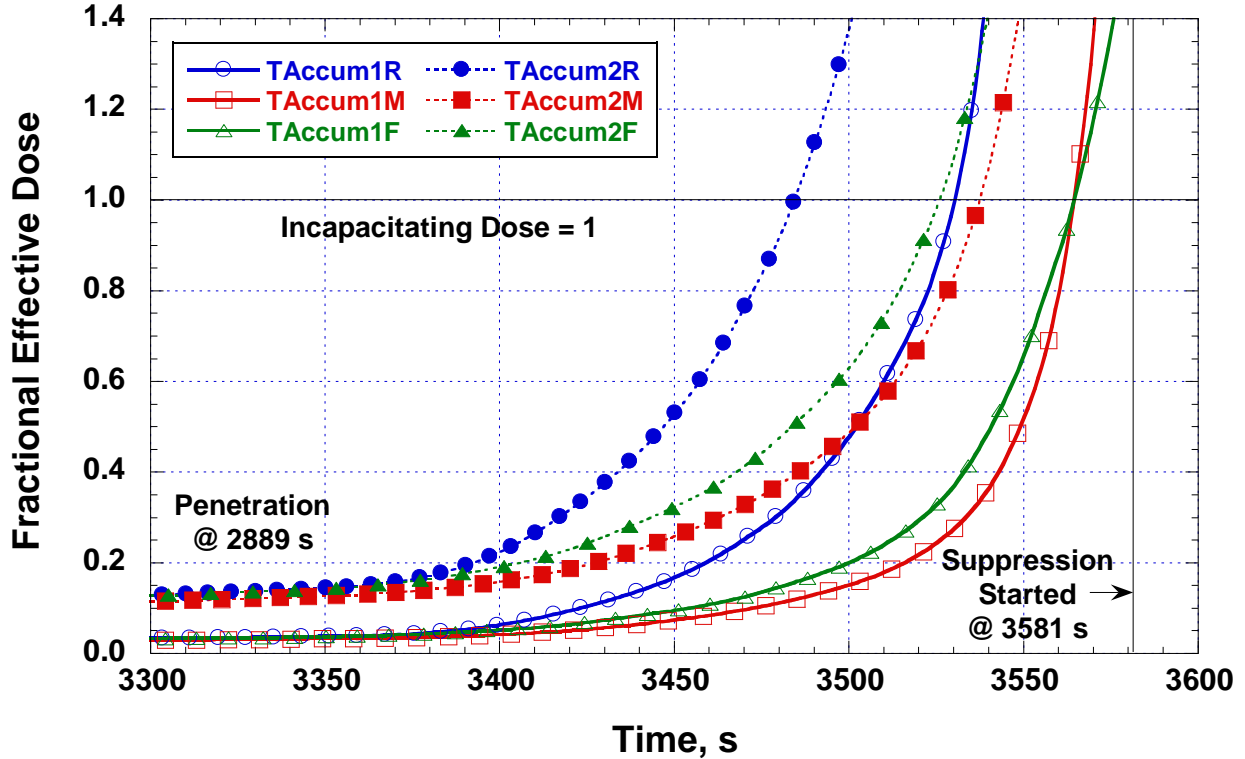


Figure 94 Fractional effective doses from thermal convection plotted versus time for the thermocouples 1.5 m from the floor at the rear (R), middle (M), and front (F) thermocouple arrays. The type 1 analysis treats occupants as fully clothed while type 2 is for more lightly clothed occupants with more skin exposure.

Combining the two thermal effects is a more practical measure of the real tenability deterioration in the motorcoach passenger compartment. The total thermal tenability FED is the sum of the radiative and thermal convection FEDs. Figure 95 shows a plot of the total thermal FEDs for the rear and middle stations for the tenability experiment. The front station was not analyzed because there was no heat flux measurement associated with that location. The rear analysis used the rear station 1.5 m thermocouple and the heat flux at 2 m. The middle analysis used the middle station 1.5 m thermocouple and the 6 m heat flux gauge.

The rear of the motorcoach became thermally untenable for fully clothed persons 3218 s after burner removal and for lightly clothed persons at 3195 s. The middle of the motorcoach became thermally untenable for fully clothed persons 3334 s after burner removal and for lightly clothed persons at 3315 s. The passenger compartment began to become untenable for all clothing types 5 min 6 s after fire penetrated it. The lag for tenability at the middle station versus the rear was about 2 min. Combining thermal convection with radiation accelerated the process to untenable conditions by about 30 s at the rear station.

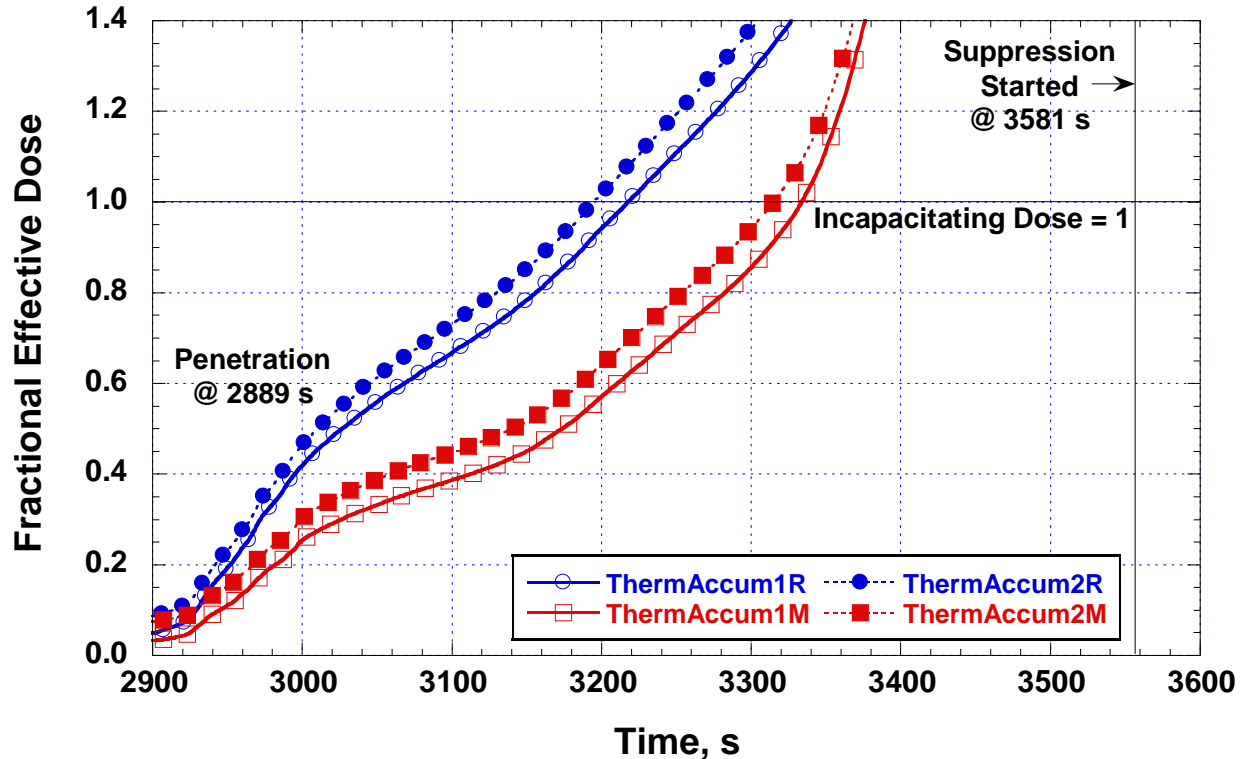


Figure 95 Fractional effective doses from radiation and convection plotted versus time for the rear (1 m) and middle (6 m) heat flux gauges and thermocouples 1.5 m above the floor. The type 1 analysis treats occupants as fully clothed while type 2 is for more lightly clothed occupants with more skin exposure.

Other Temperature Measurements

For the tenability experiment, the temperatures of the tops of the aisle seat headrests and the parcel rack doors above them were measured with thermocouples. Refer to Figure 19, Figure 20, and Figure 21 for their locations. Figure 96 shows a plot of these temperatures versus time from burner removal. Each pair of headrest and door temperatures tracked somewhat with each other which indicates that the thermal environment varied more with the axis of the motorcoach and not as much vertically at each row. The front seat seems to have been involved in the fire first followed by the middle and then rear. The front and middle parcel rack door temperatures lagged their matching headrest temperatures indicating that they were receiving heat from the flaming seats, but may not have been as involved in the fire as the seats. At the rear headrest, this was reversed indicating that the parcel rack door was being heated by the burning of the middle and front seats more so than the rear seat. At about 3510 s, the rear seat appears to ignite and the seat and door temperatures rose rapidly.

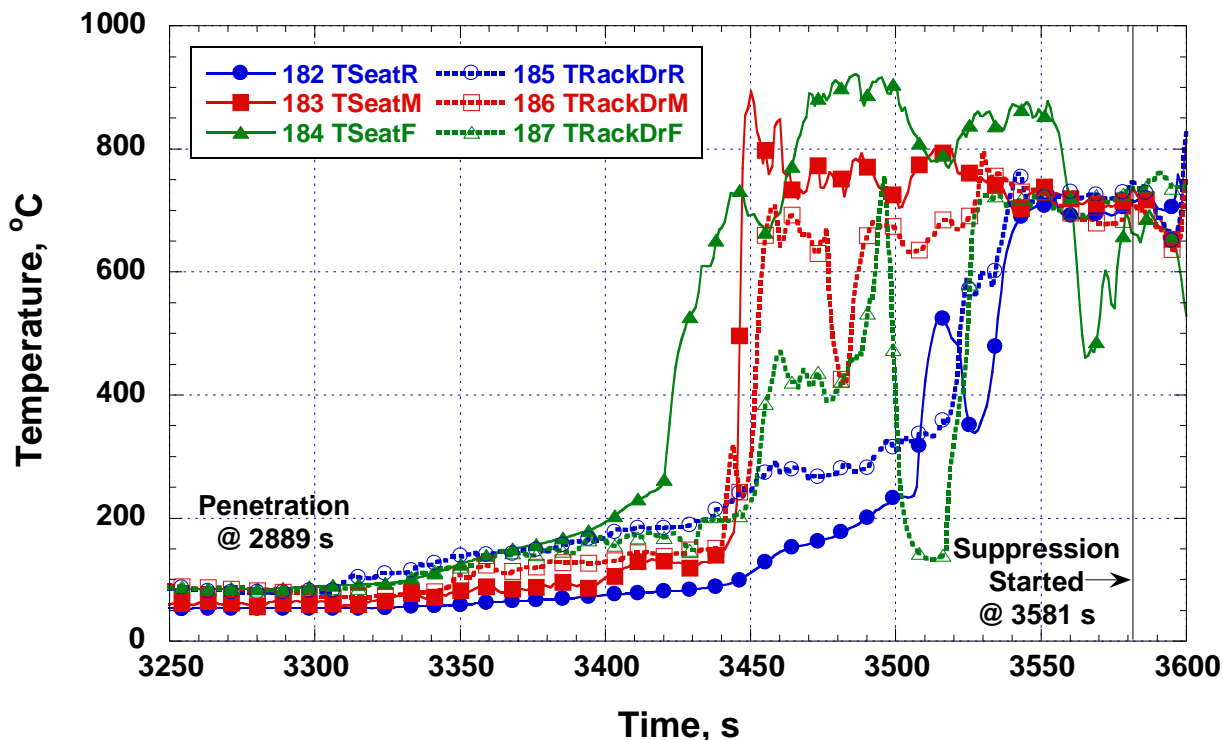


Figure 96 Seat headrest and parcel rack door temperatures plotted versus time for the tenability experiment. Locations were on or over the rear (R), middle (M), and front (F) seats.

Gas Volume Fractions

Gas volume fractions were measured for the tenability experiment. The volume fractions of oxygen (O_2), carbon dioxide (CO_2), and carbon monoxide (CO) are plotted in Figure 97 for the period about 7 min after window penetration to just after extinguishment was initiated. The volume fraction is plotted as a “dry” measurement because water was trapped out of the sample before it went through the gas analyzers. FTIR measurements of water showed about 3.5 % water vapor near the time of the largest fire just before extinguishment.

O_2 decreased at all three locations from near ambient levels over 20 % to about 19 % from 2900 s to 3000 s. From 3000 s to 3350 s, O_2 decreased slowly to about 18 % before beginning a more rapid decrease to 4 % (rear), 4.5 % (front), and 5 % (middle) when extinguishment was initiated at 3581 s.

On the same plot, CO_2 increased at all three locations from 0 % to about 1.5 % from 2900 s to 3000 s. From 3000 s to 3350 s, CO_2 rose slowly to about 2 % before beginning a more rapid rise to 12.5 % (rear) and 11.5 % (middle and front) when extinguishment was initiated at 3581 s.

Also shown in Figure 97, CO increased at all three locations from 0 % to about 0.1 % and stayed below 0.2% until about 3400 s. After 3400 s, CO rose more rapidly. CO in the rear peaked at 3.1 % and decreased slightly to 3.0 % at 3581 s when extinguishment was initiated. The middle and front CO volume fractions lagged the rear position and were only about 2.6 % at the beginning of extinguishment. Since the extinguishment process took tens of seconds and was

focused in the rear of the motorcoach, the CO volume fractions peaked at about 3.3 % about 30 s after extinguishment was started for both the front and middle positions.

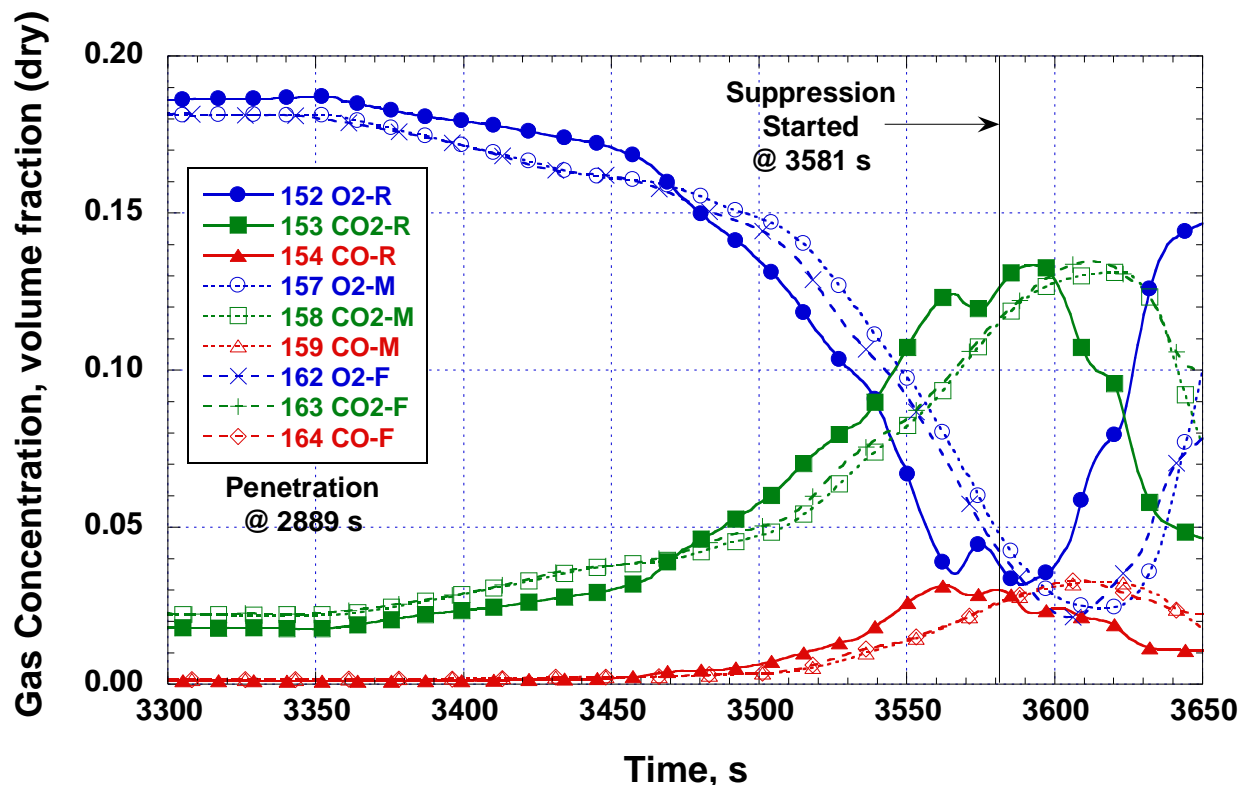


Figure 97 O₂, CO₂, and CO volume fractions measured at the rear (R), middle (M), and front (F) sampling locations plotted versus time for the tenability experiment.

Unburned hydrocarbons were measured at each sampling location. The hydrocarbon analyzers were not calibrated for levels (as methane) of over 5 %, but there were more than 5 % hydrocarbons generated. For the rear station, between 5 % and about 10 % (based on extrapolating the peak) were generated prior to the beginning of extinguishment. For the middle and front stations, levels of 4.1 % and 3.8 % were measured, respectively.

Figure 98 is a plot of some of the gases measured using FTIR at the rear sampling position in the motorcoach. The CO volume fraction is slightly lower, but comparable to the analyzer measurement at the same location. HCl peaked at about 1.5 % while HCN only reached about 500 $\mu\text{L/L}$.

Most of the FTIR measurements had uncertainties estimated at $\pm 10\%$ of the measured values, but CO and CO₂ had special uncertainty issues. The maximum CO volume fraction measured using FTIR was 2.7 % versus 3.3 % measured with the NDIR CO analyzer. For CO₂, the maximum FTIR measurement was only about 44 % of that measured by the NDIR CO₂ analyzer. There were questions about whether the appropriate calibration libraries were used as well as the possibility of stray light intruding into the FTIR cell and impacting the results at high volume fractions. While the uncertainties for the FTIR measurements of CO₂ and CO at low volume

fractions were probably good within 10 %, the high volume fractions, which were most important for our analyses, were too suspect to be included.

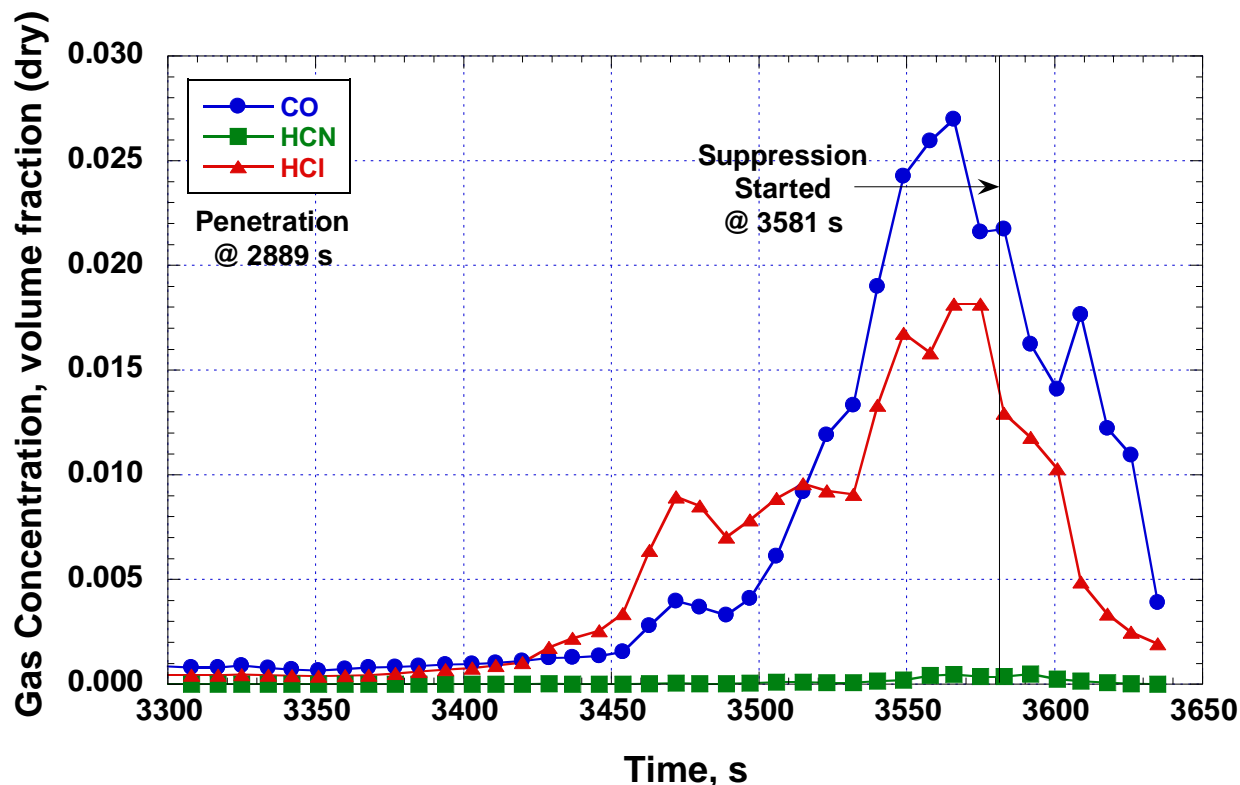


Figure 98 CO, HCN, and HCl volume fractions measured with FTIR at the rear sampling location plotted versus time for the tenability experiment.

Toxic Gas Tenability

ISO 13571 [6] was also utilized for tenability analysis for the toxic gases measured in the tenability experiment. The toxic gases considered here were CO, HCl, and HCN. CO₂ is considered as well in that it can cause more labored breathing and enhance the effects of the toxic gases.

In order to analyze the gases, some data manipulation was required. The FTIR produced data about every 8 s while the CO and CO₂ analyzers were recorded every second. The FTIR measured water vapor while the analyzers had water trapped and volume fractions were reported on a dry basis. To put the two types of data on the same basis, curve fits for water and the FTIR gases were generated and then data at every second were produced using the curve fits. Variations of the curve fits from the actual data were kept within 10 %.

The next step in the data analysis was to apply a water vapor correction to the CO and CO₂ data to put all gases on a wet basis. Water was only measured at the rear station, but three conditions supported applying the water correction to gases measured at the middle and front stations as well: (1) the water vapor volume fractions were between 1 % and 6 % leading up to extinguishment so the correction would have a relatively low impact, (2) the middle and front

stations did not lag the rear by much time so the timing of the water vapor volume fraction increase could be assumed to be similar, and (3) since the CO and CO₂ volume fraction magnitudes were comparable in the front as to the rear, the water vapor volume fraction could be assumed to be of similar magnitude to that in the rear.

If the CO₂ measurement at a given time was over 2 %, a toxicity enhancement multiplying factor, $e^{(CO_2)/5}$, was applied to the CO and HCN volume fractions due to hyperventilation caused by the high CO₂ levels. [6] Finally, HCN from the rear FTIR measurement was assumed to be uniform throughout the motorcoach and was combined with the middle and front CO measurements for some analyses.

Equation (4) defines the total FED accumulated exposure for both CO and HCN. [6] The equation has a 35 % uncertainty (specified in the standard).

$$X_{FED} = \sum_{t1}^{t2} \frac{CO}{35000} \Delta t + \sum_{t1}^{t2} \frac{\exp(HCN / 43)}{220} \Delta t \quad (4)$$

where: X_{FED} is the fractional effective dose,
 CO and HCN are gas volume fractions in $\mu\text{L/L}$,
 t is time in minutes, and
 $t1$ and $t2$ are time interval limits in minutes

The two terms are plotted separately in Figure 99 for the rear (CO and HCN), middle (CO), and front (CO) sampling positions. When acting alone, the time to incapacitation was 3516 s for rear HCN, 3526 s for rear CO, 3540 s for middle CO, and 3536 s for front CO. Combining the rear HCN with the CO for each position results in the plot in Figure 100. All of the curves converge due to the strong influence of HCN on the totals. The incapacitating dose is reached within 1 s of 3508 s for all three positions. This time to untenable conditions is 10 min 19 s after penetration.

HCl, as an upper-respiratory irritant, requires a FEC (fractional effective concentration) analysis. Equation (5) shows that it is a simple ratio of the concentration to the compromising threshold concentration. [6] The uncertainty in this equation is 50 % (specified in the standard).

$$X_{FEC} = \frac{HCl}{F_{HCl}} \quad (5)$$

where: X_{FEC} is the fractional effective concentration,
 HCl is the gas volume fraction in $\mu\text{L/L}$,
 F_{HCl} is the gas volume fraction in $\mu\text{L/L}$ of HCl expected to seriously compromise an occupant's ability to accomplish escape (1000 $\mu\text{L/L}$ from [6]),
 t is time in minutes, and
 $t1$ and $t2$ are time interval limits in minutes

The plot in Figure 101 shows that the FEC for HCl increases rapidly at 3419 s and crosses the incapacitating dose line at 3420 s which is 8 min 51 s after penetration.

Related to toxic gas tenability is asphyxiation due to oxygen vitiation. Oxygen volume fractions below 10 % are considered lethal. [48] For this experiment, this threshold was reached at 3531 s, 3543 s, and 3548 s for the rear, front, and middle stations, respectively.

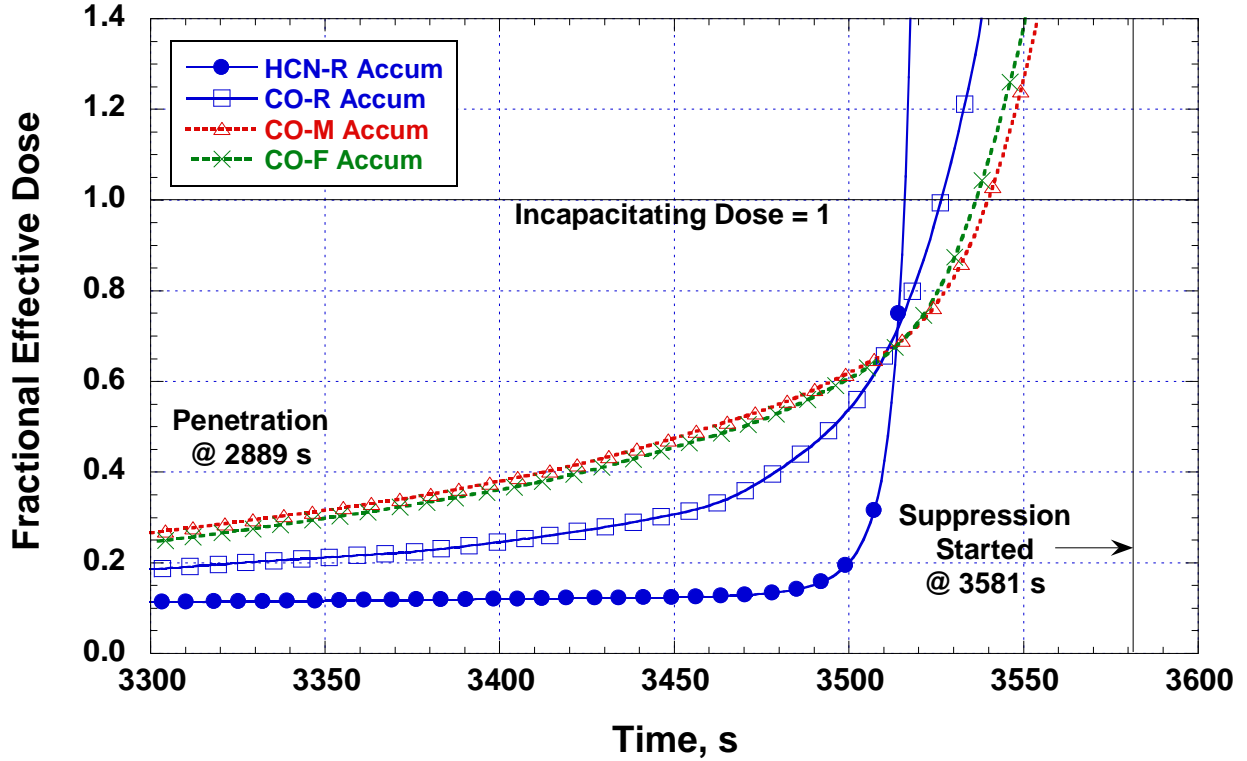


Figure 99 Fractional effective doses for HCN and CO measured at the rear (R), middle (M), and front (F) sampling locations plotted versus time for the tenability experiment.

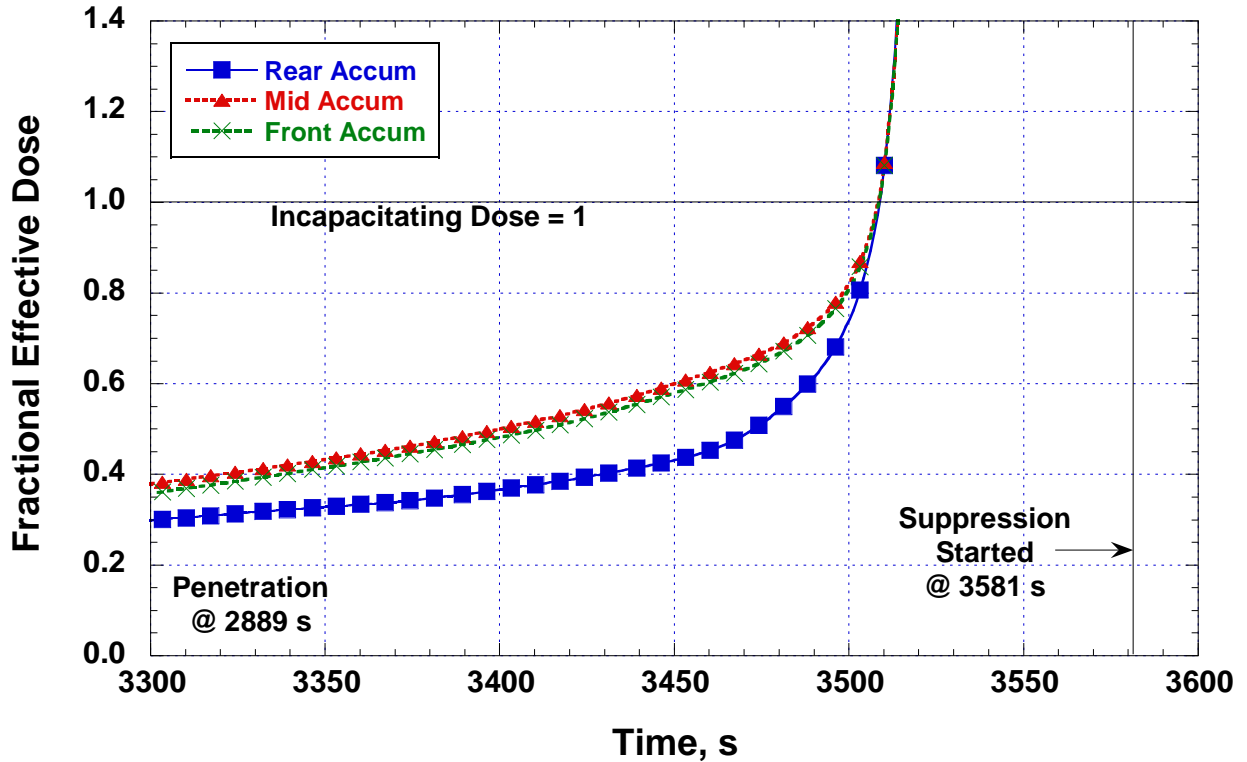


Figure 100 Total (both CO and HCN) fractional effective doses for the rear (R), middle (M), and front (F) sampling locations plotted versus time for the tenability experiment.

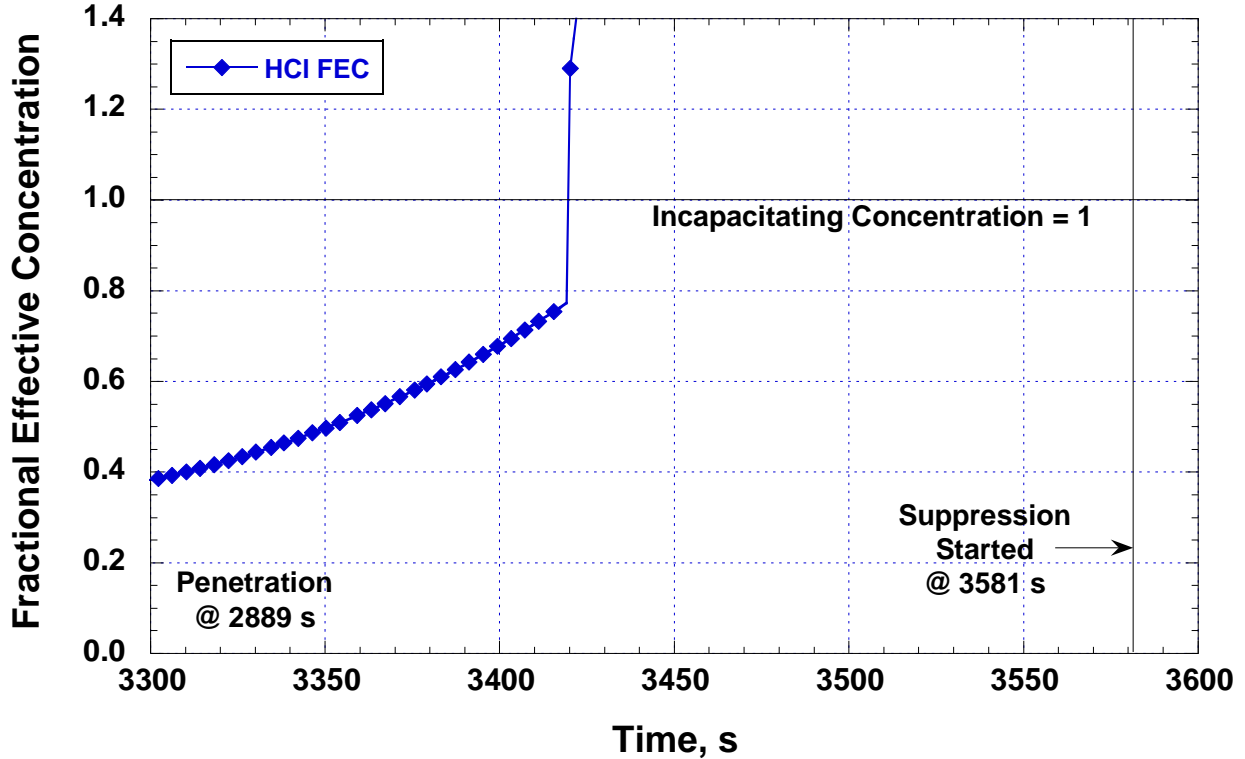


Figure 101 Fractional effective concentration for HCl measured with FTIR at the rear sampling location plotted versus time.

Table 16 lists the various hazardous conditions that were measured during the tenability experiment and the corresponding times for untenable levels to be reached from the time of fire penetration. The thermal hazards are listed as well as the gaseous ones. For the rear and middle locations, the thermal hazards reached untenable levels earlier than the other hazards. For the front location, heat flux was not measured, but the time for convective untenable conditions was comparable to those for gaseous hazards. Adding heat flux to the front location analysis could put thermal conditions as the leading hazard there, similarly to the other locations, or HCl may have been the fastest hazard at the front to reach an untenable level. Of the toxicity, asphyxiation, and irritant hazards, HCl led the others to untenable conditions by over 1.5 min. Oxygen vitiation was the last hazard to reach untenable levels. All of these hazards would normally act synergistically which would cause incapacitation leading to death earlier than any single component alone.

Table 16 Comparison of times from fire penetration to untenable conditions

Location	Time from Fire Penetration to Untenable Conditions					
	Rear		Middle		Front	
	(s)	(min:s)	(s)	(min:s)	(s)	(min:s)
Radiative (heat flux)	522	8:42	450	7:30	N/A	N/A
Convective (temperature) fully clothed	641	10:41	675	11:15	676	11:16
Convective (temperature) lightly clothed	595	9:55	648	10:48	637	10:37
Combined radiative and convective (fully clothed)	329	5:29	445	7:25	N/A	N/A
Combined radiative and convective (lightly clothed)	306	5:06	426	7:06	N/A	N/A
Carbon monoxide (CO)	637	10:37	651	10:51	647	10:47
Hydrogen cyanide (HCN)	627	10:27	*627	*10:27	*627	*10:27
Combined CO and HCN	619	10:19	619	10:19	619	10:19
Hydrogen chloride (HCl)	531	8:51	*531	*8:51	*531	*8:51
Oxygen vitiation	642	10:42	659	10:59	654	10:54

* Levels assumed at locations (middle and front) other than where measured (rear).

Visibility

The smoke measurements had indeterminate results. The instrument signal shifted dramatically at times which seemed unrelated to smoke attenuation and was possibly due to beam shifting (sometimes caused by heating of mounting apparatus). The voltage became negative during part of the experiment which precluded a meaningful analysis.

The video recording of the exit signs to determine visibility resulted in the times and distances listed in Table 17. Analysis was accomplished by viewing of the video recording and determining the times that signs could not be seen based on the judgment of the viewer. Sign visibility may have been slightly enhanced by the low level of ambient light within the motorcoach. The plot in Figure 102 shows the relationship between the visibility distance and tire ignition time. The trend in the plot shows a linear decrease in visibility distance with time. It is interesting that smoke from the tire fire resulted in nearly no visibility in the motorcoach interior even before fire penetrated into the passenger compartment.

Table 17 List of distances and time visibility ended for the tenability experiment exit signs.

Exit Sign Location from Lavatory Door (m)	Exit Sign Distance from Video Camera (m)	Time After Burner Removed for No Visibility (s)
0	12	237
2	10	411
4	8	462
6	6	589
8	4	603
10	2	711

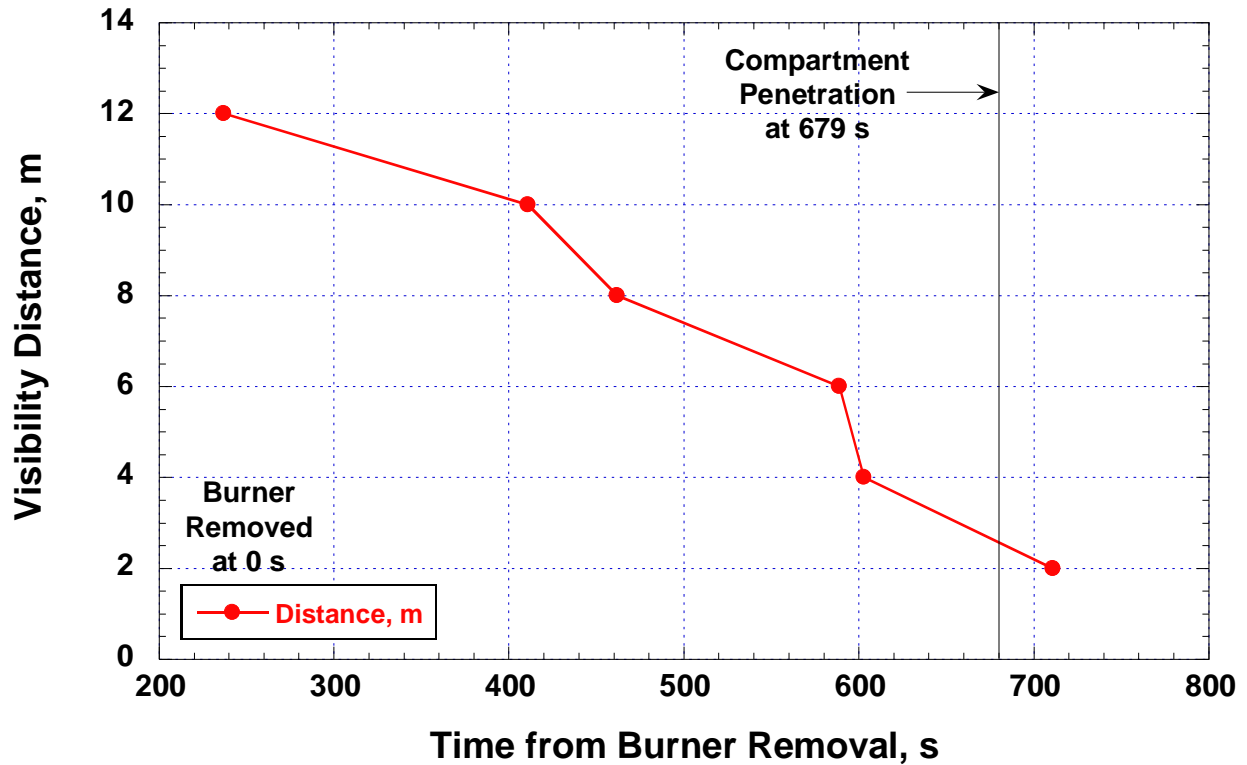


Figure 102 Visibility distance plotted versus the time from burner removal for the exit signs during the tenability experiment.

Extinguishment

Extinguishment of the tenability experiment fires required a longer period of time than any of the previous experiments. Water and foam were used on the exterior at 3581 s after burner removal, but a water hose was required on the interior. The interior fire was attacked through the doorway within 20 s of the exterior extinguishment activity. The valve for the fixed sprinkler in the ceiling was not opened. The majority of the fire was doused within 1 min. Approximately 80 L (21 gal) to 100 L (26 gal) of water and foam were required to extinguish the fire excluding subsequent cooling operations. At the time of the motorcoach's manufacture, safety equipment included a 2.3 kg (5 lb) ABC dry chemical (powder) fire extinguisher, but no water-based extinguishers.

SUMMARY OF FINDINGS AND CONCLUSIONS

Material Flammability Testing

Four motorcoach interior components (interior wall panels, parcel rack doors, seat fronts, and seat backs) were selected for the series of flammability tests which would be required if the components were used in railroad passenger cars or commercial aircraft. A limited sample of previously used interior components from particular bus models (2000 MCI E-series and 2003 to 2009 MCI J-series) was tested as a spot check of the large number of combinations of manufacturer, model, age, and component design. The performance of these typical components is considered representative of those used by other motorcoach manufacturers. Based on the flammability test results, the following are the findings and the conclusions which can be drawn:

- One interior material, the back of the seat backrest, failed the FMVSS 302 requirement by exceeding the horizontal burn rate by 25 %.
- Other than the interior wall panel, all of the other components (parcel rack doors, seat fronts, and seat backs) failed the Federal Aviation Administration (FAA) flammability requirements.
- All of the components tested failed the Federal Railroad Administration (FRA) flammability requirements.
- The poor flammability test performance of the seat components and the parcel rack door showed that they burn significantly more easily than comparable components approved for use in aircraft and railcars.
- The seats and the parcel rack doors were the first interior components involved in the tenability tire fire experiment, and they constitute a majority of the combustible interior mass. Improved flammability performance of these items may significantly increase time for fire spread and untenable conditions once a fire penetrates into the passenger compartment of a motorcoach.

Penetration Experiments

Two motorcoach tire fire experiments were conducted to investigate the mode by which tire fires penetrate the passenger compartment. A novel burner was designed to simulate frictional heating by failed axle bearings, locked brakes, or dragged blown tires with localized heating of wheel metal without substantially preheating the tire rubber. Temperatures and heat fluxes were recorded along with video and still images. Based on this specific motorcoach and the conditions of these particular experiments, the following are the findings and the conclusions which can be drawn:

- Tire fire penetration into the passenger compartment occurred from flame impingement on windows and the resulting glass breakage. This finding is in contrast with research conducted by SP [17] (on a different model motorcoach) when a non-combustible barrier was placed on the exterior above the tires and fire penetration through the windows did not occur.
- A tire fire can spread to combustible exterior fenders or panels within 2 min of a sustained fire on the tire.
- The time between the start of a self-sustained or established tire fire and window breakage by fire can be less than 5 min.

- The slow rates of rise of floor and central tunnel temperatures indicate that the floor, lavatory, and central tunnel are protected sufficiently for this particular motorcoach and are not likely pathways for passenger compartment penetration in the early stages of a tire fire prior to or immediately following window penetration.
- For the drive axle experiment, based on the rates of temperature increase observed before extinguishment, there is a possibility of an initial tire fire crossing the motorcoach by way of the drive axle within several minutes of window penetration. Window penetration on the second side would lag behind that on the primary side by the delay of the spread of fire across the axle. The tag axle experiment did not show significant heating along either axle at the center of the motorcoach or on the driver's side.
- Temperatures in the wheel well and along the axles were sufficiently high with potential to ignite or damage any combustible materials underneath the motorcoach, but the floor and interior areas near the fire were protected by stainless steel sheet metal and a layer of insulation. Additional penetration points could occur from local degradation of less protected areas, but this was not observed for the conditions experienced in these tests with the design of this particular motorcoach.
- The relatively easy extinguishment of these tire fires (less than 15 s) with foam and water suggests that these tire fires, while established, were not yet fully involved (when all tire rubber in contact with the wheel is burning simultaneously). [13] If heating of wheel metal was substantially greater for an actual moving motorcoach than it was for these experiments, it is possible that a much larger initial fire would ensue involving the whole tire when the coach stopped rolling. A tire fire which was more fully involved initially than for these tests could have a different spreading behavior which could change the timing of window penetration.
- There was a wide range of timing for window penetration as demonstrated by the first tag axle experiment which experienced penetration in less than 5 min and the tenability tag axle experiment which experienced penetration in over 11 min. It is not known why the penetration times are different. Possible reasons include: variation in the wheel burner heating which could have caused different initial fire conditions for the two tire fires, variation in window strength and performance, and natural variation in how the plumes interacted with the windows.

Fire-hardening Experiments

Three motorcoach tire fire experiments were conducted to investigate fire-hardening methods that might protect a motorcoach from tire fire penetration into the passenger compartment or at least delay penetration. The three methods were: replacing the combustible exterior panel and fender with sheet steel, applying an intumescent coating to the combustible exterior panel and fender, and installing a fire plume deflector between the fender and exterior side panel.

Temperatures and heat fluxes were recorded along with video and still images. Based on this specific motorcoach, the conditions of these particular experiments, and the particular protective designs which were attempted, the following are the findings and the conclusions which can be drawn:

- Of the three fire-hardening methods examined here, two (replacing exterior combustible components with metal or coating existing combustible panels with intumescent materials) appear to be effective approaches to improving fire safety for wheel well fires.

Replacement or treatment was effective when performed on materials located above or near the tires.

- Replacing the combustible exterior side components directly over the tires with sheet metal was the most effective design for preventing the tire fire from penetrating through the windows. For the conditions tested here, it prevented penetration, but materials behind the replacement panels approached temperatures which may have led to interior ignition and flame spread. Fire penetration was delayed approximately 30 min before the test was terminated compared to the tag axle experiments without fire-hardening.
- The intumescent coating on the combustible exterior side components near the tires was the second most effective design for preventing the tire fire from penetrating through the windows. Fire penetration did occur, but it was delayed approximately 20 min compared to the tag axle experiments without fire-hardening.
- A steel deflector shield had an indeterminate effectiveness on preventing the tire fire from penetrating through the windows. The penetration time was 5 min longer than one tag axle experiment, but was 1.5 min shorter than that for the tenability tag axle experiment. Larger deflector designs that push the fire plume further from the windows could be more effective, but could create other issues related to practical implementation.
- The ABS sensor as deployed for these experiments did not respond to heating from the adjacent wheel and hub metal consistently or sufficiently to provide an effective signal of an approaching or occurring tire fire; however, a simple temperature measurement device such as a thermocouple located near the wheel could provide early warning of adverse heating in the vicinity well before tire ignition temperatures are reached.

Tenability Experiment

One experiment was conducted to ascertain the approximate time for conditions to become untenable in the passenger compartment of a motorcoach with a tire fire. A mock up of a motorcoach front end was constructed and attached to the rear half of the test motorcoach. Temperatures, heat fluxes, gas volume fractions, and visibility were measured and analyzed with regards to tenability criteria. The calculations of accumulated doses of thermal or toxic conditions have uncertainties of up to 50 % which in turn impact the estimates for time to untenable conditions. Based on this specific motorcoach, the design of its extension, the open door and fuel loading configurations, and the conditions of these particular experiments, the following are the findings and the conclusions which can be drawn:

- Thermally untenable conditions were reached in the rear and middle of the motorcoach in less than 7 min after fire penetration. The front of the motorcoach became thermally untenable by about 11 min.
- Assuming smoke layer uniformity, carbon monoxide and hydrogen cyanide combined to make conditions untenable throughout the motorcoach at just over 11 min after fire penetration.
- Assuming smoke layer uniformity, hydrogen chloride caused untenable conditions in the rear of the motorcoach at just under 9 min after fire penetration.
- Oxygen vitiation caused untenable conditions throughout the motorcoach by 11 min after fire penetration.
- Thermal conditions were generally more severe at earlier times than toxic, irritant, or asphyxiant gas conditions.

- Combination of the incapacitating effects of thermal and toxic gas effects would shorten tenability time and time to escape.
- Visibility conditions (evaluated 1.5 m from the floor) deteriorated significantly prior to fire penetration of the motorcoach. Within 30 s after penetration, visibility decreased to less than 2 m. Poor visibility could have made egress from this motorcoach difficult several minutes before conditions became untenable.
- The combination of three pairs of seats and partial trim installation was sufficient fuel loading to cause flashover (bring to 600 °C and 20 kW/m²) in the rear half of the passenger compartment in less than 11 min after fire penetration.
- Untenable conditions for this experiment were attained with a very limited fuel loading. This suggests that the conditions and timing observed in this experiment were not the most conservative.

RECOMMENDATIONS

Based on the particular interior motorcoach components tested (from 2000 MCI E-series and 2003 to 2009 MCI J-series) and the limited experiments conducted, the following recommendations are made, but pertinence and application to other motorcoach models must be considered as well as cost-benefit analyses which have not been conducted:

- A simple temperature measurement device such as a thermocouple located near the wheel should be investigated further as a source for early warning of adverse heating and an impending tire fire.
- It is recommended that fire hardening of external components above the wheel wells be considered as part of a holistic fire safety analysis. Designs utilizing replacement of combustible materials with metal should consider the potential of heat from a tire fire to conduct through the metal to combustible materials in the motorcoach wall structure.
- To potentially lead to additional design options for hardening a motorcoach exterior against tire fires, *exterior* components should be flammability tested to examine ignition and flame spread behavior due to impinging flames or substantial radiative heat flux.
- If reduced fire spread and increased time to untenable conditions are desired, it is recommended that flammability requirements for interior components analogous to those required by FRA and/or FAA be considered. Further research is needed to quantify the impact on fire spread and time to untenable conditions of improved flammability performance of the seats and parcel rack doors.
- Flammability testing (beyond FMVSS 302) of interior components vulnerable to early ignition by tire fire and not examined in the current study is recommended, including combustible coverings of window posts and window shades. Additional research is needed to quantify their role in early fire spread immediately after tire fire penetration.

ACKNOWLEDGEMENTS

This work was sponsored by the National Highway Traffic Safety Administration.

Thanks to Marco Fernandez and the Large Fire Laboratory staff (Matt Bundy, Laurean DeLauter, Tony Chakalis, and Doris Rinehart, and Artur Chernovsky) for all of the hard work preparing for and running this challenging experimental project. Thanks to Ed Hnetkovsky for help with the burner. We're grateful to the NIST Fire Protection Group and Roy McLane and Andrew Lock of the Fire Fighting Technology Group for providing backup suppression. Equipment loans from Roy McLane, Jay McElroy, and Rick Davis were appreciated. Thanks to Nathan Marsh for conducting the FTIR measurements. Thanks to Rick Peacock for video help and Kevin McGrattan for FDS modeling. Also, the NIST Plant Division is appreciated for providing crews to move the motorcoach.

NIST thanks Randy Smith and Alex Cook of Greyhound for technical advice regarding removal and replacement of motorcoach components.

REFERENCES

- [1] National Transportation Safety Board, Motorcoach fire on Interstate 45 during Hurricane Rita evacuation near Wilmer, Texas, September 23, 2005, NTSB/HAR-07/01, NTSB, Washington, DC, February 21, 2007.
- [2] N. R. Meltzer, G. J. Ayres, M. H. Truong, Motorcoach Fire Safety Analysis, Volpe National Transportation Systems Center for Federal Motor Carrier Safety Administration, Cambridge, MA, July 2009.
- [3] E. L. Johnsson, J. C. Yang, Motorcoach Flammability Project Interim Report: Tire Fire Penetration Into the Passenger Compartment, NIST Technical Note 1653, NIST, Gaithersburg, MD, May 2010.
- [4] Braun, E., Davis, S., Klote, J.H., Levin, B.C., and Paabo, M., "Assessment of the Fire Performance of School Bus Interior Components," NISTIR 4347, National Institute of Standards and Technology, U.S. Department of Commerce, Washington DC, July 1990.
- [5] Fardell, P.J., Kumar, S., Ellwood, J.A., Rowley, J.A., and Vollam, S., "A Study of Life Threat in Bus Fires," Proceedings of INTERFLAM'93, 6th International Fire Conference, Interscience Communication Ltd., London, United Kingdom, pp.401-411 (1993).
- [6] ISO 13571:2007, Life-Threatening Components of Fire – Guidelines for the Estimation of Time Available for Escape using Fire Data, International Organization of Standardization, Geneva, Switzerland.
- [7] Cox, G. and Kumar, S., "Field Modelling of Fire in Forced Ventilated Enclosures," Combustion Science and Technology, **52** (1-3): 7-23 (1987).
- [8] Chow, W.K., "Preliminary Notes on Fire Protection in Buses," Journal of Applied Fire Science, **9** (1): 79-89 (1999).
- [9] Chow, W.K., "Flashover for Bus Fires from Empirical Equations," Journal of Fire Sciences, **19**: 81-93 (2001).
- [10] Chow, W.K., "Observation on the Two Recent Bus Fires and Preliminary Recommendations to Provide Fire Safety," International Journal on Engineering Performance-Based Fire Codes, **5** (1): 1-5 (2003).
- [11] Chow, W.K., Lam, K.C., Fong, N.K., Dong, H., Zou, G.W., and Gao, Y., "Scale Modelling Results on Smoke Spreading and Control in a Double-Deck Bus," International Journal on Engineering Performance-Based Fire Codes, **8** (4): 145-151 (2006).
- [12] ASTM Standard E648 - 09a, Standard Test Method for Critical Radiant Flux of Floor-Covering Systems Using a Radiant Heat Energy Source, ASTM International, West Conshohocken, Pennsylvania.
- [13] Peacock, R.D., Forney, G.P., Reneke, P., Portier, R., and Jones, W.W., CFAST, the Consolidated Model of Fire Growth and Smoke Transport, NIST Technical Note 1299, U.S. Department of Commerce, Washington, DC, 1993.
- [14] Hansen, P.A., "Fires in Tyres, Heat Release Rate and Response of Vehicles," SINTEF Reports, STF25 A95039, SINTEF NBL-Norwegian Fire Research Laboratory, April 1995.
- [15] Brandt, A.W., "Method for Testing the Response of Vehicles Exposed to a Fire Simulating Burning Tyres," STF22 A98833, SINTEF NBL-Norwegian Fire Research Laboratory, May 1998.
- [16] Stensaas, J.P., Jacobsen, H.C., "Testing of Different Portable Fire Extinguishers against Fires in Twin Tyres," NBL10 A01159, SINTEF NBL-Norwegian Fire Research Laboratory, December 2001.
- [17] Hammarström, R., Axelsson, J., Försth, M., Johansson, P., and Sundström, B., "Bus Fire Safety," SP Report 2008:41, SP Technical Research Institute of Sweden, 2008.
- [18] ISO 3795:1989, Road Vehicles, and Tractors and Machinery for Agriculture and Forestry -- Determination of Burning Behaviour of Interior Materials, International Organization of Standardization, Geneva, Switzerland.
- [19] ISO 5660-1:2002, Reaction-to-Fire Tests -- Heat Release, Smoke Production and Mass Loss Rate -- Part 1: Heat Release Rate (Cone Calorimeter Method), International Organization of Standardization, Geneva, Switzerland.
- [20] ISO 11925-2:2002, Reaction to Fire Tests -- Ignitability of Building Products Subjected to Direct Impingement of Flame -- Part 2: Single-Flame Source Test, International Organization of Standardization, Geneva, Switzerland.
- [21] CBUF (Combustion Behaviour of Upholstered Furniture) - Fire Safety of Upholstered Furniture - the Final Report on the CBUF Research Programme, EC Report EUR 16477 EN, Interscience Communication, London, 1994.
- [22] ISO 6941:2003, Textile Fabrics -- Burning Behaviour -- Measurement of Flame Spread Properties of Vertically Oriented Specimens, International Organization of Standardization, Geneva, Switzerland.
- [23] McGrattan, K. and Forney, G., Fire Dynamics Simulator (Version 4), User's Guide, NIST Special Publication 1019, U.S. Department of Commerce, Washington, DC, July 2004.
- [24] 49 CFR Part 571.302, Federal Motor Vehicle Safety Standards, Standard No. 302, Flammability of Interior Materials, National Highway Traffic Safety Administration, Department of Transportation.

- [25] United Nations Economic Commission for Europe (ECE), Regulation No. 118, Uniform Technical Descriptions Concerning the Burning Behaviour of Materials Used in the Interior Construction of Certain Categories of Motor Vehicles.
- [26] 49 CFR Part 238.103, Passenger Equipment Safety Standards, Fire Safety, Federal Railroad Administration, Department of Transportation.
- [27] 14 CFR Part 25.853, Compartment Interiors, Federal Aviation Administration, Department of Transportation.
- [28] Axelsson, J., Johansson, P., Petzall, J., and Hagerupsen, A., "Fire Safety in Buses," Proceedings of Fire and Materials Conference, San Francisco, California, 2007.
- [29] Digges, K.H., Gann, R.G., Grayson, S.J., Hirschler, M.M., Lyon, R.E., Purser, D.A., Quintiere, J.G., Stephenson, R.R., and Tewarson, A., "Improving Survivability in Motor Vehicle Fires," Proceedings of INTERFLAM'07, 11th International Fire Conference, Interscience Communication Ltd., London, United Kingdom, pp. 135-143 (2007).
- [30] Underwriters Laboratories, "Investigation of the Fire Performance of Materials and Products for Use in U.S. Railcar and Bus Applications," UL Final Report, Northbrook, IL, June 16, 2008.
- [31] Informal Document No. GRSG-95-19, 21-24 October 2008.
- [32] ISO 5658-2:2006, Reaction to Fire Tests -- Spread of Flame -- Part 2: Lateral Spread on Building and Transport Products in Vertical Configuration, International Organization of Standardization, Geneva, Switzerland.
- [33] ISO 5659-2:2006, Plastics -- Smoke Generation -- Part 2: Determination of Optical Density by a Single-Chamber Test, International Organization of Standardization, Geneva, Switzerland.
- [34] ISO 9239-1:2002, Reaction to Fire Tests for Floorings -- Part 1: Determination of the Burning Behaviour using a Radiant Heat Source, International Organization of Standardization, Geneva, Switzerland.
- [35] prCEN/TS 45545-2:2008, Railway Applications - Fire Protection on Railway Vehicles - Part 2: Requirements for Fire Behaviour of Materials and Components, European Committee for Standardization, Brussels, Belgium.
- [36] ASTM Standard C1166 - 06, Standard Test Method for Flame Propagation of Dense and Cellular Elastomeric Gaskets and Accessories, ASTM International, West Conshohocken, Pennsylvania.
- [37] ASTM Standard D3675 - 09, Standard Test Method for Surface Flammability of Flexible Cellular Materials Using a Radiant Heat Energy Source, ASTM International, West Conshohocken, Pennsylvania.
- [38] ASTM Standard E119 - 09, Standard Test Methods for Fire Tests of Building Construction and Materials, ASTM International, West Conshohocken, Pennsylvania.
- [39] ASTM Standard E162 - 09, Standard Test Method for Surface Flammability of Materials Using a Radiant Heat Energy Source, ASTM International, West Conshohocken, Pennsylvania.
- [40] ASTM Standard E662 - 09, Standard Test Method for Specific Optical Density of Smoke Generated by Solid Materials, ASTM International, West Conshohocken, Pennsylvania.
- [41] "Aircraft Materials Fire Test Handbook," Final Report DOT/FAA/AR-00/12, April 2000, Department of Transportation, Federal Aviation Administration.
- [42] R. A. Bryant, T. J. Ohlemiller, E. L. Johnsson, A. P. Hamins, B. S. Grove, W. F. Guthrie, A. Maranghides, G. W. Mulholland, The NIST 3 Megawatt Quantitative Heat Release Rate Facility, NIST Special Publication 1007, NIST, Gaithersburg, MD, December 2003.
- [43] C. Huggett, Estimation of Rate of Heat Release by Means of Oxygen Consumption Measurements, *Fire and Materials* **4** (2), 61-65 (1980).
- [44] L. G. Blevins, W. M. Pitts, Modeling of Bare and Aspirated Thermocouples in Compartment Fires, *Fire Safety Journal*, **33** Volume 33, Issue 4, November 1999, 239-259.
- [45] W. M. Pitts, A.V. Murthy, J. L. deRis, J. R. Filtz, K. Nygard; D. Smith, I. Wetterlund, Round Robin Study of Total Heat Flux Gauge Calibration at Fire Laboratories, *Fire Safety Journal*, Vol. 41, No. 6, 459-475, September 2006.
- [46] J. F. Krasny, W. J. Parker, V. Babrauskas, *Fire Behavior of Upholstered Furniture and Mattresses*, William Andrew Publishing, LLC, Norwich, NY (2001).
- [47] NFPA; *Fire Protection Handbook*, 20th Edition. National Fire Protection Assoc., Quincy, MA, Cote, A. E.; Grant, C. C.; Hall, J. R., Jr.; Solomon, R. E., Editor(s), 2008.
- [48] D.A. Purser, Assessment of Hazards to Occupants from Smoke, Toxic Gases and Heat. *The SFPE Handbook of Fire Protection Engineering* 4th ed, DiNenno P.J (ed.), National Fire Protection Association, Quincy, MA, 2009, pp. 2/96 - 2/193.

APPENDICES

Appendix A. Data Channel Description and Hook-up Lists

Penetration and Fire Hardening Experiments

LFL MIDAS Hookup Sheet Instrument and Channel Description	LabView file: LFLMIDASCenterMotorCoach031709 .vi	Series:	Motorcoach Fires - Johnsson			Revision Date: 3/24/09			
Main Channels	Location Description	Overall Channel Number	Abbr.	MIDAS Station	Mod.	Mod. Ch. No.	Conv. Units	Wire	Gain
5 V Marker Channel	At MIDAS Center	0	5VMarker	Center	1	0	V	Cu	1
Tamb	At MIDAS Center station	1	Tamb	Center	1	1	°C	TC	100
Total Heat Flux Gauge Rear/Side (SN127848)	See Table 9	2	HFRS	Center	1	2	kW/m	Cu	100
Total Heat Flux Gauge Front/Side (SN128324)	See Table 9	3	HFFS	Center	1	3	kW/m	Cu	100
Total Heat Flux Gauge Rear/Down (SN128321)	See Table 9	4	HFRD	Center	1	4	kW/m	Cu	100
Total Heat Flux Gauge Front/Down (SN127841)	See Table 9	5	HFFD	Center	1	5	kW/m	Cu	100
Temperature of Total HF Gauge Rear/Side (SN127848)	See Table 9	6	THFRS	Center	1	6	°C	TC	100
Temperature of Total HF Gauge Front/Side (SN128324)	See Table 9	7	THFFS	Center	1	7	°C	TC	100
Temperature of Total HF Gauge Rear/Down (SN128321)	See Table 9	8	THFRD	Center	1	8	°C	TC	100
Temperature of Total HF Gauge Front/Down (SN127841)	See Table 9	9	THFFD	Center	1	9	°C	TC	100
Window Temperature Outside Array 1 TC 1	79 cm up from bottom of glass	10	O1T1	Center	1	10	°C	TC	100
Window Temperature Outside Array 1 TC 2	41 cm up from bottom of glass	11	O1T2	Center	1	11	°C	TC	100
Window Temperature Outside Array 1 TC 3	3 cm up from bottom of glass	12	O1T3	Center	1	12	°C	TC	100
Window Temperature Outside Array 1 TC 4	35 cm down from bottom of glass	13	O1T4	Center	1	13	°C	TC	100
Window Temperature Outside Array 2 TC 1	79 cm up from bottom of glass	14	O2T1	Center	1	14	°C	TC	100
Window Temperature Outside Array 2 TC 2	41 cm up from bottom of glass	15	O2T2	Center	1	15	°C	TC	100
Window Temperature Outside Array 2 TC 3	3 cm up from bottom of glass	16	O2T3	Center	1	16	°C	TC	100
Window Temperature Outside Array 2 TC 4	35 cm down from bottom of glass	17	O2T4	Center	1	17	°C	TC	100
Window Temperature Outside Array 3 TC 1	79 cm up from bottom of glass	18	O3T1	Center	1	18	°C	TC	100
Window Temperature Outside Array 3 TC 2	41 cm up from bottom of glass	19	O3T2	Center	1	19	°C	TC	100
Window Temperature Outside Array 3 TC 3	3 cm up from bottom of glass	20	O3T3	Center	1	20	°C	TC	100
Window Temperature Outside Array 3 TC 4	35 cm down from bottom of glass	21	O3T4	Center	1	21	°C	TC	100
Window Temperature Outside Array 4 TC 1	79 cm up from bottom of glass	22	O4T1	Center	1	22	°C	TC	100
Window Temperature Outside Array 4 TC 2	41 cm up from bottom of glass	23	O4T2	Center	1	23	°C	TC	100
Window Temperature Outside Array 4 TC 3	3 cm up from bottom of glass	24	O4T3	Center	1	24	°C	TC	100
Window Temperature Outside Array 4 TC 4	35 cm down from bottom of glass	25	O4T4	Center	1	25	°C	TC	100
Window Temperature Outside Array 5 TC 1	79 cm up from bottom of glass	26	O5T1	Center	1	26	°C	TC	100
Window Temperature Outside Array 5 TC 2	41 cm up from bottom of glass	27	O5T2	Center	1	27	°C	TC	100

THIS IS A PREDECISIONAL DRAFT INTERIM REPORT

Main Channels	Location Description	Overall Channel Number	Abbr.	MIDAS Station	Mod.	Mod. Ch. No.	Conv. Units	Wire	Gain
Window Temperature Outside Array 5 TC 3	3 cm up from bottom of glass	28	O5T3	Center	1	28	°C	TC	100
Window Temperature Outside Array 5 TC 4	35 cm down from bottom of glass	29	O5T4	Center	1	29	°C	TC	100
Window Temperature Outside Array 6 TC 1	79 cm up from bottom of glass	30	O6T1	Center	1	30	°C	TC	100
Window Temperature Outside Array 6 TC 2	41 cm up from bottom of glass	31	O6T2	Center	1	31	°C	TC	100
Window Temperature Outside Array 6 TC 3	3 cm up from bottom of glass	32	O6T3	Center	2	0	°C	TC	100
Window Temperature Outside Array 6 TC 4	35 cm down from bottom of glass	33	O6T4	Center	2	1	°C	TC	100
Window Temperature Outside Array 7 TC 1	79 cm up from bottom of glass	34	O7T1	Center	2	2	°C	TC	100
Window Temperature Outside Array 7 TC 2	41 cm up from bottom of glass	35	O7T2	Center	2	3	°C	TC	100
Window Temperature Outside Array 7 TC 3	3 cm up from bottom of glass	36	O7T3	Center	2	4	°C	TC	100
Window Temperature Outside Array 7 TC 4	35 cm down from bottom of glass	37	O7T4	Center	2	5	°C	TC	100
Window Temperature Outside Array 8 TC 1	79 cm up from bottom of glass	38	O8T1	Center	2	6	°C	TC	100
Window Temperature Outside Array 8 TC 2	41 cm up from bottom of glass	39	O8T2	Center	2	7	°C	TC	100
Window Temperature Outside Array 8 TC 3	3 cm up from bottom of glass	40	O8T3	Center	2	8	°C	TC	100
Window Temperature Outside Array 8 TC 4	35 cm down from bottom of glass	41	O8T4	Center	2	9	°C	TC	100
Window Temperature Outside Array 9 TC 1	79 cm up from bottom of glass	42	O9T1	Center	2	10	°C	TC	100
Window Temperature Outside Array 9 TC 2	41 cm up from bottom of glass	43	O9T2	Center	2	11	°C	TC	100
Window Temperature Outside Array 9 TC 3	3 cm up from bottom of glass	44	O9T3	Center	2	12	°C	TC	100
Window Temperature Outside Array 9 TC 4	35 cm down from bottom of glass	45	O9T4	Center	2	13	°C	TC	100
Window Temperature Outside Array 10 TC 1	79 cm up from bottom of glass	46	O10T1	Center	2	14	°C	TC	100
Window Temperature Outside Array 10 TC 2	41 cm up from bottom of glass	47	O10T2	Center	2	15	°C	TC	100
Window Temperature Outside Array 10 TC 3	3 cm up from bottom of glass	48	O10T3	Center	2	16	°C	TC	100
Window Temperature Outside Array 10 TC 4	35 cm down from bottom of glass	49	O10T4	Center	2	17	°C	TC	100
Window Temperature Outside Array 11 TC 1	79 cm up from bottom of glass	50	O11T1	Center	2	18	°C	TC	100
Window Temperature Outside Array 11 TC 2	41 cm up from bottom of glass	51	O11T2	Center	2	19	°C	TC	100
Window Temperature Outside Array 11 TC 3	3 cm up from bottom of glass	52	O11T3	Center	2	20	°C	TC	100
Window Temperature Outside Array 11 TC 4	35 cm down from bottom of glass	53	O11T4	Center	2	21	°C	TC	100
Window Temperature Outside Array 12 TC 1	79 cm up from bottom of glass	54	O12T1	Center	2	22	°C	TC	100
Window Temperature Outside Array 12 TC 2	41 cm up from bottom of glass	55	O12T2	Center	2	23	°C	TC	100
Window Temperature Outside Array 12 TC 3	3 cm up from bottom of glass	56	O12T3	Center	2	24	°C	TC	100
Window Temperature Outside Array 12 TC 4	35 cm down from bottom of glass	57	O12T4	Center	2	25	°C	TC	100
Window Temperature Inside Array 1 TC 0.5	17 cm above Array 1 TC1	58	I1T0	Center	2	26	°C	TC	100
Window Temperature Inside Array 1 TC 1	79 cm up from bottom of glass	59	I1T1	Center	2	27	°C	TC	100
Window Temperature Inside Array 1 TC 2	41 cm up from bottom of glass	60	I1T2	Center	2	28	°C	TC	100
Window Temperature Inside Array 1 TC 3	3 cm up from bottom of glass	61	I1T3	Center	2	29	°C	TC	100
Window Temperature Inside Array 2 TC 0.5	17 cm above Array 2 TC1	62	I2T0	Center	2	30	°C	TC	100
Window Temperature Inside Array 2 TC 1	79 cm up from bottom of glass	63	I2T1	Center	2	31	°C	TC	100
Window Temperature Inside Array 2 TC 2	41 cm up from bottom of glass	64	I2T2	Center	3	0	°C	TC	100
Window Temperature Inside Array 2 TC 3	3 cm up from bottom of glass	65	I2T3	Center	3	1	°C	TC	100

THIS IS A PREDECISIONAL DRAFT INTERIM REPORT

Main Channels	Location Description	Overall Channel Number	Abbr.	MIDAS Station	Mod.	Mod. Ch. No.	Conv. Units	Wire	Gain
Window Temperature Inside Array 3 TC 0.5	17 cm above Array 3 TC1	66	I3T0	Center	3	2	°C	TC	100
Window Temperature Inside Array 3 TC 1	79 cm up from bottom of glass	67	I3T1	Center	3	3	°C	TC	100
Window Temperature Inside Array 3 TC 2	41 cm up from bottom of glass	68	I3T2	Center	3	4	°C	TC	100
Window Temperature Inside Array 3 TC 3	3 cm up from bottom of glass	69	I3T3	Center	3	5	°C	TC	100
Window Temperature Inside Array 4 TC 0.5	17 cm above Array 4 TC1	70	I4T0	Center	3	6	°C	TC	100
Window Temperature Inside Array 4 TC 1	79 cm up from bottom of glass	71	I4T1	Center	3	7	°C	TC	100
Window Temperature Inside Array 4 TC 2	41 cm up from bottom of glass	72	I4T2	Center	3	8	°C	TC	100
Window Temperature Inside Array 4 TC 3	3 cm up from bottom of glass	73	I4T3	Center	3	9	°C	TC	100
Window Temperature Inside Array 5 TC 0.5	17 cm above Array 5 TC1	74	I5T0	Center	3	10	°C	TC	100
Window Temperature Inside Array 5 TC 1	79 cm up from bottom of glass	75	I5T1	Center	3	11	°C	TC	100
Window Temperature Inside Array 5 TC 2	41 cm up from bottom of glass	76	I5T2	Center	3	12	°C	TC	100
Window Temperature Inside Array 5 TC 3	3 cm up from bottom of glass	77	I5T3	Center	3	13	°C	TC	100
Window Temperature Inside Array 6 TC 0.5	17 cm above Array 6 TC1	78	I6T0	Center	3	14	°C	TC	100
Window Temperature Inside Array 6 TC 1	79 cm up from bottom of glass	79	I6T1	Center	3	15	°C	TC	100
Window Temperature Inside Array 6 TC 2	41 cm up from bottom of glass	80	I6T2	Center	3	16	°C	TC	100
Window Temperature Inside Array 6 TC 3	3 cm up from bottom of glass	81	I6T3	Center	3	17	°C	TC	100
Window Temperature Inside Array 7 TC 0.5	17 cm above Array 7 TC1	82	I7T0	Center	3	18	°C	TC	100
Window Temperature Inside Array 7 TC 1	79 cm up from bottom of glass	83	I7T1	Center	3	19	°C	TC	100
Window Temperature Inside Array 7 TC 2	41 cm up from bottom of glass	84	I7T2	Center	3	20	°C	TC	100
Window Temperature Inside Array 7 TC 3	3 cm up from bottom of glass	85	I7T3	Center	3	21	°C	TC	100
Window Temperature Inside Array 8 TC 0.5	17 cm above Array 8 TC1	86	I8T0	Center	3	22	°C	TC	100
Window Temperature Inside Array 8 TC 1	79 cm up from bottom of glass	87	I8T1	Center	3	23	°C	TC	100
Window Temperature Inside Array 8 TC 2	41 cm up from bottom of glass	88	I8T2	Center	3	24	°C	TC	100
Window Temperature Inside Array 8 TC 3	3 cm up from bottom of glass	89	I8T3	Center	3	25	°C	TC	100
Window Temperature Inside Array 9 TC 0.5	17 cm above Array 9 TC1	90	I9T0	Center	3	26	°C	TC	100
Window Temperature Inside Array 9 TC 1	79 cm up from bottom of glass	91	I9T1	Center	3	27	°C	TC	100
Window Temperature Inside Array 9 TC 2	41 cm up from bottom of glass	92	I9T2	Center	3	28	°C	TC	100
Window Temperature Inside Array 9 TC 3	3 cm up from bottom of glass	93	I9T3	Center	3	29	°C	TC	100
Window Temperature Inside Array 10 TC 0.5	17 cm above Array 10 TC1	94	I10T0	Center	3	30	°C	TC	100
Window Temperature Inside Array 10 TC 1	79 cm up from bottom of glass	95	I10T1	Center	3	31	°C	TC	100
Window Temperature Inside Array 10 TC 2	41 cm up from bottom of glass	96	I10T2	Center	4	0	°C	TC	100
Window Temperature Inside Array 10 TC 3	3 cm up from bottom of glass	97	I10T3	Center	4	1	°C	TC	100
Window Temperature Inside Array 11 TC 0.5	17 cm above Array 11 TC1	98	I11T0	Center	4	2	°C	TC	100
Window Temperature Inside Array 11 TC 1	79 cm up from bottom of glass	99	I11T1	Center	4	3	°C	TC	100
Window Temperature Inside Array 11 TC 2	41 cm up from bottom of glass	100	I11T2	Center	4	4	°C	TC	100
Window Temperature Inside Array 11 TC 3	3 cm up from bottom of glass	101	I11T3	Center	4	5	°C	TC	100
Window Temperature Inside Array 12 TC 0.5	17 cm above Array 12 TC1	102	I12T0	Center	4	6	°C	TC	100
Window Temperature Inside Array 12 TC 1	79 cm up from bottom of glass	103	I12T1	Center	4	7	°C	TC	100

THIS IS A PREDECISIONAL DRAFT INTERIM REPORT

Main Channels	Location Description	Overall Channel Number	Abbr.	MIDAS Station	Mod.	Mod. Ch. No.	Conv. Units	Wire	Gain
Window Temperature Inside Array 12 TC 2	41 cm up from bottom of glass	104	I12T2	Center	4	8	°C	TC	100
Window Temperature Inside Array 12 TC 3	3 cm up from bottom of glass	105	I12T3	Center	4	9	°C	TC	100
Inside Ignited Wheel Screwed On Back 12 o'clock Position	0° position facing outside of wheel	106	TIWh12	Center	4	10	°C	TC	100
Inside Ignited Wheel Screwed On Back 3 o'clock Position	90° position facing outside of wheel	107	TIWh3	Center	4	11	°C	TC	100
Inside Ignited Wheel Screwed On Back 6 o'clock Position	180° position facing outside of wheel	108	TIWh6	Center	4	12	°C	TC	100
Inside Ignited Wheel Screwed On Back 9 o'clock Position	270° position facing outside of wheel	109	TIWh9	Center	4	13	°C	TC	100
At Wheel/Tire Interface of Ignited Tire 12 o'clock Position	0° position facing outside of tire	110	TITi12	Center	4	14	°C	TC	100
At Wheel/Tire Interface of Ignited Tire 3 o'clock Position	90° position facing outside of tire	111	TITi3	Center	4	15	°C	TC	100
At Wheel/Tire Interface of Ignited Tire 6 o'clock Position	180° position facing outside of tire	112	TITi6	Center	4	16	°C	TC	100
At Wheel/Tire Interface of Ignited Tire 9 o'clock Position	270° position facing outside of tire	113	TITi9	Center	4	17	°C	TC	100
Inside Non-Ignited Wheels (Ignition Side) Taped On Back 12 o'clock Position	NOT USED	114	TNWh12	Center	4	18	°C	TC	100
At Wheel/Tire Interface of Non-Ignited Tire (Ignition Side)	NOT USED	115	TNTi12	Center	4	19	°C	TC	100
Inside the Wheel Well Above the Tires (Ignition Side) Behind Rear Tire		116	TIWWRear	Center	4	20	°C	TC	100
Inside the Wheel Well Above the Tires (Ignition Side) Rear Tire Center		117	TIWWRearC	Center	4	21	°C	TC	100
Inside the Wheel Well Above the Tires (Ignition Side) Middle		118	TIWWMid	Center	4	22	°C	TC	100
Inside the Wheel Well Above the Tires (Ignition Side) Front Tire Center		119	TIWWFrontC	Center	4	23	°C	TC	100
Inside the Wheel Well Above the Tires (Ignition Side) In Front of Front Tire		120	TIWWFront	Center	4	24	°C	TC	100
At Rear Wheel/Tire Interface (Unignited Side) 12 o'clock Position	NOT USED	121	TURTi12	Center	4	25	°C	TC	100
At Front Wheel/Tire Interface (Unignited Side) 12 o'clock Position	NOT USED	122	TUFTi12	Center	4	26	°C	TC	100
Inside the Wheel Well Above the Tires (Unignited Side) Rear Tire Center		123	TUWWRearC	Center	4	27	°C	TC	100
Inside the Wheel Well Above the Tires (Unignited Side) Front Tire Center		124	TUWWFrontC	Center	4	28	°C	TC	100
Joint of Floor with Lavatory Near Tank, Outside Corner of Outside Wall and Lavatory Wall		125	TLXWallCorn	Center	4	29	°C	TC	100
Joint of Floor with Lavatory Near Tank, Inside Joint of Lavatory Wall and Floor		126	TLMidJoint	Center	4	30	°C	TC	100

THIS IS A PREDECISIONAL DRAFT INTERIM REPORT

Main Channels	Location Description	Overall Channel Number	Abbr.	MIDAS Station	Mod.	Mod. Ch. No.	Conv. Units	Wire	Gain
Joint of Floor with Lavatory Near Tank, Rear Joint Inside Lavatory of Outside Wall and Lavatory Wall		127	TLXWallJoint	Center	4	31	°C	TC	100
Along Floor Joint With Wall Above Tires 46 cm Next TC	46 cm rearward of TFWWRear	128	TFWWRear46	Center	5	0	°C	TC	100
Along Floor Joint With Wall Above Tires Behind Rear Tire	aligned over wheel well TC TIWWRear	129	TFWWRear	Center	5	1	°C	TC	100
Along Floor Joint With Wall Above Tires Rear Tire Center	aligned over wheel well TC TIWWRearC	130	TFWWRearC	Center	5	2	°C	TC	100
Along Floor Joint With Wall Above Tires Middle of Tires	aligned over wheel well TC TIWWMid	131	TFWWMid	Center	5	3	°C	TC	100
Along Floor Joint With Wall Above Tires Front Tire Center	aligned over wheel well TC TIWWFrontC	132	TFWWFrontC	Center	5	4	°C	TC	100
Along Floor Joint With Wall Above Tires in Front of Front Tire	aligned over wheel well TC TIWWFront	133	TFWWFront	Center	5	5	°C	TC	100
Along Floor Joint With Wall Above Tires 46 cm in Front of Previous TC	46 cm forward of TFWWFront	134	TFWWFront46	Center	5	6	°C	TC	100
Horizontal Rake Along Tag Axle Passenger Side		135	TTagAxleP	Center	5	7	°C	TC	100
Horizontal Rake Along Tag Axle Bus Center		136	TTagAxleC	Center	5	8	°C	TC	100
Horizontal Rake Along Tag Axle Driver's Side		137	TTagAxleD	Center	5	9	°C	TC	100
Horizontal Rake Along Drive Axle Passenger Side		138	TDrAxleP	Center	5	10	°C	TC	100
Horizontal Rake Along Drive Axle Bus Center		139	TDrAxleC	Center	5	11	°C	TC	100
Horizontal Rake Along Drive Axle Driver's Side		140	TDrAxleD	Center	5	12	°C	TC	100
Inside Central Tunnel Wiring/ Fuel Line Track Behind Rear Tires	align w/wheel well TCs	141	TWireTrkR	Center	5	13	°C	TC	100
Inside Central Tunnel Wiring/ Fuel Line Track Middle of Tires	align w/wheel well TCs	142	TWireTrkC	Center	5	14	°C	TC	100
Inside Central Tunnel Wiring/ Fuel Line Track In Front of Drive Axle	align w/wheel well TCs	143	TWireTrkF	Center	5	15	°C	TC	100
Total Heat Flux Gauge Seat (SN127842)	See Table 2	144	HFSeat	Center	5	16	kW/m	Cu	100
Temperature of Total Heat Flux Gauge Seat (SN127842)	See Table 2	145	THFSeat	Center	5	17	°C	TC	100
Smoke Detector 1	Only used for overnight monitoring	146	SM1	Center	5	18	V	Cu	1
Smoke Detector 2	Only used for overnight monitoring	147	SM2	Center	5	19	V	Cu	1
Extra TC Temperature 1		148	TX1	Center	5	20	°C	TC	100
Extra TC Temperature 2		149	TX2	Center	5	21	°C	TC	100
Extra TC Temperature 3		150	TX3	Center	5	22	°C	TC	100
Extra TC Temperature 4		151	TX4	Center	5	23	°C	TC	100
Created Channels									
Event Marker 1		152	Event1	Center					
Event Marker 2		153	Event2	Center					

Tenability Experiment

LFL MIDAS Hookup Sheet Instrument and Channel Description	LabView file: LFLMIDASCenterMotorCoach111809 .vi	Series:	Motorcoach Fires - Johnsson			Revision Date: 11/18/09				
Main Channels	Location Description	Overall Channel Number	Abbr.	MIDAS Station	Mod.	Mod. Ch. No.	Conv. Units	Wire	Gain	
5 V Marker Channel	At MIDAS Center	0	5VMarker	Center	1	0	V	Cu	1	
Tamb	At MIDAS Center station	1	Tamb	Center	1	1	°C	TC	100	
Total Heat Flux Gauge Rear/Side (SN127848)	See Table 10	2	HF1m	Center	1	2	kw/m2	Cu	100	
Total Heat Flux Gauge Front/Side (SN128324)	See Table 10	3	HF2m	Center	1	3	kw/m2	Cu	100	
Total Heat Flux Gauge Rear/Down (SN128321)	See Table 10	4	HF3m	Center	1	4	kw/m2	Cu	100	
Total Heat Flux Gauge Front/Down (SN127841)	See Table 10	5	HF4m	Center	1	5	kw/m2	Cu	100	
Temperature of Total Heat Flux Gauge Rear/Side (SN127848)	See Table 10	6	THF1m	Center	1	6	°C	TC	100	
Temperature of Total Heat Flux Gauge Front/Side (SN128324)	See Table 10	7	THF2m	Center	1	7	°C	TC	100	
Temperature of Total Heat Flux Gauge Rear/Down (SN128321)	See Table 10	8	THF3m	Center	1	8	°C	TC	100	
Temperature of Total Heat Flux Gauge Front/Down (SN127841)	See Table 10	9	THF4m	Center	1	9	°C	TC	100	
Window Temperature Outside Array 1 TC 1	79 cm up from bottom	10	O1T1	Center	1	10	°C	TC	100	
Window Temperature Outside Array 1 TC 2	41 cm up from bottom	11	O1T2	Center	1	11	°C	TC	100	
Window Temperature Outside Array 1 TC 3	3 cm up from bottom	12	O1T3	Center	1	12	°C	TC	100	
Window Temperature Outside Array 1 TC 4	35 cm down from bottom	13	O1T4	Center	1	13	°C	TC	100	
Window Temperature Outside Array 2 TC 1	79 cm up from bottom	14	O2T1	Center	1	14	°C	TC	100	
Window Temperature Outside Array 2 TC 2	41 cm up from bottom	15	O2T2	Center	1	15	°C	TC	100	
Window Temperature Outside Array 2 TC 3	3 cm up from bottom	16	O2T3	Center	1	16	°C	TC	100	
Window Temperature Outside Array 2 TC 4	35 cm down from bottom	17	O2T4	Center	1	17	°C	TC	100	
Window Temperature Outside Array 3 TC 1	79 cm up from bottom	18	O3T1	Center	1	18	°C	TC	100	
Window Temperature Outside Array 3 TC 2	41 cm up from bottom	19	O3T2	Center	1	19	°C	TC	100	
Window Temperature Outside Array 3 TC 3	3 cm up from bottom	20	O3T3	Center	1	20	°C	TC	100	
Window Temperature Outside Array 3 TC 4	35 cm down from bottom	21	O3T4	Center	1	21	°C	TC	100	
Window Temperature Outside Array 4 TC 1	79 cm up from bottom	22	O4T1	Center	1	22	°C	TC	100	
Window Temperature Outside Array 4 TC 2	41 cm up from bottom	23	O4T2	Center	1	23	°C	TC	100	
Window Temperature Outside Array 4 TC 3	3 cm up from bottom	24	O4T3	Center	1	24	°C	TC	100	
Window Temperature Outside Array 4 TC 4	35 cm down from bottom	25	O4T4	Center	1	25	°C	TC	100	
Window Temperature Outside Array 5 TC 1	79 cm up from bottom	26	O5T1	Center	1	26	°C	TC	100	
Window Temperature Outside Array 5 TC 2	41 cm up from bottom	27	O5T2	Center	1	27	°C	TC	100	
Window Temperature Outside Array 5 TC 3	3 cm up from bottom	28	O5T3	Center	1	28	°C	TC	100	

THIS IS A PREDECISIONAL DRAFT INTERIM REPORT

Main Channels	Location Description	Overall Channel Number	Abbr.	MIDAS Station	Mod.	Mod. Ch. No.	Conv. Units	Wire	Gain
Window Temperature Outside Array 5 TC 4	35 cm down from bottom	29	O5T4	Center	1	29	°C	TC	100
Window Temperature Outside Array 6 TC 1	79 cm up from bottom	30	O6T1	Center	1	30	°C	TC	100
Window Temperature Outside Array 6 TC 2	41 cm up from bottom	31	O6T2	Center	1	31	°C	TC	100
Window Temperature Outside Array 6 TC 3	3 cm up from bottom	32	O6T3	Center	2	0	°C	TC	100
Window Temperature Outside Array 6 TC 4	35 cm down from bottom	33	O6T4	Center	2	1	°C	TC	100
Window Temperature Outside Array 7 TC 1	79 cm up from bottom	34	O7T1	Center	2	2	°C	TC	100
Window Temperature Outside Array 7 TC 2	41 cm up from bottom	35	O7T2	Center	2	3	°C	TC	100
Window Temperature Outside Array 7 TC 3	3 cm up from bottom	36	O7T3	Center	2	4	°C	TC	100
Window Temperature Outside Array 7 TC 4	35 cm down from bottom	37	O7T4	Center	2	5	°C	TC	100
Window Temperature Outside Array 8 TC 1	79 cm up from bottom	38	O8T1	Center	2	6	°C	TC	100
Window Temperature Outside Array 8 TC 2	41 cm up from bottom	39	O8T2	Center	2	7	°C	TC	100
Window Temperature Outside Array 8 TC 3	3 cm up from bottom	40	O8T3	Center	2	8	°C	TC	100
Window Temperature Outside Array 8 TC 4	35 cm down from bottom	41	O8T4	Center	2	9	°C	TC	100
Window Temperature Outside Array 9 TC 1	79 cm up from bottom	42	O9T1	Center	2	10	°C	TC	100
Window Temperature Outside Array 9 TC 2	41 cm up from bottom	43	O9T2	Center	2	11	°C	TC	100
Window Temperature Outside Array 9 TC 3	3 cm up from bottom	44	O9T3	Center	2	12	°C	TC	100
Window Temperature Outside Array 9 TC 4	35 cm down from bottom	45	O9T4	Center	2	13	°C	TC	100
Window Temperature Outside Array 10 TC 1	79 cm up from bottom	46	O10T1	Center	2	14	°C	TC	100
Window Temperature Outside Array 10 TC 2	41 cm up from bottom	47	O10T2	Center	2	15	°C	TC	100
Window Temperature Outside Array 10 TC 3	3 cm up from bottom	48	O10T3	Center	2	16	°C	TC	100
Window Temperature Outside Array 10 TC 4	35 cm down from bottom	49	O10T4	Center	2	17	°C	TC	100
Window Temperature Outside Array 11 TC 1	79 cm up from bottom	50	O11T1	Center	2	18	°C	TC	100
Window Temperature Outside Array 11 TC 2	41 cm up from bottom	51	O11T2	Center	2	19	°C	TC	100
Window Temperature Outside Array 11 TC 3	3 cm up from bottom	52	O11T3	Center	2	20	°C	TC	100
Window Temperature Outside Array 11 TC 4	35 cm down from bottom	53	O11T4	Center	2	21	°C	TC	100
Window Temperature Outside Array 12 TC 1	79 cm up from bottom	54	O12T1	Center	2	22	°C	TC	100
Window Temperature Outside Array 12 TC 2	41 cm up from bottom	55	O12T2	Center	2	23	°C	TC	100
Window Temperature Outside Array 12 TC 3	3 cm up from bottom	56	O12T3	Center	2	24	°C	TC	100
Window Temperature Outside Array 12 TC 4	35 cm down from bottom	57	O12T4	Center	2	25	°C	TC	100
Window Temperature Inside Array 1 TC 0.5	17 cm above TC1	58	I1T0	Center	2	26	°C	TC	100
Window Temperature Inside Array 1 TC 1	79 cm up from bottom	59	I1T1	Center	2	27	°C	TC	100
Window Temperature Inside Array 1 TC 2	41 cm up from bottom	60	I1T2	Center	2	28	°C	TC	100
Window Temperature Inside Array 1 TC 3	3 cm up from bottom	61	I1T3	Center	2	29	°C	TC	100
Window Temperature Inside Array 2 TC 0.5	17 cm above TC1	62	I2T0	Center	2	30	°C	TC	100
Window Temperature Inside Array 2 TC 1	79 cm up from bottom	63	I2T1	Center	2	31	°C	TC	100
Window Temperature Inside Array 2 TC 2	41 cm up from bottom	64	I2T2	Center	3	0	°C	TC	100
Window Temperature Inside Array 2 TC 3	3 cm up from bottom	65	I2T3	Center	3	1	°C	TC	100
Window Temperature Inside Array 3 TC 0.5	17 cm above TC1	66	I3T0	Center	3	2	°C	TC	100

THIS IS A PREDECISIONAL DRAFT INTERIM REPORT

Main Channels	Location Description	Overall Channel Number	Abbr.	MIDAS Station	Mod.	Mod. Ch. No.	Conv. Units	Wire	Gain
Window Temperature Inside Array 3 TC 1	79 cm up from bottom	67	I3T1	Center	3	3	°C	TC	100
Window Temperature Inside Array 3 TC 2	41 cm up from bottom	68	I3T2	Center	3	4	°C	TC	100
Window Temperature Inside Array 3 TC 3	3 cm up from bottom	69	I3T3	Center	3	5	°C	TC	100
Window Temperature Inside Array 4 TC 0.5	17 cm above TC1	70	I4T0	Center	3	6	°C	TC	100
Window Temperature Inside Array 4 TC 1	79 cm up from bottom	71	I4T1	Center	3	7	°C	TC	100
Window Temperature Inside Array 4 TC 2	41 cm up from bottom	72	I4T2	Center	3	8	°C	TC	100
Window Temperature Inside Array 4 TC 3	3 cm up from bottom	73	I4T3	Center	3	9	°C	TC	100
Window Temperature Inside Array 5 TC 0.5	17 cm above TC1	74	I5T0	Center	3	10	°C	TC	100
Window Temperature Inside Array 5 TC 1	79 cm up from bottom	75	I5T1	Center	3	11	°C	TC	100
Window Temperature Inside Array 5 TC 2	41 cm up from bottom	76	I5T2	Center	3	12	°C	TC	100
Window Temperature Inside Array 5 TC 3	3 cm up from bottom	77	I5T3	Center	3	13	°C	TC	100
Window Temperature Inside Array 6 TC 0.5	17 cm above TC1	78	I6T0	Center	3	14	°C	TC	100
Window Temperature Inside Array 6 TC 1	79 cm up from bottom	79	I6T1	Center	3	15	°C	TC	100
Window Temperature Inside Array 6 TC 2	41 cm up from bottom	80	I6T2	Center	3	16	°C	TC	100
Window Temperature Inside Array 6 TC 3	3 cm up from bottom	81	I6T3	Center	3	17	°C	TC	100
Window Temperature Inside Array 7 TC 0.5	17 cm above TC1	82	I7T0	Center	3	18	°C	TC	100
Window Temperature Inside Array 7 TC 1	79 cm up from bottom	83	I7T1	Center	3	19	°C	TC	100
Window Temperature Inside Array 7 TC 2	41 cm up from bottom	84	I7T2	Center	3	20	°C	TC	100
Window Temperature Inside Array 7 TC 3	3 cm up from bottom	85	I7T3	Center	3	21	°C	TC	100
Window Temperature Inside Array 8 TC 0.5	17 cm above TC1	86	I8T0	Center	3	22	°C	TC	100
Window Temperature Inside Array 8 TC 1	79 cm up from bottom	87	I8T1	Center	3	23	°C	TC	100
Window Temperature Inside Array 8 TC 2	41 cm up from bottom	88	I8T2	Center	3	24	°C	TC	100
Window Temperature Inside Array 8 TC 3	3 cm up from bottom	89	I8T3	Center	3	25	°C	TC	100
Window Temperature Inside Array 9 TC 0.5	17 cm above TC1	90	I9T0	Center	3	26	°C	TC	100
Window Temperature Inside Array 9 TC 1	79 cm up from bottom	91	I9T1	Center	3	27	°C	TC	100
Window Temperature Inside Array 9 TC 2	41 cm up from bottom	92	I9T2	Center	3	28	°C	TC	100
Window Temperature Inside Array 9 TC 3	3 cm up from bottom	93	I9T3	Center	3	29	°C	TC	100
Window Temperature Inside Array 10 TC 0.5	17 cm above TC1	94	I10T0	Center	3	30	°C	TC	100
Window Temperature Inside Array 10 TC 1	79 cm up from bottom	95	I10T1	Center	3	31	°C	TC	100
Window Temperature Inside Array 10 TC 2	41 cm up from bottom	96	I10T2	Center	4	0	°C	TC	100
Window Temperature Inside Array 10 TC 3	3 cm up from bottom	97	I10T3	Center	4	1	°C	TC	100
Window Temperature Inside Array 11 TC 0.5	17 cm above TC1	98	I11T0	Center	4	2	°C	TC	100
Window Temperature Inside Array 11 TC 1	79 cm up from bottom	99	I11T1	Center	4	3	°C	TC	100
Window Temperature Inside Array 11 TC 2	41 cm up from bottom	100	I11T2	Center	4	4	°C	TC	100
Window Temperature Inside Array 11 TC 3	3 cm up from bottom	101	I11T3	Center	4	5	°C	TC	100
Window Temperature Inside Array 12 TC 0.5	17 cm above TC1	102	I12T0	Center	4	6	°C	TC	100
Window Temperature Inside Array 12 TC 1	79 cm up from bottom	103	I12T1	Center	4	7	°C	TC	100
Window Temperature Inside Array 12 TC 2	41 cm up from bottom	104	I12T2	Center	4	8	°C	TC	100

THIS IS A PREDECISIONAL DRAFT INTERIM REPORT

Main Channels	Location Description	Overall Channel Number	Abbr.	MIDAS Station	Mod.	Mod. Ch. No.	Conv. Units	Wire	Gain
Window Temperature Inside Array 12 TC 3	3 cm up from bottom	105	I12T3	Center	4	9	°C	TC	100
Inside Ignited Wheel Screwed On Back 12 o'clock Position		106	TIWh12	Center	4	10	°C	TC	100
Inside Ignited Wheel Screwed On Back 3 o'clock Position		107	TIWh3	Center	4	11	°C	TC	100
Inside Ignited Wheel Screwed On Back 6 o'clock Position		108	TIWh6	Center	4	12	°C	TC	100
Inside Ignited Wheel Screwed On Back 9 o'clock Position		109	TIWh9	Center	4	13	°C	TC	100
At Wheel/Tire Interface of Ignited Tire 12 o'clock Position		110	TITi12	Center	4	14	°C	TC	100
At Wheel/Tire Interface of Ignited Tire 3 o'clock Position		111	TITi3	Center	4	15	°C	TC	100
At Wheel/Tire Interface of Ignited Tire 6 o'clock Position		112	TITi6	Center	4	16	°C	TC	100
At Wheel/Tire Interface of Ignited Tire 9 o'clock Position		113	TITi9	Center	4	17	°C	TC	100
ABS Sensor Tag Axle Wheel		114	ABSTag	Center	4	18	°C	V	1
At Wheel/Tire Interface of Non-Ignited Tire (Ignition Side)		115	TNTi12	Center	4	19	°C	TC	100
Inside the Wheel Well Above the Tires (Ignition Side) Behind Rear Tire		116	TIWWRear	Center	4	20	°C	TC	100
Inside the Wheel Well Above the Tires (Ignition Side) Rear Tire Center		117	TIWWRearC	Center	4	21	°C	TC	100
Inside the Wheel Well Above the Tires (Ignition Side) Middle		118	TIWWMid	Center	4	22	°C	TC	100
Inside the Wheel Well Above the Tires (Ignition Side) Front Tire Center		119	TIWWFrontC	Center	4	23	°C	TC	100
Inside the Wheel Well Above the Tires (Ignition Side) In Front of Front Tire		120	TIWWFront	Center	4	24	°C	TC	100
bad channel		121	bad	Center	4	25	V	V	1
ABS Sensor Temperature Tag Axle Wheel		122	TABSTag	Center	4	26	°C	TC	100
Inside the Wheel Well Above the Tires (Unignited Side) Rear Tire Center		123	TUWWRearC	Center	4	27	°C	TC	100
Inside the Wheel Well Above the Tires (Unignited Side) Front Tire Center		124	TUWWFrontC	Center	4	28	°C	TC	100
Joint of Floor with Lavatory Near Tank, Outside Corner of Outside Wall and Lavatory Wall		125	TLXWallCorn	Center	4	29	°C	TC	100
Joint of Floor with Lavatory Near Tank, Inside Joint of Lavatory Wall and Floor		126	TLMidJoint	Center	4	30	°C	TC	100
Joint of Floor with Lavatory Near Tank, Rear Joint Inside Lavatory of Outside Wall and Lavatory Wall		127	TLXWallJoint	Center	4	31	°C	TC	100
Along Floor Joint With Wall Above Tires 46 cm Next TC	align w/wheel well TCs	128	TFWWRear46	Center	5	0	°C	TC	100
Along Floor Joint With Wall Above Tires Behind Rear Tire	align w/wheel well TCs	129	TFWWRear	Center	5	1	°C	TC	100

THIS IS A PREDECISIONAL DRAFT INTERIM REPORT

Main Channels	Location Description	Overall Channel Number	Abbr.	MIDAS Station	Mod.	Mod. Ch. No.	Conv. Units	Wire	Gain
Along Floor Joint With Wall Above Tires Rear Tire Center	align w/wheel well TCs	130	TFWWRearC	Center	5	2	°C	TC	100
Along Floor Joint With Wall Above Tires Middle of Tires	align w/wheel well TCs	131	TFWWMid	Center	5	3	°C	TC	100
Along Floor Joint With Wall Above Tires Front Tire Center	align w/wheel well TCs	132	TFWWFrontC	Center	5	4	°C	TC	100
Along Floor Joint With Wall Above Tires in Front of Front Tire	align w/wheel well TCs	133	TFWWFront	Center	5	5	°C	TC	100
Along Floor Joint With Wall Above Tires 46 cm in Front of Previous TC	align w/wheel well TCs	134	TFWWFront46	Center	5	6	°C	TC	100
Horizontal Rake Along Tag Axle Passenger Side		135	TTagAxleP	Center	5	7	°C	TC	100
Horizontal Rake Along Tag Axle Bus Center		136	TTagAxleC	Center	5	8	°C	TC	100
Horizontal Rake Along Tag Axle Driver's Side		137	TTagAxleD	Center	5	9	°C	TC	100
Horizontal Rake Along Drive Axle Passenger Side		138	TDrAxleP	Center	5	10	°C	TC	100
Horizontal Rake Along Drive Axle Bus Center		139	TDrAxleC	Center	5	11	°C	TC	100
Horizontal Rake Along Drive Axle Driver's Side		140	TDrAxleD	Center	5	12	°C	TC	100
Inside Wiring/ Fuel Line Track Behind Rear Tires	align w/wheel well TCs	141	TWireTrkR	Center	5	13	°C	TC	100
Inside Wiring/ Fuel Line Track Middle of Tires	align w/wheel well TCs	142	TWireTrkC	Center	5	14	°C	TC	100
Inside Wiring/ Fuel Line Track In Front of Drive Axle	align w/wheel well TCs	143	TWireTrkF	Center	5	15	°C	TC	100
Total Heat Flux Gauge Seat (SN127842)		144	HF6m	Center	5	16	kw/m2	Cu	100
Temperature of Total Heat Flux Gauge Seat (SN127842)		145	THF6m	Center	5	17	°C	TC	100
Smoke Meter/Smoke Detector 1		146	SM1	Center	5	18	V	Cu	1
Smoke Detector 2		147	SM2	Center	5	19	V	Cu	1
Steel Panel Backside Temp, 1/2 Way Up Rearward of Tag Wheel		148	TPanRear	Center	5	20	°C	TC	100
Steel Panel Backside Temp, 1/2 Way Up Centered Above Tag Wheel		149	TPanRearC	Center	5	21	°C	TC	100
Steel Panel Backside Temp, 1/2 Way Up Centered Between Wheels		150	TPanMid	Center	5	22	°C	TC	100
Steel Panel Backside Temp, 1/2 Way Up Centered Above Drive Wheel		151	TPanFrontC	Center	5	23	°C	TC	100
Oxygen - Rear		152	O2-R	Center	5	24	Vol fr	Cu	1
Carbon Dioxide - Rear		153	CO2-R	Center	5	25	Vol fr	Cu	1
Carbon Monoxide - Rear		154	CO-R	Center	5	26	Vol fr	Cu	1
Total Unburned Hydrocarbons - Rear		155	UH-R	Center	5	27	Vol fr	Cu	1
Dewpoint - Rear		156	DP-R	Center	5	28	°C	Cu	1
Oxygen - Middle		157	O2-M	Center	5	29	Vol fr	Cu	1
Carbon Dioxide - Middle		158	CO2-M	Center	5	30	Vol fr	Cu	1
Carbon Monoxide - Middle		159	CO-M	Center	5	31	Vol fr	Cu	1

THIS IS A PREDECISIONAL DRAFT INTERIM REPORT

Main Channels	Location Description	Overall Channel Number	Abbr.	MIDAS Station	Mod.	Mod. Ch. No.	Conv. Units	Wire	Gain
Total Unburned Hydrocarbons - Middle		160	UH-M	Center	6	0	Vol fr	Cu	1
Dewpoint - Middle		161	DP-M	Center	6	1	°C	Cu	1
Oxygen - Front		162	O2-F	Center	6	2	Vol fr	Cu	1
Carbon Dioxide - Front		163	CO2-F	Center	6	3	Vol fr	Cu	1
Carbon Monoxide - Front		164	CO-F	Center	6	4	Vol fr	Cu	1
Total Unburned Hydrocarbons - Front		165	UH-F	Center	6	5	Vol fr	Cu	1
Dewpoint - Front		166	DP-F	Center	6	6	°C	Cu	1
Rear Thermocouple Array TC 180 cm up, 18 cm down		167	TRear180	Center	6	7	°C	TC	100
Rear Thermocouple Array TC 150 cm up, 48 cm down		168	TRear150	Center	6	8	°C	TC	100
Rear Thermocouple Array TC 120 cm up, 78 cm down		169	TRear120	Center	6	9	°C	TC	100
Rear Thermocouple Array TC 60 cm up, 138 cm down		170	TRear60	Center	6	10	°C	TC	100
Rear Thermocouple Array TC 30 cm up, 168 cm down		171	TRear30	Center	6	11	°C	TC	100
Middle Thermocouple Array TC 180 cm up, 18 cm down		172	TMiddle180	Center	6	12	°C	TC	100
Middle Thermocouple Array TC 150 cm up, 48 cm down		173	TMiddle150	Center	6	13	°C	TC	100
Middle Thermocouple Array TC 120 cm up, 78 cm down		174	TMiddle120	Center	6	14	°C	TC	100
Middle Thermocouple Array TC 60 cm up, 138 cm down		175	TMiddle60	Center	6	15	°C	TC	100
Middle Thermocouple Array TC 30 cm up, 168 cm down		176	TMiddle30	Center	6	16	°C	TC	100
Front Thermocouple Array TC 180 cm up, 18 cm down		177	TFront180	Center	6	17	°C	TC	100
Front Thermocouple Array TC 150 cm up, 48 cm down		178	TFront150	Center	6	18	°C	TC	100
Front Thermocouple Array TC 120 cm up, 78 cm down		179	TFront120	Center	6	19	°C	TC	100
Front Thermocouple Array TC 60 cm up, 138 cm down		180	TFront60	Center	6	20	°C	TC	100
Front Thermocouple Array TC 30 cm up, 168 cm down		181	TFront30	Center	6	21	°C	TC	100
Thermocouple Rear Inner Seat Top Center of Headrest		182	TSeatR	Center	6	22	°C	TC	100
Thermocouple Middle Inner Seat Top Center of Headrest		183	TSeatM	Center	6	23	°C	TC	100
Thermocouple Front Inner Seat Top Center of Headrest		184	TSeatF	Center	6	24	°C	TC	100
Thermocouple Above Rear Inner Seat On Parcel Rack Door		185	TRackDrR	Center	6	25	°C	TC	100
Thermocouple Above Middle Inner Seat On Parcel Rack Door		186	TRackDrM	Center	6	26	°C	TC	100
Thermocouple Above Front Inner Seat On Parcel Rack Door		187	TRackDrF	Center	6	27	°C	TC	100
Created Channels									
Event Marker 1		188	Event1	Center					
Event Marker 2		189	Event2	Center					

Appendix B. Photographs

Penetration Experiments



Figure 103 Tag axle wheel heating penetration experiment showing burner, shield, melted hub, and early thermal damage to tire.



Figure 104 Tag axle wheel heating penetration experiment about 2.5 minutes after the burner was removed showing the large quantity of black smoke on the far (driver's) side of the motorcoach.



Figure 105 Exterior fire damage due to tag axle wheel heating penetration experiment



Figure 106 Exterior view of window damage after tag axle wheel heating penetration experiment.



Figure 107 Interior view of window damage after tag axle wheel heating penetration experiment.



Figure 108 Damage to wall behind exterior panel after tag axle wheel heating penetration experiment.



Figure 109 Damage to back side of exterior panel showing little penetration of fire through the GRP.



Figure 110 Motorcoach ready for start of drive axle wheel heating penetration experiment.



Figure 111 Positioning of burner for drive axle wheel heating penetration experiment.



Figure 112 Close up view of burner near beginning of drive axle wheel heating penetration experiment.



Figure 113 Drive axle wheel heating penetration experiment showing smoke coming from the external air vents.



Figure 114 Drive axle wheel heating penetration experiment just over 1 min after burner was removed.



Figure 115 Drive axle wheel heating penetration experiment showing large fire plumes on each tire.



Figure 116 Drive axle wheel heating penetration experiment showing smoke on driver's side 4 min after burner removed.



Figure 117 Interior view of damage to the window over the tag axle after the drive axle wheel heating penetration experiment fire.



Figure 118 Interior view of damage to the window over the drive axle after the drive axle wheel heating penetration experiment fire.

Fire-Hardening Experiments



Figure 119 Steel exterior panel fire-hardening experiment at the beginning of suppression.



Figure 120 Steel exterior panel fire-hardening experiment paper-covered wall foam damage from fire.



Figure 121 Intumescent coating fire-hardening experiment close-up of coated fender.



Figure 122 Intumescent coating fire-hardening experiment damage to coated fender and exterior panel.

Tenability Experiment



Figure 123 Tenability experiment at the beginning of suppression.



Figure 124 Tenability experiment seat damage from fire.



Figure 125 Tenability experiment seat and parcel rack damage from fire.



Figure 126 Tenability experiment seat damage from fire.